NAVAL POSTGRADUATE SCHOOL
Monterey, California

AD-A284 180

DTIC
S ELECTE D
SEP 0 9 1994
F

THESIS

A TRIANGULATION METHOD FOR PASSIVE RANGING
by
Gerasimos Pelegris
June 1994
Thesis Advisor: Ron J. Pieper
Thesis Co-Advisor: A. W. Cooper

Approved for public release; distribution is unlimited.

94-29287

DTIC QUALITY INSPECTED 3

94 9 07 130

REPORT DOCUMENTATION PAGE		Form Approved OMB No. 0704

Public reporting burden for this collection of information is estimated to average 1 hour per response, includ   the time for reviewing instruction, searching existing data sources, gathering and maintaining the data needed, and completing and reviewing the collection of information. Send comments regarding this burden estimate or any other aspect of this collection of information, including suggestions for reducing this burden, to Washington headquarters Services, Directorate for Information Operations and Reports, 1215 Jefferson Davis Highway, Suite 1204, Arlington, VA 22202-4302, and to the Office of Management and Budget, Paperwork Reduction Project (0704-0188) Washington DC 20503.

1. AGENCY USE ONLY *(Leave blank)*	2. REPORT DATE June 1994	3. REPORT TYPE AND DATES COVERED Master's Thesis
4. TITLE AND SUBTITLE A Triangulation Method for Passive Ranging		5. FUNDING NUMBERS
6. AUTHOR(S) Gerasimos Pelegris		
7. PERFORMING ORGANIZATION NAME(S) AND ADDRESS(ES) Naval Postgraduate School Monterey CA 93943-5000		8. PERFORMING ORGANIZATION REPORT NUMBER
9. SPONSORING/MONITORING AGENCY NAME(S) AND ADDRESS(ES)		10. SPONSORING/MONITORING AGENCY REPORT NUMBER

11. SUPPLEMENTARY NOTES The views expressed in this thesis are those of the author and do not reflect the official policy or position of the Department of Defense or the U.S. Government.

12a. DISTRIBUTION/AVAILABILITY STATEMENT Approved for public release; distribution unlimited	12b. DISTRIBUTION CODE A

13. ABSTRACT *(maximum 200 words)* A method for passive ranging based on the principle of triangulation is considered. In the basic triangulation scheme that is a single baseline model the precision in the bearing readings can be related to the precision in the range estimation. For some target orientations the precision in the triangulated target is completely lost. This phenomenon is known as "geometric dilution." A proposed orthogonal dual baseline scheme eliminates the "geometric dilution" effect. The performance of each of the two orthogonal baselines depends on the orientation. For specific target orientations the triangulation range measurements for the two baselines are equivalent. The dual baseline scheme would require "smart electronics" which would switch between baselines at crossover points in the range estimation precision. It is shown that the crossover points depend primarily on the ratio of the two baselines. A general expression for the maximum triangulation range consistent with limitations in minimum tolerance precision in range estimation is derived. The dependency between maximum range and target orientation are presented in polar form. Limitations in the dual baseline model due to physical limitation created by the optical horizon are also considered.

14. SUBJECT TERMS Baseline, Dual baseline, Triangulation, Passive ranging.			15. NUMBER OF PAGES 118
			16. PRICE CODE
17. SECURITY CLASSIFICATION OF REPORT Unclassified	18. SECURITY CLASSIFICATION OF THIS PAGE Unclassified	19. SECURITY CLASSIFICATION OF ABSTRACT Unclassified	20. LIMITATION OF ABSTRACT UL

DTIC QUALITY INSPECTED 3

A TRIANGULATION METHOD FOR PASSIVE RANGING

by

Gerasimos Pelegris
Lieutenant Colonel, Greek Army
B.S. Greek Army Military Academy, 1974

Submitted in partial fulfillment
of the requirements for the degree of

MASTER OF SCIENCE IN ELECTRICAL ENGINEERING
MASTER OF SCIENCE IN APPLIED PHYSICS

from the

NAVAL POSTGRADUATE SCHOOL
June 1994
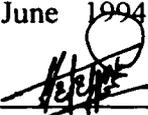
Author : _____
Gerasimos Pelegris
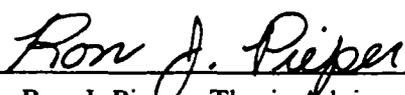
Approved by: _____
Ron J. Pieper, Thesis Advisor
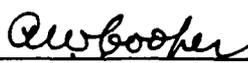
_____
A. W. Cooper, Thesis Co-Advisor

_____
Michael A. Morgan, Chairman
Department of Electrical and Computer Engineering

_____
W. B. Colson, Chairman Physics Department

ABSTRACT

A method for passive ranging based on the principle of triangulation is considered.

In the basic triangulation scheme that is a single baseline model the precision in the bearing

readings can be related to the precision in the range estimation. For some target orienta-

tions the precision in the triangulated target range is completely lost. This phenomenon is

known as "geometric dilution." A proposed orthogonal dual baseline scheme eliminates

the "geometric dilution" effect. The performance of each of the two orthogonal baselines

depends on target orientation. For specific target orientations the triangulation range mea-

surements for the two baselines are equivalent. The dual baseline scheme would require

"smart electronics" which would switch between baselines at crossover points in the range

estimation precision. It is shown that the crossover points depend primarily on the ratio of

the two baselines. A general expression for the maximum triangulation range consistent

with limitations in minimum tolerance precision in range estimation is derived. The depen-

dency between maximum range and target orientation are presented in polar form. Limita-

tions in the dual baseline model due to physical limitation created by the optical horizon

are also considered.

iii

TABLE OF CONTENTS

I. INTRODUCTION

A. REVIEW OF PRIOR WORK

Recent technological developments can turn an active radar system into a target for anti-radiation missiles (ARM). In essence, a system designed to provide security against missile attacks can become a security hazard. This thesis will present a methodology of passive ranging based on triangulation and the use of IR sensors which could be implemented on various kinds of military platforms. IR sensors provide for passive surveillance and target identification and tracking, but targeting and fire control require a minimum range to target.

Passive ranging is the Holy Grail of the defense community. The passive interrogation of a scene greatly restricts the domain of applicable countermeasures. Therefore, with passive ranging the security of the intelligence operation is less likely to be compromised.

Various passive ranging schemes based on the radiating characteristics of a target have been proposed. These can be classified under a variety of descriptors such as: time difference of arrival (TDOA), frequency difference of arrival (FDOA), and angle difference location (ADL) [Ref. 1], [Ref. 2]. The first two schemes, TDOA and FDOA require that RF modulation be present on the target's electromagnetic spectrum [Ref. 3]. Since the thrust of this thesis is to focus on a potential ADL technique triangulation, which requires only a target's unmodulated IR signature, no further discussion on TDOA or FDOA

1

methods will be included. Several methods for using atmospheric attenuation to predict target range passively are covered in the next paragraph.

In the early 1960's several patents were approved which related IR signal's atmospheric attenuation to range. The first of these was based on the atmospheric absorption of radiation from targets which have strong water vapor or carbon dioxide bands [Ref. 4]. The scheme includes signal chopping, optical beam splitting, and controlled absorption of the CO_2 band in a reference path. A nulling circuit, which uses a partially transmitting wedge driven by a servomotor, balances the two signals. The error signal is then directly related to the amount of energy in the CO_2 band of the original IR signal received. This error signal can be related to the length of the attenuation path, i.e., range. A second patent [Ref. 5] is again based on the principle of preferential atmospheric absorption of IR radiation for some bands. However, in this case the authors proposes that if a target's total and filtered radiation intensities are known, and if the effective radiation coefficients for total and filtered bands could be ascertained, then ratios of measured intensities can be related through analysis to the unknown range. The inventors of this patent also use a chopper and comparison circuitry. Recent NPS theses have examined the passive ranging problem using similar concepts [Ref. 6], [Ref. 7], [Ref. 8].

The principle of the parallax effect, as applied in the optical range finder [Ref. 9], has been modified to process IR signals. In this scheme, introduced as a patent [Ref. 10], the measurement of a parallax angle between two imaging sensors and a known baseline will permit calculation of the range to a target. Another 60's patent [Ref. 11] suggests a model for calculation closure time, the approximate time it will take one body to collide with

2

another. This parameter depends on range. The inventors show that the closure time can be calculated from the time rate of change of the target's passively detected radiant energy. They provide a circuit for this application.

With the development of IRST passive sensors [Ref. 12], renewed interest in ADL methods has occurred. In particular these devices are available on a rotating (30 rpm) platform and can predict bearing azimuth data on low flying targets. A platform for an IRST device is shown in Figure 1. The bearing resolution of such devices is classified; however an interesting mathematical model for predicting resolution for targets in the presence of noise has been proposed [Ref. 13].
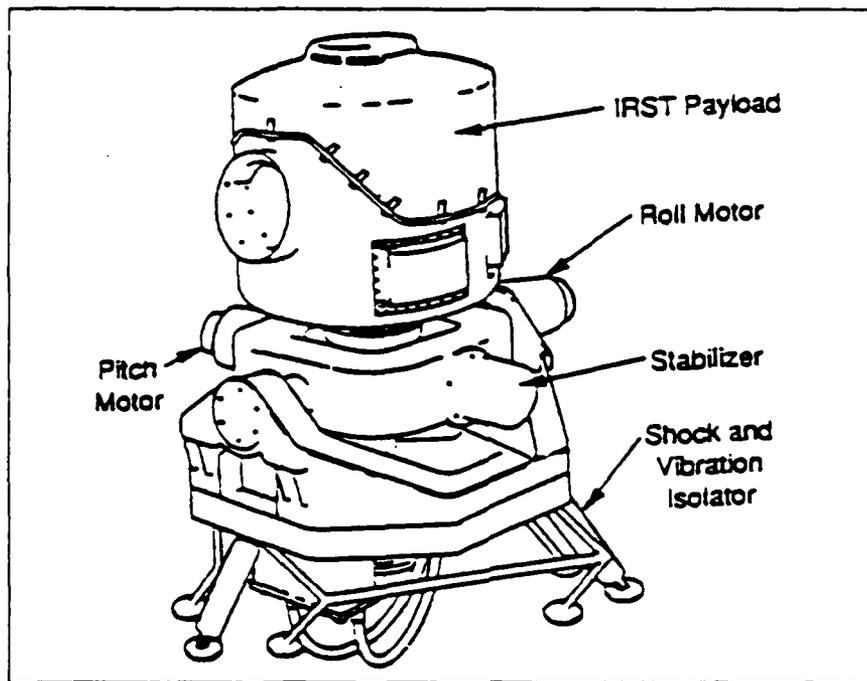
Figure 1: IRST sensor platform (After Ref. 12)

Most of the ADL methods are based on using two sensors, i.e., a single baseline approach (SBL) [Ref. 14], [Ref. 15]. In the late 70's a multiple sensor scheme based on a technique known as circulation [Ref. 16], which employs an interactive least squares algorithm, has been investigated. Although the method eliminates the problem of "geometric dilution" the scheme can exhibit convergence problems. More recently a preliminary study on an analytic dual baseline method has been introduced [Ref. 17]. This description is based on an approximate model for estimating the range sensitivity. Further developments on this dual baseline model will be presented in this thesis.

B.   THESIS OVERVIEW

Chapter I covers the literature review and the thesis overview. In Chapter II the single baseline analysis is developed, and the lack of precision in a triangulated range is related to the lack of precision in the bearing measurements. It is shown that the precision of the triangulation method for targets alligned with the single baseline is completely lost. This problem is known as "geometric dilution." Chapter III explores the applicability of a dual baseline scheme in order to circumvent this problem. In Chapter IV the dual baseline model is applied to characterize a maximum range for triangulation consistent with a minimum precision in the measurement. The development in this chapter leads to a physical polar representation for R_{max} in terms of target orientation. Two paradigms, quadrature addition and the more conservative sum of absolutes, are considered. In Chapter V the limitations in range estimation due to earth's curvature are evaluated and included with the dual baseline model. Some interesting qualifications for predicting the characteristics of

4

the polar plots studied in Chapter IV are provided in Chapter VI . Chapter VII provides the conclusions.

Appendix A is the list of symbols provided for convenience in alphabetical order. In order not to complicate the main text some of the more mathematical derivations have been relegated to the Appendices B, C, and D. In Appendix B details on approximations made on the single baseline model are presented. In Appendix C, an exact mathematical expression or the single baseline triangulated range in terms of IRST sensors bearing is derived. In Appendix D two paradigms for error estimation are analyzed. It is shown that the sum of absolutes estimation is more conservative than estimation via quadrature addition. Appendix E is a collection of the programs used in generating the plots seen in the thesis.

II. BACKGROUND ANALYSIS

A. THE TRIANGULATION CONCEPT

The eye-brain system undoubtedly works in a fairly sophisticated manner in order to extract information from parallax. The geometric considerations of the corresponding passive sensor problem are fairly simple. In principle, the range prediction can be made with 100% accuracy; in practice the limitations in the accuracy of the measurements in orientation bearings introduce an error in the range prediction. The sensitivity for the range prediction to variation in the bearing accuracy is dependent on target orientation, the distance between the points of observation or baseline, and the range to the target. Currently IRST bearings do not include elevation data. For targets which appear coming over the horizon this should not represent a significant deficiency in the model. Therefore, the model to be presented predicts horizontal range, not the slant range.

B. SINGLE BASELINE MODEL

A single baseline model, involving two sensors, located at the ends of a baseline, can be analyzed for conditions sufficient for triangulation. Starting from Figure 2 the points at which bearing measurements are made, A and C, are located at a distance R_1 and R_2 respectively from the target at T. Although no measurements are made at point B it serves as a convenient symmetrical reference between observation points A and C. The range R is defined as the distance from point B to the target. The characteristics of the single

6

baseline model in terms of symmetric variables R and θ greatly facilitates the dual baseline analysis presented later. The distance between the points A and C is the baseline (BL). The initial objective of this analysis will be to relate the range R to the measurables in the problem, i.e., baseline (BL) and orientation (θ_1 and θ_2). The next step in the procedure will be to perform a sensitivity analysis with respect to variation in the orientation variables, θ_1 and θ_2.

The significant assumptions of the model are:

(1) There is no error in the baseline measurement;

(2) The tolerances in the bearing measurements are known, and will be denoted $\Delta\theta_1$ and $\Delta\theta_2$;

(3) The discrepancy between horizontal path range and slant-path range is not significant.

1. A single baseline analysis

From the Figure 2, the apex angles satisfy the following relation

$$\theta_3 = \theta_2 - \theta_1 = \theta_4 + \theta_5 \tag{1}$$

Another relation between the apex angles and θ_1, θ_2 is obtained from the Law of Sines

$$\sin\theta_4 = \frac{BL}{2R}\sin\theta_2 \tag{2a}$$

$$\sin\theta_5 = \frac{BL}{2R}\sin\theta_1 \tag{2b}$$

7

Through expansion of (1) it follows that

$$\sin(\theta_2 - \theta_1) = \sin\theta_4\cos\theta_5 + \cos\theta_4\sin\theta_5 \tag{3a}$$

and

$$\sin(\theta_2 - \theta_1) = \frac{BL}{2R}\left[\sin\theta_2\sqrt{1 - \left(\frac{BL}{2R}\sin\theta_1\right)^2} + \sin\theta_1\sqrt{1 - \left(\frac{BL}{2R}\sin\theta_2\right)^2}\right] \tag{3b}$$

Solving (3) for the range R, it follows that

$$R = \frac{BL}{2}\left[\frac{\sin\theta_2\sqrt{1 - \left(\frac{BL}{2R}\sin\theta_1\right)^2} + \sin\theta_1\sqrt{1 - \left(\frac{BL}{2R}\sin\theta_2\right)^2}}{\sin(\theta_2 - \theta_1)}\right] \tag{4}$$

An exact expression for $R/BL(\theta_1, \theta_2)$ can be obtained using symbolic mathematical processing. See Appendix C. The immediate objective is to obtain an expression for the range sensitivity in terms of the bearing angles θ_1 and θ_2, which will be in the form

$$\frac{\Delta R}{R} = f_1(\theta_1, \theta_2)\Delta\theta_1 + f_2(\theta_1, \theta_2)\Delta\theta_2 \tag{5}$$

In order to not distract the reader, the mathematical details in obtaining the range sensitivity appear in Appendix B, and the final expression for it is

$$\frac{\Delta R}{R} = \left[\frac{\sqrt{1-\left(\frac{BL}{2R}\sin\theta_2\right)^2}\left(\cos\theta_1+\sin\theta_1\cot(\theta_2-\theta_1)\right)-\sin\theta_2\sqrt{1-\left(\frac{BL}{2R}\sin\theta_2\right)^2}\left(\cot(\theta_2-\theta_1)-\frac{\left(\frac{BL}{2R}\right)^2\sin\theta_1\cos\theta_1}{1-\left(\frac{BL}{2R}\sin\theta_1\right)^2}\right)}{\sin\theta_2\sqrt{1-\left(\frac{BL}{2R}\sin\theta_1\right)^2}+\sin\theta_1\sqrt{1-\left(\frac{BL}{2R}\sin\theta_2\right)^2}} \right](\Delta\theta_1)+$$

$$+\left[\frac{\sqrt{1-\left(\frac{BL}{2R}\sin\theta_1\right)^2}\left(\cos\theta_2-\sin\theta_2\cot(\theta_2-\theta_1)\right)-\sin\theta_1\sqrt{1-\left(\frac{BL}{2R}\sin\theta_2\right)^2}\left(\cot(\theta_2-\theta_1)+\frac{\left(\frac{BL}{2R}\right)^2\sin\theta_2\cos\theta_2}{1-\left(\frac{BL}{2R}\sin\theta_2\right)^2}\right)}{\sin\theta_2\sqrt{1-\left(\frac{BL}{2R}\sin\theta_1\right)^2}+\sin\theta_1\sqrt{1-\left(\frac{BL}{2R}\sin\theta_2\right)^2}} \right](\Delta\theta_2) \qquad (6)$$

where it is understood that $\Delta\theta_1$, and $\Delta\theta_2$ are assumed to be zero mean random variables

A statistical model for eliminating "systematic error" has been proposed using a scheme based on a method known as circulation [Ref. 16]. Furthermore, the ratio "a" of rms values for $\Delta\theta_2$ and $\Delta\theta_1$ can be used and the final expression for the normalized variation in R can be written as follows

$$\left(\frac{\Delta R}{R}\frac{1}{\Delta\theta}\right) = \left(\frac{\sqrt{1-\left(\frac{BL}{2R}\sin\theta_2\right)^2}\left(\cos\theta_1+\sin\theta_1\cot(\theta_2-\theta_1)\right)+\sin\theta_2\sqrt{1-\left(\frac{BL}{2R}\sin\theta_1\right)^2}\left(\cot(\theta_2-\theta_1)-\frac{\left(\frac{BL}{2R}\right)^2\sin\theta_1\cos\theta_2}{1-\left(\frac{BL}{2R}\sin\theta_1\right)^2}\right)}{\sin\theta_2\sqrt{1-\left(\frac{BL}{2R}\sin\theta_1\right)^2}+\sin\theta_1\sqrt{1-\left(\frac{BL}{2R}\sin\theta_2\right)^2}} \right)\cdot\chi_1+$$

$$\left(\frac{\sqrt{1-\left(\frac{BL}{2R}\sin\theta_1\right)^2}\left(\cos\theta_2-\sin\theta_2\cot(\theta_2-\theta_1)\right)-\sin\theta_1\sqrt{1-\left(\frac{BL}{2R}\sin\theta_2\right)^2}\left(\cot(\theta_2-\theta_1)+\frac{\left(\frac{BL}{2R}\right)^2\sin\theta_2\cos\theta_2}{1-\left(\frac{BL}{2R}\sin\theta_2\right)^2}\right)}{\sin\theta_2\sqrt{1-\left(\frac{BL}{2R}\sin\theta_1\right)^2}+\sin\theta_1\sqrt{1-\left(\frac{BL}{2R}\sin\theta_2\right)^2}} \right)\cdot\chi_2\cdot a \qquad (7)$$

where χ_1 and χ_2 are independent random variables having zero mean and unity standard deviation, and

$$a = \frac{\sqrt{\langle\theta_2^2\rangle}}{\sqrt{\langle\theta_1^2\rangle}} \qquad (8)$$

It is noteworthy that (7) depends on R, θ_1, and θ_2 instead of the symmetrically defined variables R and θ. Additional relations are needed at this point in order to express (7) and (8) in terms of the symmetrically defined variables R and θ. From the Law of Cosines, applied to Figure 2, it follows that

$$\left(\frac{R_2}{BL}\right)^2 = \left(\frac{R}{BL}\right)^2 + \left(\frac{1}{2}\right)^2 + \left(\frac{R}{BL}\right)\cos\theta \qquad (9a)$$

and

$$\left(\frac{R_1}{BL}\right)^2 = \left(\frac{R}{BL}\right)^2 + \left(\frac{1}{2}\right)^2 - \left(\frac{R}{BL}\right)\cos\theta \qquad (9b)$$

From the Law of Sines, applied also to Figure 2, it follows that

$$\sin\theta_2 = \sin\theta\frac{\left(\frac{R}{BL}\right)}{\left(\frac{R_1}{BL}\right)} \qquad (10a)$$

$$\sin\theta_1 = \sin\theta\frac{\left(\frac{R}{BL}\right)}{\left(\frac{R_2}{BL}\right)} \qquad (10b)$$

and, again from the Law of Sines applied to the same figure

$$\sin(\theta_2 - \theta_1) = \sin(\theta_4 + \theta_5) = \frac{BL}{R_1}\sin\theta_1 = \frac{BL}{R_2}\sin\theta_2 \qquad (11)$$

10

Finally, along with the trigonometric rule

$$\cot x = \frac{\sqrt{1-\sin^2 x}}{\sin x} \tag{12}$$

substitution of (8), (9), and (10) into (7), which is the normalized sensitivity of the range, limits the dependence of variables to R and θ only. Although this expression is not shown explicitly in this form, it is readily evaluated in its implicit form via the substitution procedure.

2. Approximate single baseline analysis (R>>BL)

To appreciate the factors that primarily limit the accuracy in the predicted value for R it can be instructive to consider a simpler formulation of the problem. Consistent with the conditions of assumption 3 the ratio of the range to the baseline can be considered much bigger than one (R/BL>>1). After application of this assumption to (3) the second order terms in BL/2R can be neglected, leading from (4) to

$$R \cong \frac{BL}{2}\left(\frac{\sin\theta_2+\sin\theta_1}{\sin(\theta_2-\theta_1)}\right) = \frac{R_1+R_2}{2} \tag{13}$$

and the normalized variation in range would be

$$\frac{\Delta R}{R} = \left(\frac{\cos\theta_1}{\sin\theta_2+\sin\theta_1} + \cot(\theta_2-\theta_1)\right)(\Delta\theta_1) + \left(\frac{\cos\theta_2}{\sin\theta_2+\sin\theta_1} - \cot(\theta_2-\theta_1)\right)(\Delta\theta_2) \tag{14}$$

11

Equation (6) representing the normalized variation in R can then be expressed

$$\left(\frac{\Delta R}{R}\frac{1}{\Delta\theta}\right) \equiv \left(\frac{\cos\theta_1}{\sin\theta_2+\sin\theta_1} + \cot(\theta_2-\theta_1)\right)\cdot\chi_1 + \left(\frac{\cos\theta_2}{\sin\theta_2+\sin\theta_1} - \cot(\theta_2-\theta_1)\right)\cdot\chi_2\cdot a \tag{15}$$

where again χ_1 and χ_2 are independent random variables having zero mean and unity standard deviation, and "a" is defined by (8). Equation (15) can re-expressed in terms of R and θ after taking into account (9) through (12). Again the details appear in Appendix B.

3. Approximate single baseline analysis (R>>BL, R=R_1=R_2)

From the Law of Sines, Equation (8), it follows that

$$R_1 = \frac{BL}{\sin(\theta_2-\theta_1)}\sin\theta_1 \tag{16a}$$

and

$$R_2 = \frac{BL}{\sin(\theta_2-\theta_1)}\sin\theta_2 \tag{16b}$$

Working with (12), and (13) the reasonable assumption R=R_1 =R_2 can be made and (14) is easily converted into the approximate form

$$\frac{\Delta R}{R} \equiv \left(\frac{1}{2}\cot\theta_1 + \cot(\theta_2-\theta_1)\right)(\Delta\theta_1) + \left(\frac{1}{2}\cot\theta_2 - \cot(\theta_2-\theta_1)\right)(\Delta\theta_2) \tag{17}$$

12

after noting that $R \cong R_1 \cong R_2$ implies

$$\sin \theta_1 \cong \sin \theta_2 \cong \sin \theta \qquad (18)$$

Furthermore from (16)

$$\sin(\theta_2 - \theta_1) = \frac{BL}{R} \sin \theta \qquad (19)$$

and substitution of (18), and (19) into (17) leads to

$$\frac{\Delta R}{R} \cong \left(\frac{1}{2} \frac{\sqrt{1-\sin^2\theta}}{\sin\theta} + \frac{\sqrt{1-\left(\frac{BL}{R}\sin\theta\right)^2}}{\frac{BL}{R}\sin\theta} \right)(\Delta\theta_1) + \left(\frac{1}{2} \frac{\sqrt{1-\sin^2\theta}}{\sin\theta} - \frac{\sqrt{1-\left(\frac{BL}{R}\sin\theta\right)^2}}{\frac{BL}{R}\sin\theta} \right)(\Delta\theta_2) \qquad (20)$$

Using the ratio "a" of $\Delta\theta_2$ and $\Delta\theta_1$ applied to (19), it follows that

$$\left(\frac{\Delta R}{R} \frac{1}{\Delta\theta} \right) = \left(\frac{1}{2} \frac{\sqrt{1-\sin^2\theta}}{\sin\theta} + \frac{\sqrt{1-\left(\frac{BL}{R}\sin\theta\right)^2}}{\frac{BL}{R}\sin\theta} \right) \cdot \chi_1 + \left(\frac{1}{2} \frac{\sqrt{1-\sin^2\theta}}{\sin\theta} - \frac{\sqrt{1-\left(\frac{BL}{R}\sin\theta\right)^2}}{\frac{BL}{R}\sin\theta} \right) \cdot \chi_2 \cdot a \qquad (21)$$

This expression represents the normalized sensitivity in terms of the correct symmetrically defined variables, R and θ.

4. Comparison of single baseline models

In order to continue the triangulation analysis a comparison between the three single baseline models, Equations (7), (15), and (21), has to be made. Due to very complicated expressions that stand for the three models a reasonable comparison of them can

13

complicated expressions that stand for the three models a reasonable comparison of them can be made through graphical representation. In order to compare the three approximate forms for the range sensitivity, the independence of the random variables χ_1 and χ_2 should be considered. Since all three approximate expressions for the range sensitivity are of the form

$$\frac{\Delta R}{R}\frac{1}{\Delta\theta} = (term1) \cdot \chi_1 + (term2) \cdot \chi_2 \tag{22}$$

the natural method of comparison is to take

$$\left| \frac{\Delta R}{R}\frac{1}{\Delta\theta} \right| = \sqrt{(term1)^2 + (term2)^2} \tag{23}$$

or equivalently the coefficients of the sensitivity add in quadrature. This, as suggested in Appendix D, may not be the most conservative estimate for the sensitivity. However for purposes of evaluating the accuracy of the approximate model (21) relative to (7) and (15) it is adequate. The three approximation levels of the range sensitivity expressed in Equations (7), (15), and (21) are compared in the Figures 3, 4, and 5 for three values of the range to baseline ratio, and for ratio of bearing errors 0, 1 and 2.

5. Observations

Scrutinization of Figures 3, 4, and 5 indicates only small discrepancies between the approximate solutions. It is concluded that the approximations of Equation (21),

14

characteristic of all the single baseline figures are worth noting. First the range sensitivity is highest for angles close to $0°$ and $180°$. This is the well known "geometric dilution" [Ref. 14] that is characteristic of all the single baseline methods. In terms of measurements a high normalized sensitivity would result in a high level of inaccuracy. This provides the motivation for exploring the dual baseline method which is the focus of the later chapters. Because the range sensitivity normalization is done with the respect to $\Delta\theta_1$ the effect of increasing "a" is to amplify the term proportional to $\Delta\theta_2$. Therefore, as seen from the figures, there is an overall increase in the normalized range sensitivity. Lastly, the farther the triangulated target is from the baseline the more inaccurate the measurement. This is also confirmed by the increase in the normalized range sensitivity of Figures 5a, 5b, and 5c over the respective counterparts of Figures 3, and 4.
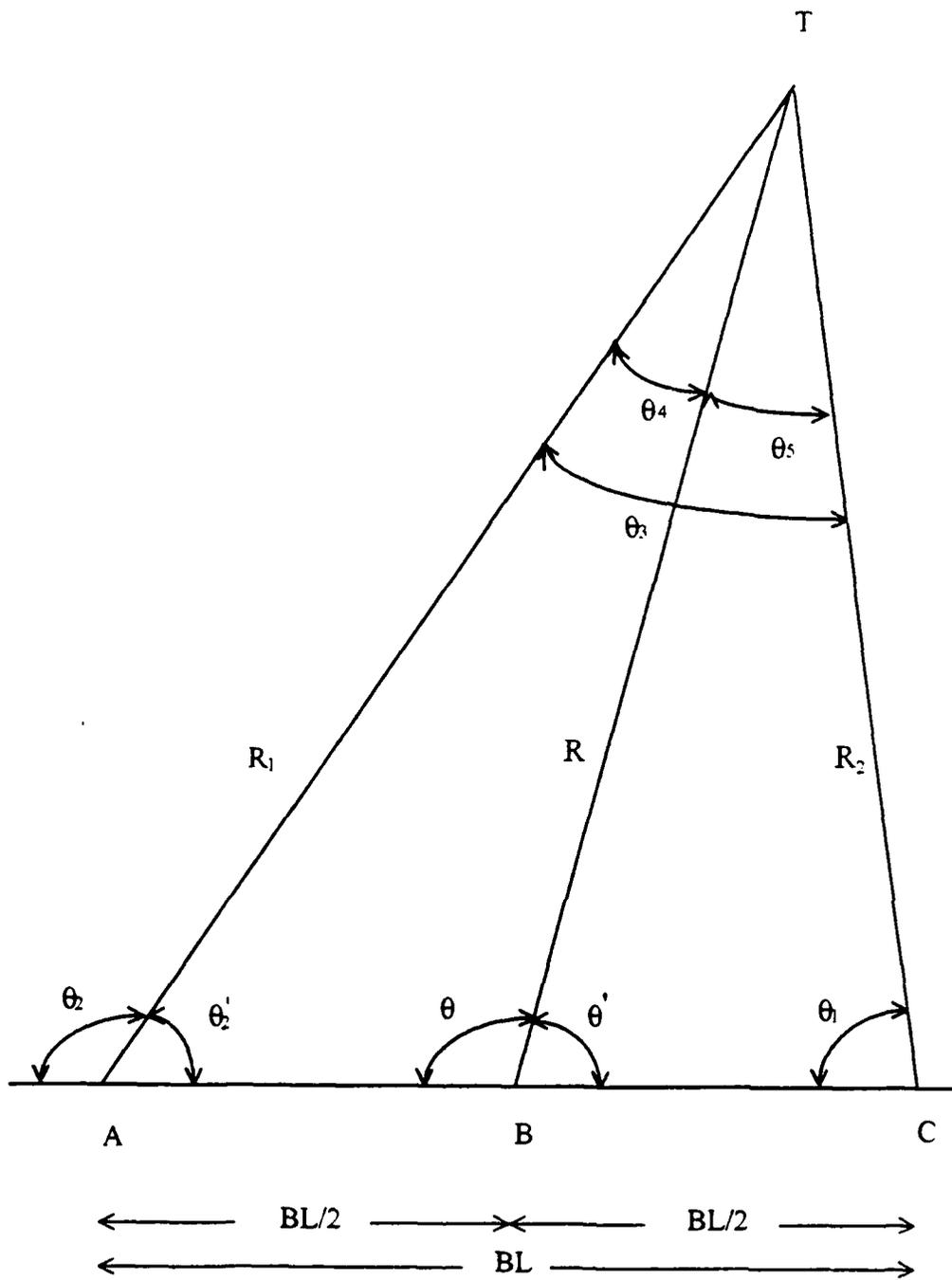
Figure 2: Geometry for the single baseline model

16
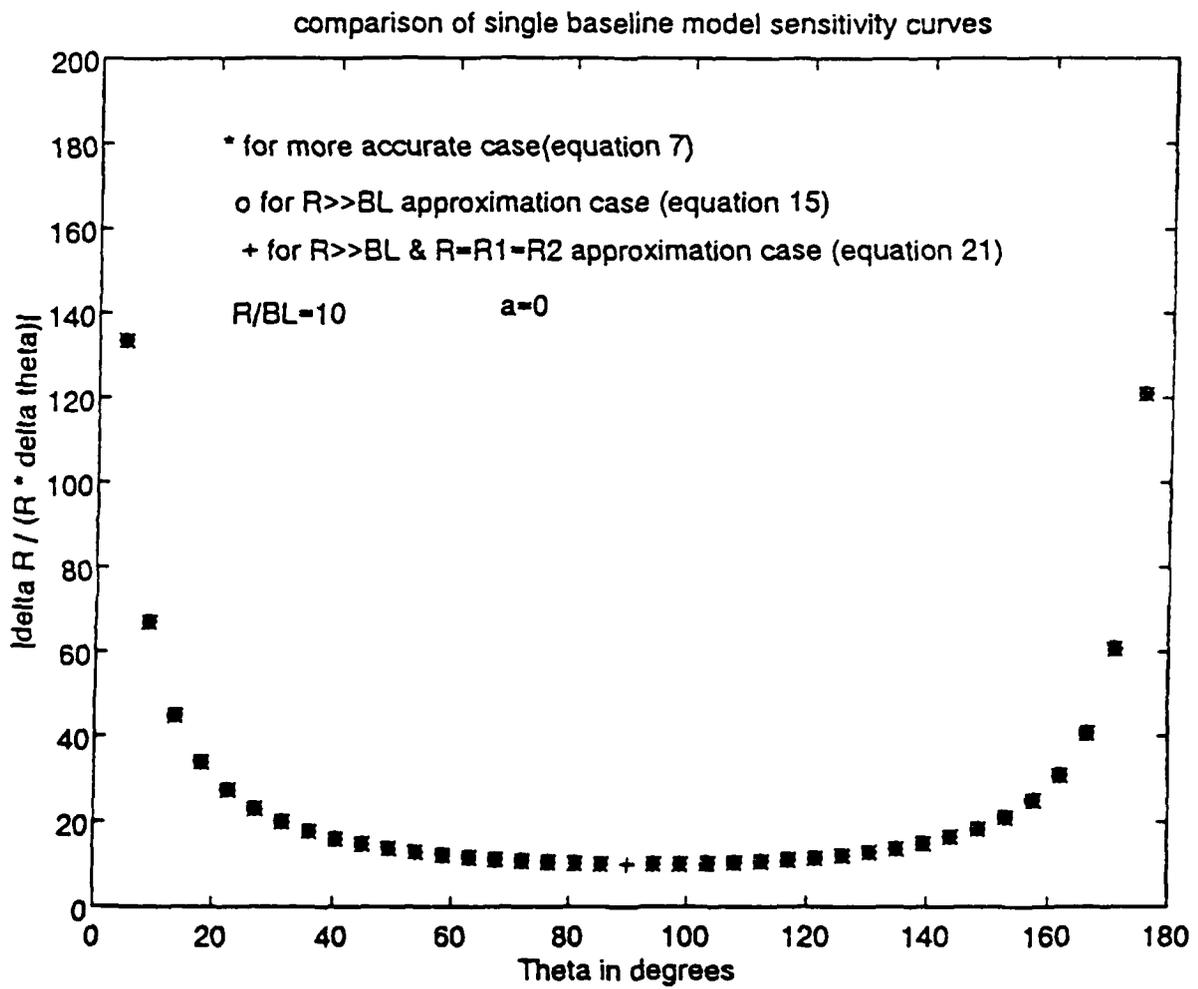
Figure 3a: Single baseline model sensitivity curves for R/BL=10 & *a*=0
(via program in Appendix E. A)

17

comparison of single baseline sensitivity curves

* for more accurate case(equation 7)

o for R>>BL approximation case (equation 15)

+ for R>>BL & R=R1=R2 approximation case (equation 21)

R/BL=10   a=1

|delta R / (R * delta theta)|

Theta in degrees
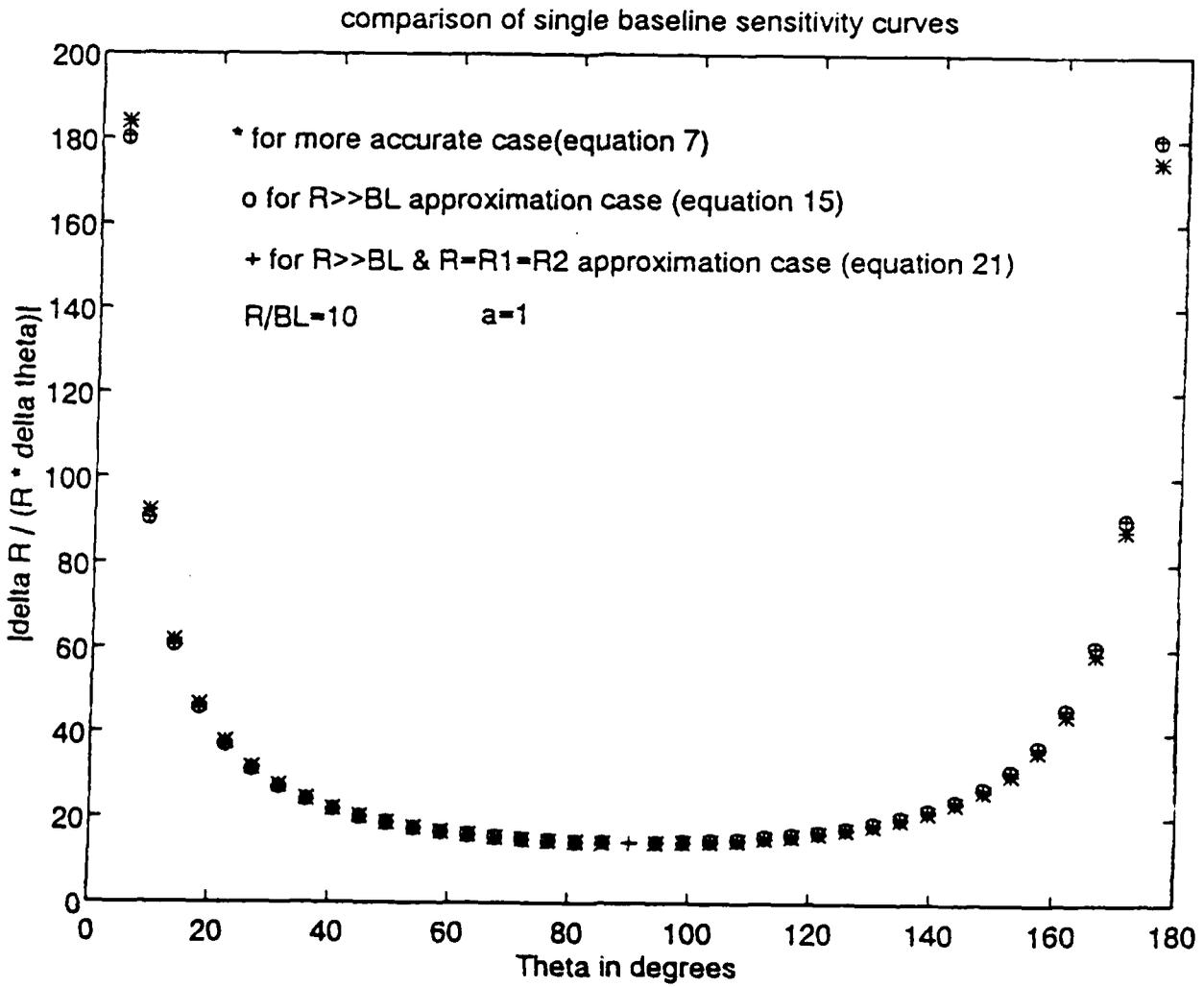
Figure 3b : Single baseline model sensitivity curves for R/BL=10 & a=1
(via program in Appendix E. A)

18

comparison of single baseline model sensitivity curves

* for more accurate case(equation 7)

o for R>>BL approximation case (equation 15)

+ for R>>BL & R=R1=R2 approximation case (equation 21)

R/BL=10   a=2
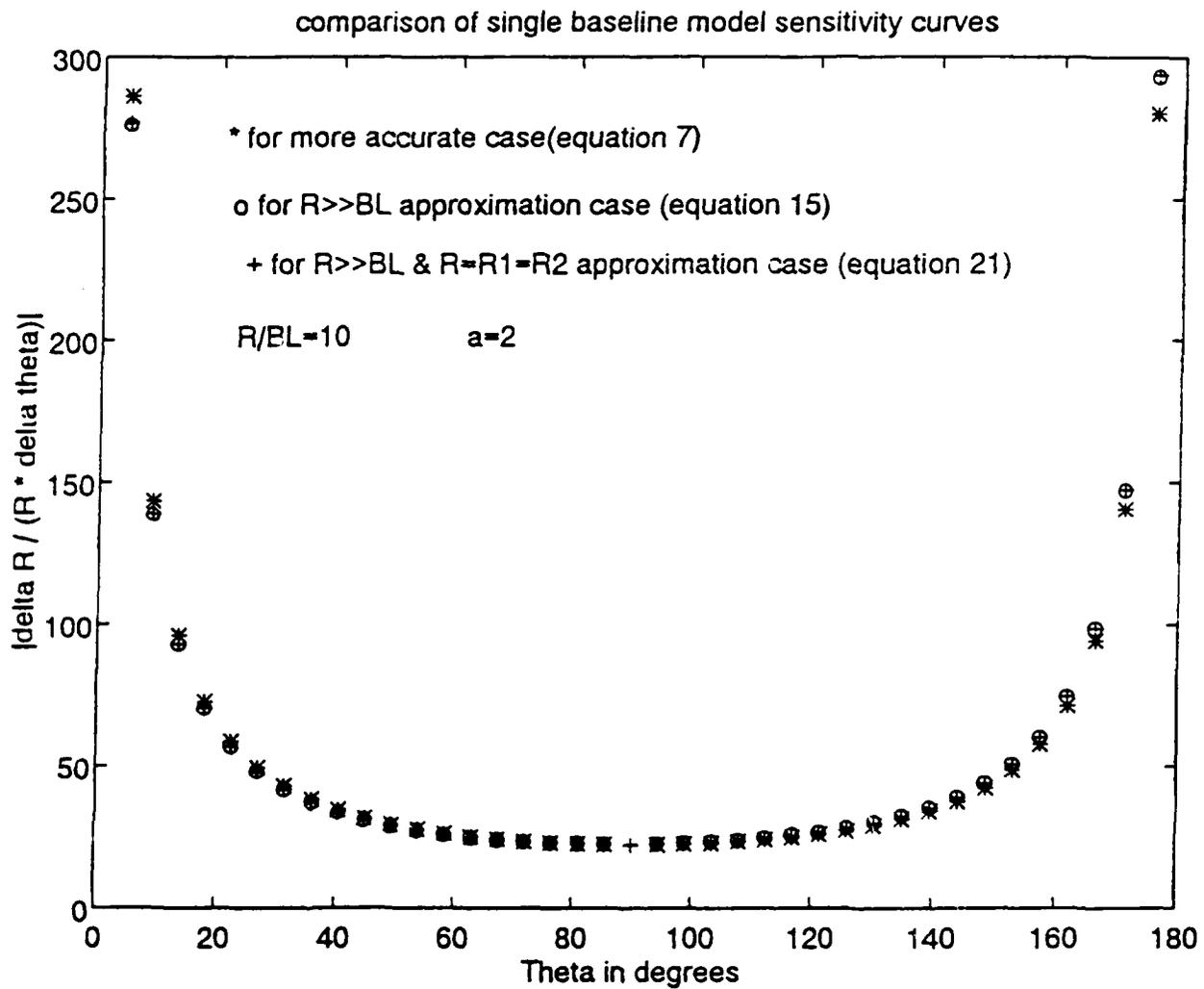
Figure 3c   Single baseline model sensitivity curves for R/BL=10 & a=2
(via program in Appendix E. A)

19

comparison of single baseline model sensitivity curves
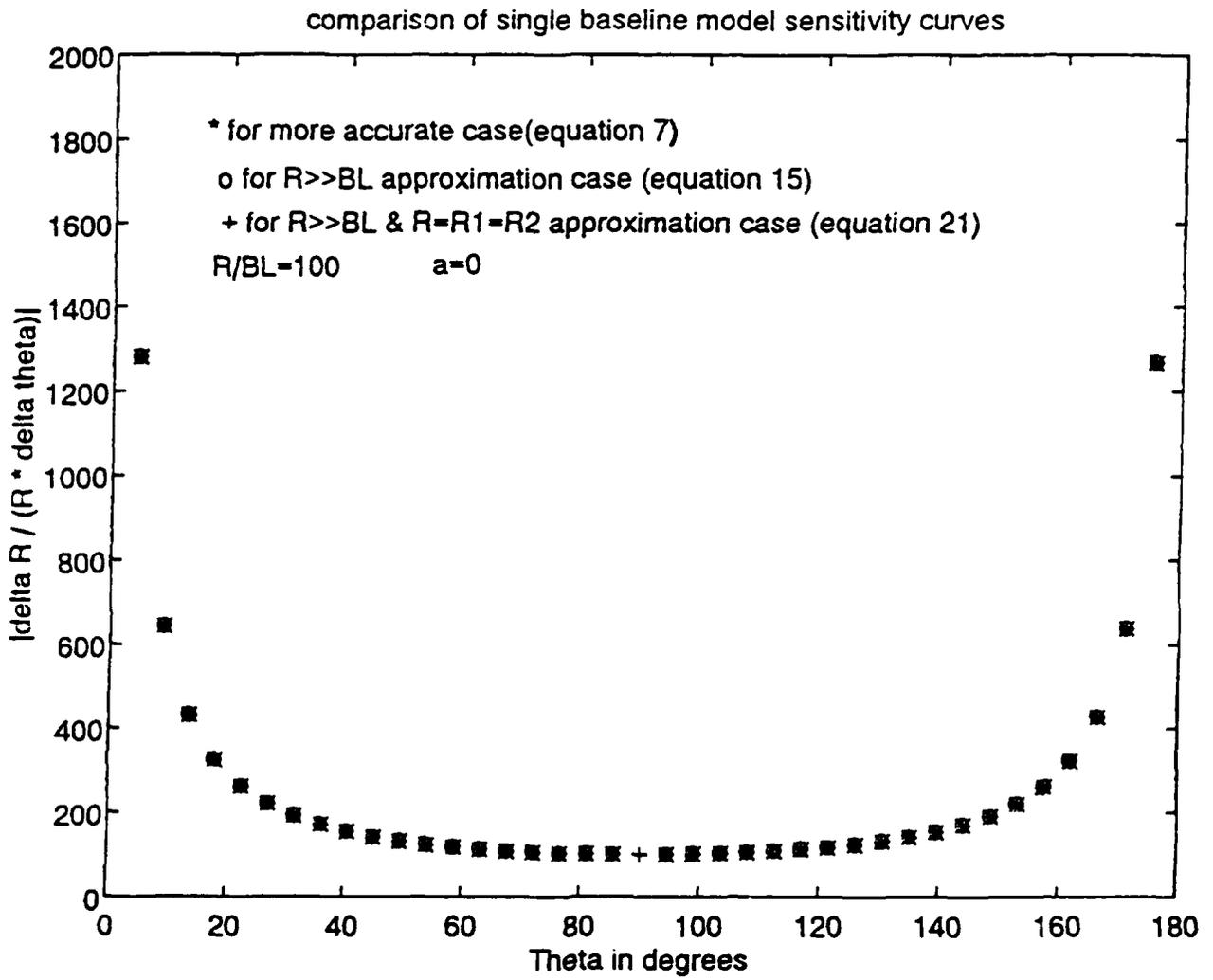
Figure 4a : Single baseline model sensitivity curves for R/BL=100 & σ=0
(via program in Appendix E. A)

comparison of single baseline model sensitivity curves

* for more accurate case(equation 7)

o for R>>BL approximation case (equation 15)

+ for R>>BL & R=R1=R2 approximation case (equation 21)

R/BL=100   a=1

x-axis: Theta in degrees

y-axis: |delta R / (R * delta theta)|
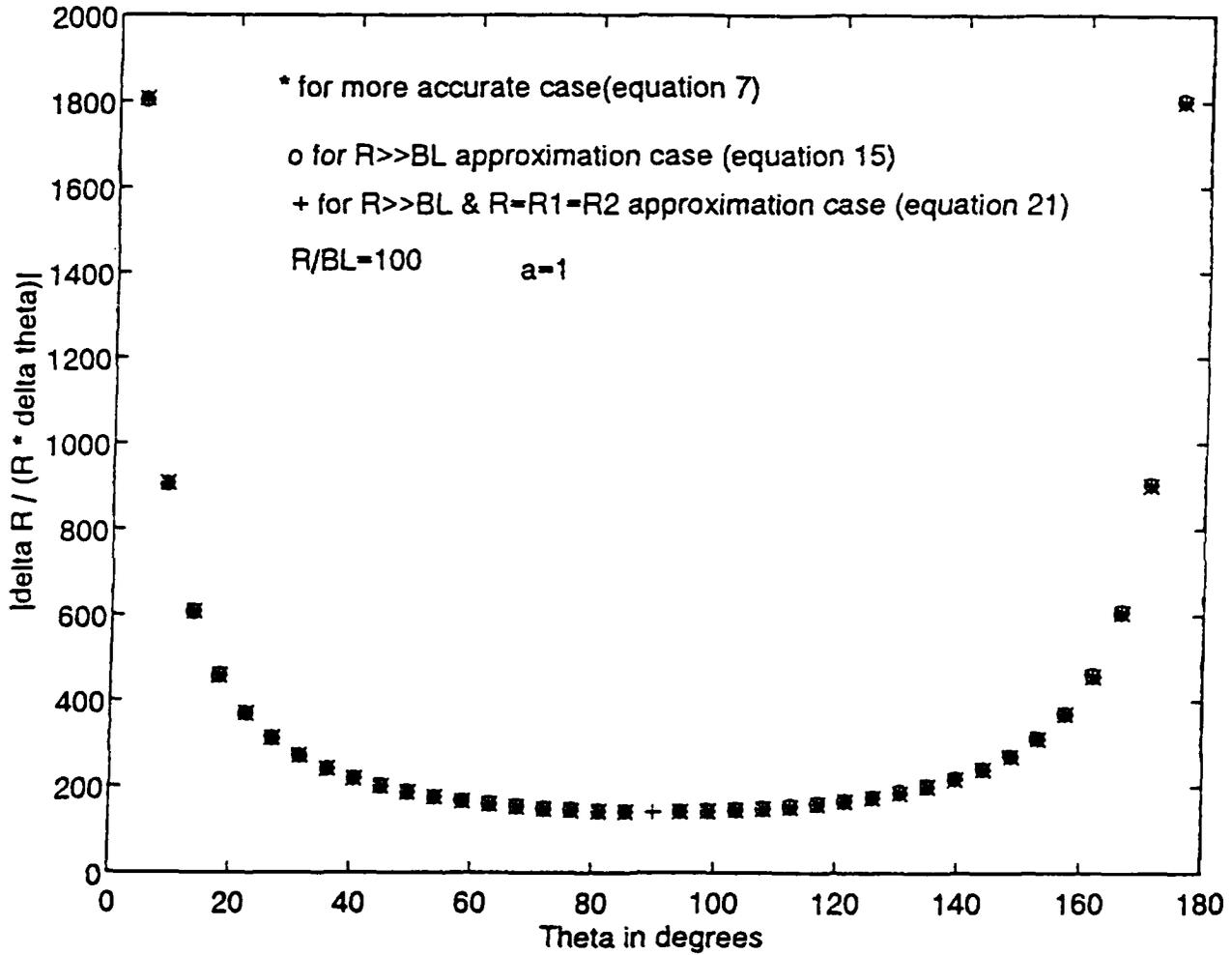
Figure 4b   Single baseline model sensitivity curves for R/BL=100 & a=1
(via program in Appendix E. A)

comparison of single baseline model sensitivity curves

* for more accurate case(equation 7)

o for R>>BL approximation case (equation 15)

+ for R>>BL & R=R1=R2 approximation case (equation 21)
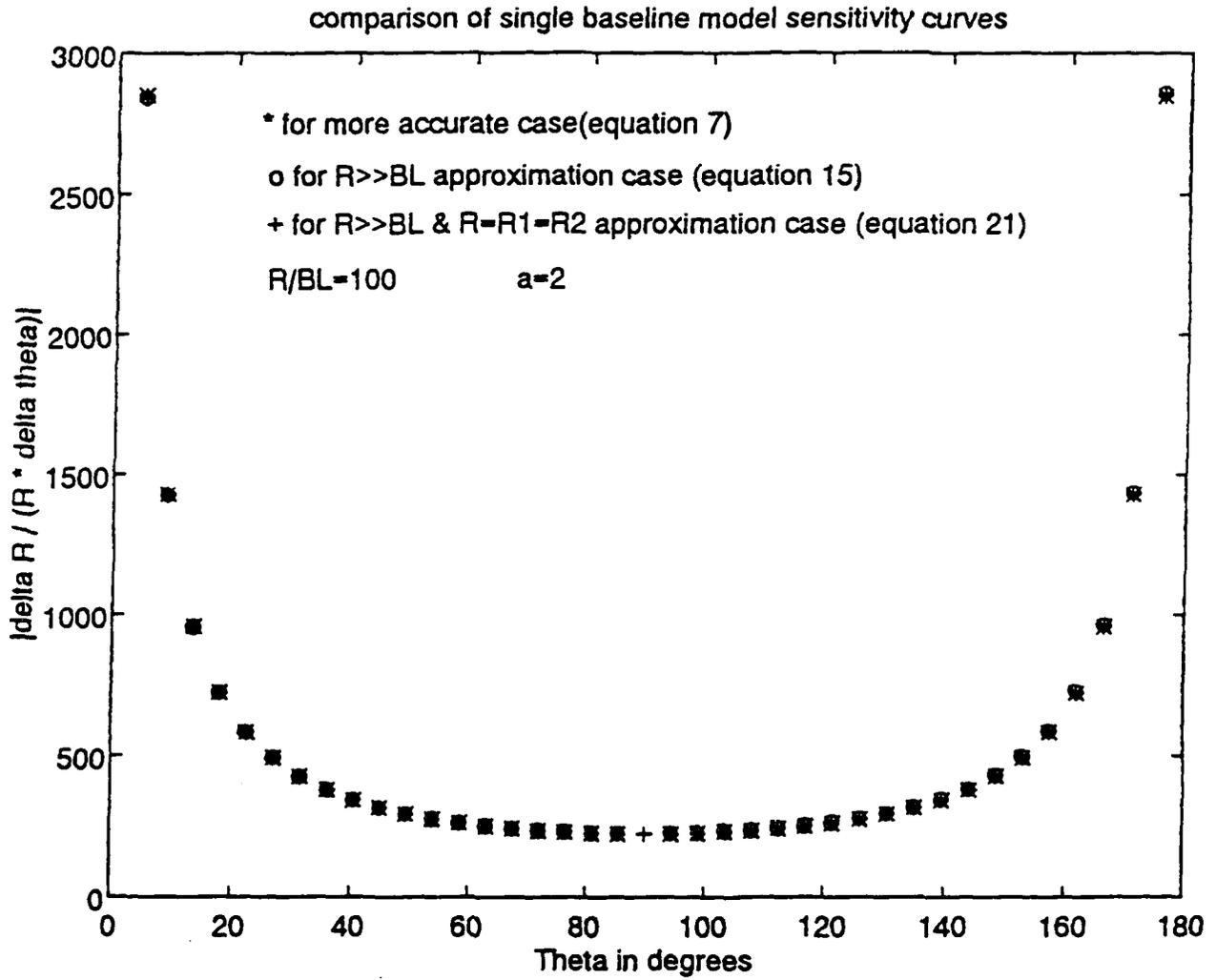
R/BL=100   a=2

Figure 4c : Single baseline model sensitivity curves for R/BL=100 & a=2
(via program in Appendix E. A)

22
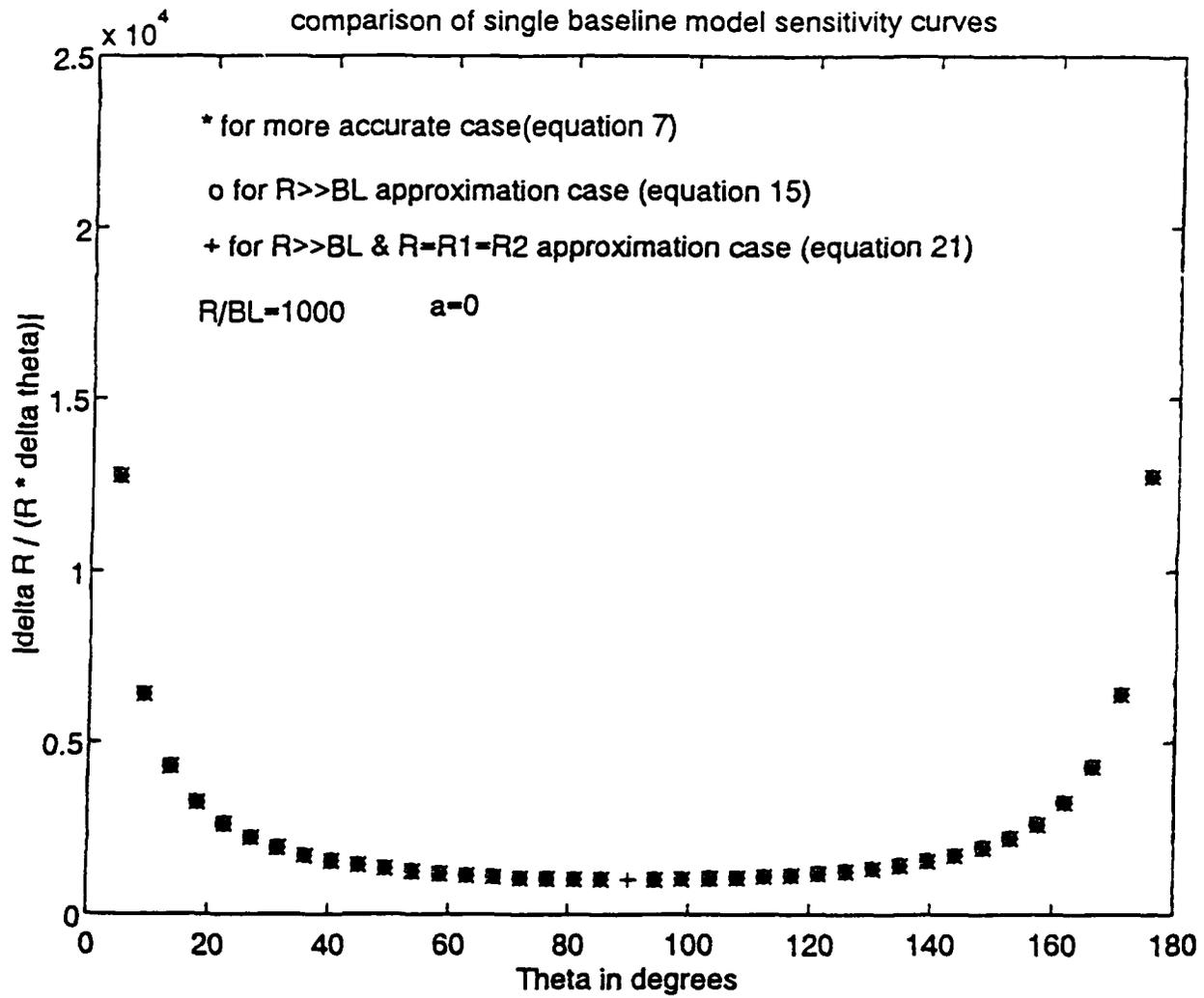
Figure 5a : Single baseline model sensitivity curves for R/BL=1000 & α=0
(via program in Appendix E. A)
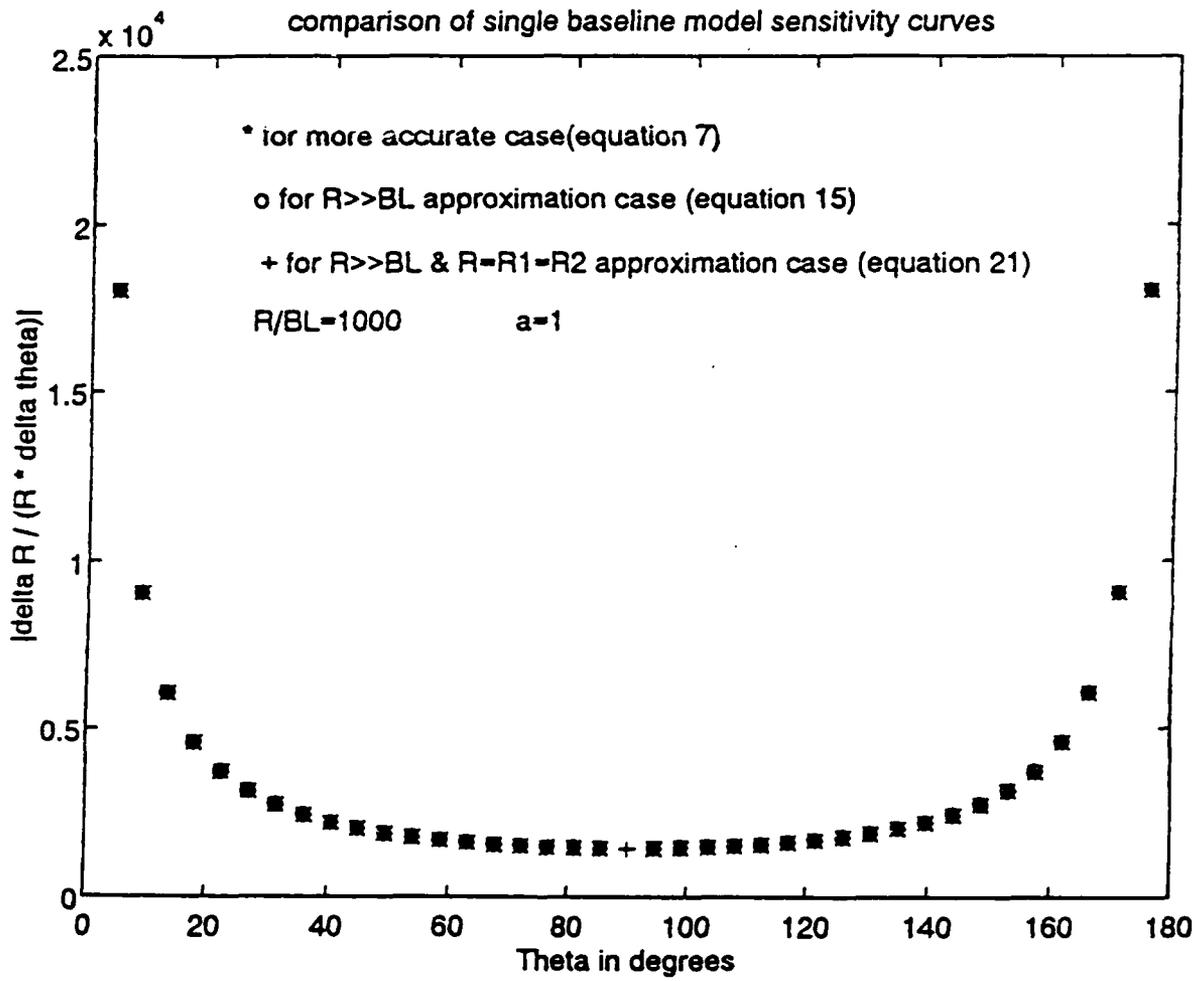
Figure 5b : Single baseline model sensitivity curves for R/BL=1000 & *a*=1
(via program in Appendix E. A)
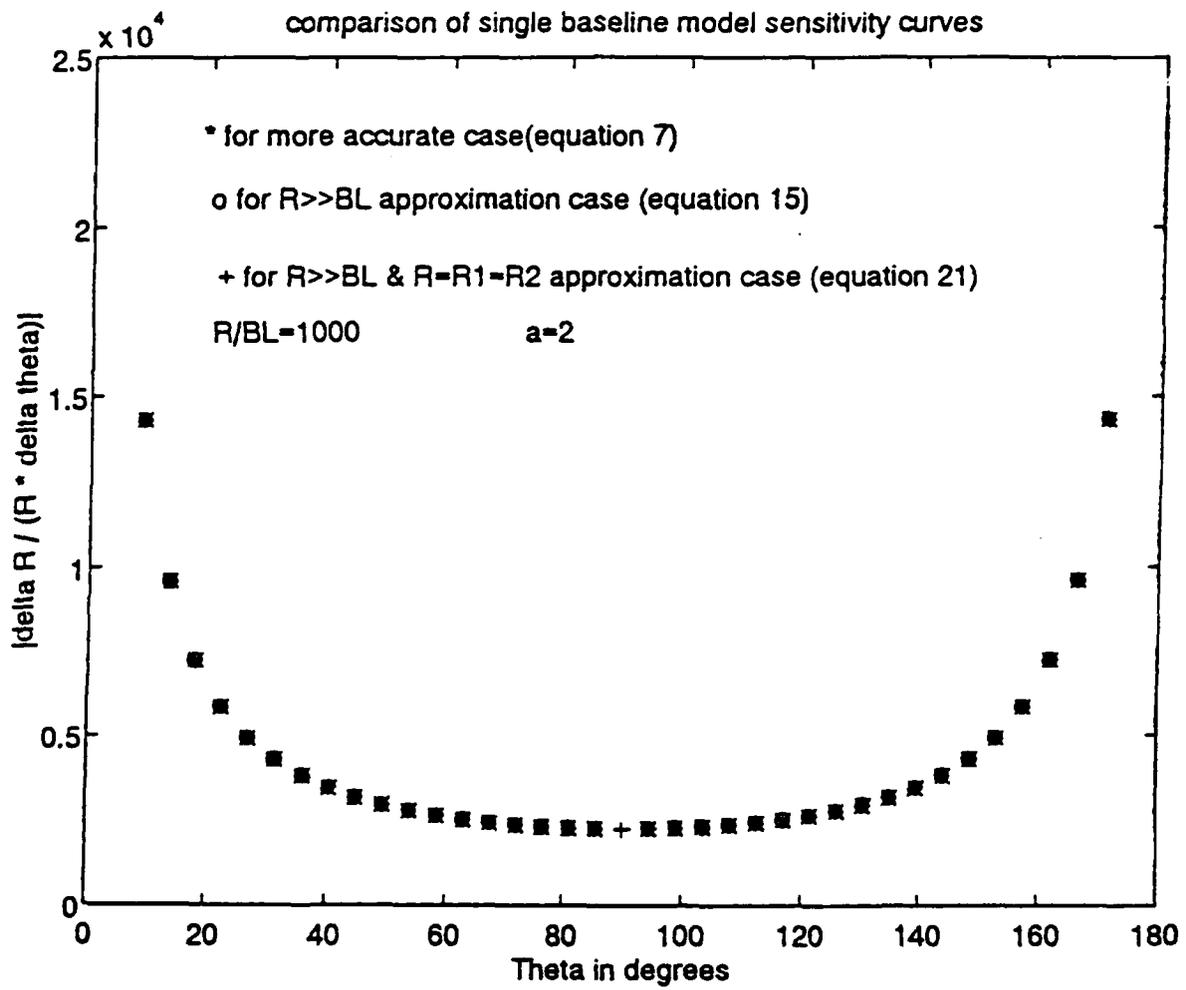
Figure 5c : Single baseline model sensitivity curves for R/BL=1000 & a=2
(via program in Appendix E. A)

25

III. DUAL BASELINE MODEL

A. DUAL BASELINE MODEL ANALYSIS

Figure 6 shows a dual baseline model. The two baselines of the model are taken to be orthogonal and they are referred to as the long base line (LBL) and the short baseline (SBL) system. The features and the relations of the single baseline model analysis are applicable here but the superscripts S and L will be used to distinguish the two systems. Furthermore, some new relations between the angles are needed, in order to express the short baseline (SBL) model in terms of the same variables R and θ, as in the long baseline (LBL) model.

B. GENERAL CONSIDERATIONS

From the Figure 6 it is clear that

$$\cos\theta^S = \cos(\theta - 90°) = \sin\theta \tag{24}$$

similarly

$$\sin\theta^S = -\cos\theta \tag{25}$$

Therefore from Equations (9), (24), and (25)

$$\left(\frac{R_2^L}{LBL}\right)^2 = \left(\frac{R}{LBL}\right)^2 + \left(\frac{1}{2}\right) + \left(\frac{R}{LBL}\right)\cos\theta \tag{26a}$$

$$\left(\frac{R_1^L}{LBL}\right)^2 = \left(\frac{R}{LBL}\right)^2 + \left(\frac{1}{2}\right)^2 - \left(\frac{R}{LBL}\right)\cos\theta \qquad (26b)$$

$$\left(\frac{R_2^S}{SBL}\right)^2 = \left(\frac{R}{SBL}\right)^2 + \left(\frac{1}{2}\right)^2 + \left(\frac{R}{SBL}\right)\sin\theta \qquad (26c)$$

$$\left(\frac{R_1^S}{SBL}\right)^2 = \left(\frac{R}{SBL}\right)^2 + \left(\frac{1}{2}\right)^2 - \left(\frac{R}{SBL}\right)\sin\theta \qquad (26d)$$

Similarly, from Equations (10), (24), and (25) it follows that

$$\sin\theta_1^L = \sin\theta\frac{\left(\frac{R}{LBL}\right)}{\left(\frac{R_2^L}{LBL}\right)} \qquad \sin\theta_2^L = \sin\theta\frac{\left(\frac{R}{LBL}\right)}{\left(\frac{R_1^L}{LBL}\right)} \qquad (27a, b)$$

$$\sin\theta_1^S = -\cos\theta\frac{\left(\frac{R}{SBL}\right)}{\left(\frac{R_2^S}{SBL}\right)} \qquad \sin\theta_2^S = -\cos\theta\frac{\left(\frac{R}{SBL}\right)}{\left(\frac{R_1^S}{SBL}\right)} \qquad (27c, d)$$

and from Equations (11), (24), and (25)

$$\sin\left(\theta_2^L - \theta_1^L\right) = \frac{LBL}{R_1^L}\sin\theta_1^L = \frac{LBL}{R_2^L}\sin\theta_2^L \qquad (28a)$$

$$\sin\left(\theta_2^S - \theta_1^S\right) = \frac{SBL}{R_1^S}\sin\theta_1^s = \frac{SBL}{R_2^S}\sin\theta_2^S \qquad (28b)$$

27

For computation of $\left(\frac{\Delta R}{R}\frac{1}{\Delta\theta}\right)^L$ let

$$\left(\frac{R_1}{BL}\right)\to\left(\frac{R_1^L}{LBL}\right)\qquad\left(\frac{R_2}{BL}\right)\to\left(\frac{R_2^L}{LBL}\right)\qquad\theta_1\to\theta_1^L\qquad\theta_2\to\theta_2^L\qquad\text{(29a, b, c, d)}$$

and follow substitution (26a, b) and (27a, b). For computation of $\left(\frac{\Delta R}{R}\frac{1}{\Delta\theta}\right)^S$ let

$$\left(\frac{R_1}{BL}\right)\to\left(\frac{R_1^S}{SBL}\right)\qquad\left(\frac{R_2}{BL}\right)\to\left(\frac{R_2^S}{SBL}\right)\qquad\theta_1\to\theta_1^S\qquad\theta_2\to\theta_2^S\qquad\text{(30a, b, c, d)}$$

and follow substitutions (26c, d) and (27c, d). In Appendix B expressions for $\left(\frac{\Delta R}{R}\frac{1}{\Delta\theta}\right)^L$

and $\left(\frac{\Delta R}{R}\frac{1}{\Delta\theta}\right)^S$ are shown for the various levels of approximation introduced in the previous single baseline description. As noted in this chapter the approximations R>>BL, and $R_1=R_2=R$ are quite good, and the dual baseline results (see (21)) for this case are provided here for later reference

$$\left(\frac{\Delta R}{R}\frac{1}{\Delta\theta}\right)^L=\left(\frac{1}{2}\frac{\sqrt{1-\sin^2\theta}}{\sin\theta}+\frac{\sqrt{1-\left(\frac{LBL}{R}\sin\theta\right)^2}}{\left(\frac{LBL}{R}\sin\theta\right)}\right)\cdot\chi_1^L+\left(\frac{1}{2}\frac{\sqrt{1-\sin^2\theta}}{\sin\theta}-\frac{\sqrt{1-\left(\frac{LBL}{R}\sin\theta\right)^2}}{\left(\frac{LBL}{R}\sin\theta\right)}\right)\cdot\chi_2^L\cdot a^L\ (31a)$$

$$\left(\frac{\Delta R}{R}\frac{1}{\Delta\theta}\right)^S=\left(\frac{1}{2}\frac{\sqrt{1-\cos^2\theta}}{(-\cos\theta)}+\frac{\sqrt{1-\left(\frac{SBL}{R}\cos\theta\right)^2}}{\left(\frac{SBL}{R}(-\cos\theta)\right)}\right)\cdot\chi_1^S+\left(\frac{1}{2}\frac{\sqrt{1-\cos^2\theta}}{(-\cos\theta)}-\frac{\sqrt{1-\left(\frac{SBL}{R}\cos\theta\right)^2}}{\left(\frac{SBL}{R}(-\cos\theta)\right)}\right)\cdot\chi_2^S\cdot a^S(31b)$$

28

where χ_1^L, χ_2^L, χ_1^S, χ_2^S are independent random variables having zero mean and unity standard deviation, and

$$\alpha^L = \frac{\sqrt{\langle(\theta_2^L)^2\rangle}}{\sqrt{\langle(\theta_1^L)^2\rangle}} \qquad\qquad \alpha^S = \frac{\sqrt{\langle(\theta_2^S)^2\rangle}}{\sqrt{\langle(\theta_1^S)^2\rangle}} \qquad (32a, b)$$

C. SENSITIVITY CURVES FOR THE DUAL BASELINE SCHEME

The expressions $\left(\frac{\Delta R}{R}\frac{1}{\Delta\theta}\right)^L$, and $\left(\frac{\Delta R}{R}\frac{1}{\Delta\theta}\right)^S$ in (31) represent the normalized sensitivity for the long and the short baseline system respectively, in terms of the symmetrical dependent variables, R and θ. It is obvious from (31) that the sensitivities of both long and short baseline systems depend heavily on the terms (R/LBL), (R/SBL), $\Delta\theta_1^L$, $\Delta\theta_2^L$, $\Delta\theta_1^S$, and $\Delta\theta_2^S$. To illustrate the dependence of the sensitivities to the above mentioned terms some examples will be introduced with the use of (31) which, after (23), becomes

$$\left(\frac{\Delta R}{R}\frac{1}{\Delta\theta}\right)^L = \sqrt{\left(\frac{1}{2}\frac{\sqrt{1-\sin^2\theta}}{\sin\theta}+\frac{\sqrt{1-\left(\frac{LBL}{R}\sin\theta\right)^2}}{\left(\frac{LBL}{R}\sin\theta\right)}\right)^2 + \left[\left(\frac{1}{2}\frac{\sqrt{1-\sin^2\theta}}{\sin\theta}-\frac{\sqrt{1-\left(\frac{LBL}{R}\sin\theta\right)^2}}{\left(\frac{LBL}{R}\sin\theta\right)}\right)\cdot\alpha^L\right]^2} \quad (33a)$$

$$\left(\frac{\Delta R}{R}\frac{1}{\Delta\theta}\right)^S = \sqrt{\left(\frac{1}{2}\frac{\sqrt{1-\cos^2\theta}}{(-\cos\theta)}+\frac{\sqrt{1-\left(\frac{SBL}{R}\cos\theta\right)^2}}{\left(\frac{SBL}{R}(-\cos\theta)\right)}\right)^2 + \left[\left(\frac{1}{2}\frac{\sqrt{1-\cos^2\theta}}{(-\cos\theta)}-\frac{\sqrt{1-\left(\frac{SBL}{R}\cos\theta\right)^2}}{\left(\frac{SBL}{R}(-\cos\theta)\right)}\right)\cdot\alpha^S\right]^2} \quad (33b)$$

29

where as previously described the terms are added in quadrature. However geometrical considerations, described in Appendix D, suggest that a more conservative gauge for range sensitivity is based on addition of absolutes

$$\left| \frac{\Delta R}{R} \frac{1}{\Delta\theta} \right| = |(term1)| + |(term2)| \tag{34}$$

under this assumption Equation (31) would be evaluated according to

$$\left| \left(\frac{\Delta R}{R} \frac{1}{\Delta\theta} \right)^{L} \right| = \left| \frac{1}{2} \frac{\sqrt{1-\sin^2\theta}}{\sin\theta} + \frac{\sqrt{1-\left(\frac{LBL}{R}\sin\theta\right)^2}}{\left(\frac{LBL}{R}\sin\theta\right)} \right| + \left| \left(\frac{1}{2} \frac{\sqrt{1-\sin^2\theta}}{\sin\theta} - \frac{\sqrt{1-\left(\frac{LBL}{R}\sin\theta\right)^2}}{\left(\frac{LBL}{R}\sin\theta\right)} \right) \cdot a^{L} \right| \tag{35a}$$

$$\left| \left(\frac{\Delta R}{R} \frac{1}{\Delta\theta} \right)^{S} \right| = \left| \frac{1}{2} \frac{\sqrt{1-\cos^2\theta}}{(-\cos\theta)} + \frac{\sqrt{1-\left(\frac{SBL}{R}\cos\theta\right)^2}}{\left(\frac{SBL}{R}(-\cos\theta)\right)} \right| + \left| \left(\frac{1}{2} \frac{\sqrt{1-\cos^2\theta}}{(-\cos\theta)} - \frac{\sqrt{1-\left(\frac{SBL}{R}\cos\theta\right)^2}}{\left(\frac{SBL}{R}(-\cos\theta)\right)} \right) \cdot a^{S} \right| \tag{35b}$$

It can be seen from Appendix D that for the discussion given, (35) for $a^{L} = a^{S} = 1$ is nominally more conservative than (33). Furthermore for $a^{L} = a^{S} = 0$, Equation (33) and Equation (35) are equivalent.

D. EXAMPLES

The examples discussed in this chapter will be based on the sensitivity expression using quadrature addition, Equation (33). The concepts applied are equally applicable to the

more conservative equation (35). MATLAB programs for evaluating (33) are provided in Appendix E. As a first example take

$$\frac{R}{LBL} = 100 \qquad\qquad \frac{R}{SBL} = 600 \qquad\qquad\qquad \text{(36a, b)}$$

$$a^L = 2 \qquad\qquad a^S = 1 \qquad\qquad\qquad \text{(36c, d)}$$

After substitution of the data into (33) and plotting it the results are shown on Figure 7. As a second example take

$$\frac{R}{LBL} = 1000 \qquad\qquad \frac{R}{SBL} = 5000 \qquad\qquad\qquad \text{(37a, b)}$$

$$a^L = 1 \qquad\qquad a^S = 1 \qquad\qquad\qquad \text{(37c, d)}$$

The plots following substitution of (36), and (37) into (33) are shown in Figure 8. In both Figures 7 and 8 the performance of the short baseline system will exceed that of the long baseline for angles close to 0° and 180°. For Figures 7 and 8 those crossing points are approximately +17° and +15°, respectively. To appreciate the utility of the analysis take a simple example (i.e., that one sensor on each baseline has no bearing error, while the bearing errors of the remaining sensors are equal). Then the situation can be described as follows:

$$\Delta\theta_1^L = \Delta\theta_1^S = \Delta\theta \qquad\qquad\qquad \text{(38a)}$$

$$\Delta\theta_2^L = \Delta\theta_2^S = 0 \qquad (38b)$$

thus, the long and the short parts of (33) after setting $a^L = a^S = 0$ become

$$\left(\frac{\Delta R}{R}\frac{1}{\Delta\theta}\right)^L = \frac{1}{2}\frac{\sqrt{1-\sin^2\theta}}{\sin\theta} + \frac{\sqrt{1-\left(\frac{LBL}{R}\sin\theta\right)^2}}{\frac{LBL}{R}\sin\theta} \qquad (39a)$$

$$\left(\frac{\Delta R}{R}\frac{1}{\Delta\theta}\right)^S = \frac{1}{2}\frac{\sqrt{1-\cos^2\theta}}{\cos\theta} + \frac{\sqrt{1-\left(\frac{SBL}{R}\cos\theta\right)^2}}{\frac{SBL}{R}\cos\theta} \qquad (39b)$$

which permit the plotting of the sensitivities versus θ. This was done for the conditions

$$\frac{R}{LBL} = 1000 \qquad \text{and} \qquad \frac{R}{SBL} = 5000 \qquad (40a, b)$$

and the results are represented on Figure 9. Note, as expected, the LBL does better over a wider range of angles. Around $\theta=170°$ and $\theta=10°$ there is a crossover point for which the short baseline system would produce more accurate range measurements at angles $\theta<10°$ and $\theta>170°$. For illustration of the use of the curves assume that the bearing resolution is $\Delta\theta_1^L = \Delta\theta_2^S = \Delta\theta = 0.1$ mr and the range to the target is 20 Km. Note according to (39) this implies long and short baselines of 20 m and 4 m, respectively. For $\theta=90°$, the LBL best case, the uncertainty in the long baseline range measurement from (39a) is

$$\Delta R_{meas}^L = R \cdot \Delta\theta \cdot \tan\psi^L \qquad (41)$$

32

where ΔR^L is the uncertainty in the long baseline range, and

$$\psi^L = a\tan\left(\sqrt{\left(\frac{R}{LBL}\right)^2 - 1}\right) \qquad (42)$$

Then, the range measured by the long baseline will be

$$R^L_{meas} = R \pm \Delta R^L_{meas} \qquad (43a)$$

$$R^L_{meas} = 20\ Km \pm 2.0\ Km \quad (LBL) \qquad (43b)$$

For $\theta=0°$ (or $180°$), the SBL best case, the uncertainty in the short baseline range measurement from equation (39b) is

$$\Delta R^S_{meas} = R \cdot \Delta\theta \cdot \tan\psi^S \qquad (44)$$

where ΔR^S is the uncertainty in the short baseline range, and

$$\psi^S = a\tan\left(\sqrt{\left(\frac{R}{SBL}\right)^2 - 1}\right) \qquad (45)$$

Thus, the range measured by the short baseline will be

$$R^S_{meas} = R \pm \Delta R^S_{meas} \qquad (46a)$$

$$R^S_{meas} = 20\ Km \pm 10\ Km \quad (SBL) \qquad (46b)$$

33

Although the inaccuracy in the measured value for R may be tolerable in the LBL case, the

SBL range estimate is probably not acceptable. Figure 9 shows what happens to the nor-

malized range sensitivity versus θ for fixed range. For the dual baseline scheme the meas-

urement accuracy is at a minimum at the crossover points. For the conditions taken this

occurs at θ=+10° and θ=+170°.

E.   RANGE LIMITATIONS FOR FIXED TARGET ORIENTATION

Range sensitivity curves plotted versus range for the principal directions θ = 0° and θ

= 90° could be applied to predict maximum bearing error and/or minimum baselines in or-

der to accurately triangulate targets at desired distance limits. Under the assumptions in-

troduced by (38) the normalized range sensitivities are given in (39), which for the single

baseline model becomes

$$\left(\frac{\Delta R}{R}\frac{1}{\Delta\theta}\right) = \frac{1}{2}\frac{\sqrt{1-\sin^2(\theta)}}{\sin(\theta)} + \frac{\sqrt{1-\left(\frac{BL}{R}\sin(\theta)\right)^2}}{\left(\frac{BL}{R}\sin(\theta)\right)} \qquad (47)$$

Equation (47) is plotted with R/BL=100 to R/BL=1000, and for angle θ=90°, 45°,and 22.5°

on Figure 10. In order to clarify the application of Figure 10 to dual baseline triangulation,

an example is presented based on the following conditions

$$LBL=20.0 \; m \qquad SBL=4.0 \; m \qquad \text{(48a, b)}$$

$$\theta=90° \qquad \Delta\theta=0.1 \; mr \qquad \text{(48c, d)}$$

and precision in range $< 5\%$, that means

$$\frac{\Delta R}{R} \leq 0.05 \qquad (48e)$$

From (48d), and (48e) the range sensitivity is evaluated as

$$\left(\frac{\Delta R}{R}\frac{1}{\Delta\theta}\right) \leq 500 \qquad (49)$$

and therefore from Figure 10 the range to baseline ratio is found to be

$$\frac{R}{BL} \leq 550 \qquad (50)$$

This condition is applicable to both the long and short baseline. In both cases the 90" condition (48c) imposes the interpretation that the target appears along a line which is perpendicular to the baseline.

For the LBL case it follows from Equation (48a) that

$$R_{LBL} \leq 550 \times 20\,m = 11\,km \qquad (51a)$$

and similarly for the SBL case

$$R_{SBL} \leq 550 \times 4.0\,m = 2.2\,km \qquad (51b)$$

35

This demonstrates that the target must be significantly closer to be triangulated with 5% accuracy if the oncoming direction is perpendicular to the short baseline. Nonetheless, as previously mentioned, the closest unresolved range will occur for the previously noted crossover angle. To demonstrate the relevance of this issue, Figure 11 shows the plot of (47) for the angles $\theta=90°$, $\theta=80°$, and $\theta=10°$. The angle $10°$ was chosen because it represents the approximate crossover point for the conditions (38). After referring to Figure 11 it is seen that the performance for the $\theta=10°$ case is about six times worse than the $\theta=90°$ case. Using the LBL baseline (51a) the range detected by the long baseline would be approximately

$$R \leq 1.8\,km \ (@ \ 10°) \tag{52}$$

which is, as expected, worse than either of the baseline performances (51). It should be noted that for a crossover point the long base line and short baseline performances are the same. This can be checked by using the $\theta=80°$ curve with the SBL data.

F. COMMENTS ON THE EXAMPLES AND ANALYSIS

The primary objective of the preceding examples and discussion has been to demonstrate a feasible modeling scheme for dual baseline triangulation. The results of this chapter demonstrate several features of the dual baseline scheme. The problem of "geometrical dilution" discussed in Chapter I can be avoided by using two orthogonal baselines. In general the larger baseline will have a higher measurement accuracy. Because of typical ship structure it is assumed that a second baseline would not be conveniently as long. The

36

scheme would require some "smart electronics" which would switch between baselines at a performance crossover point. As seen from the discussion in section D the maximum triangulation range, for a fixed range sensitivity, can be predicted for particular target orientations, i.e., fixed θ. In the chapter to follow this concept is extended by solving for R_{max} versus θ under conditions of constant range sensitivity.
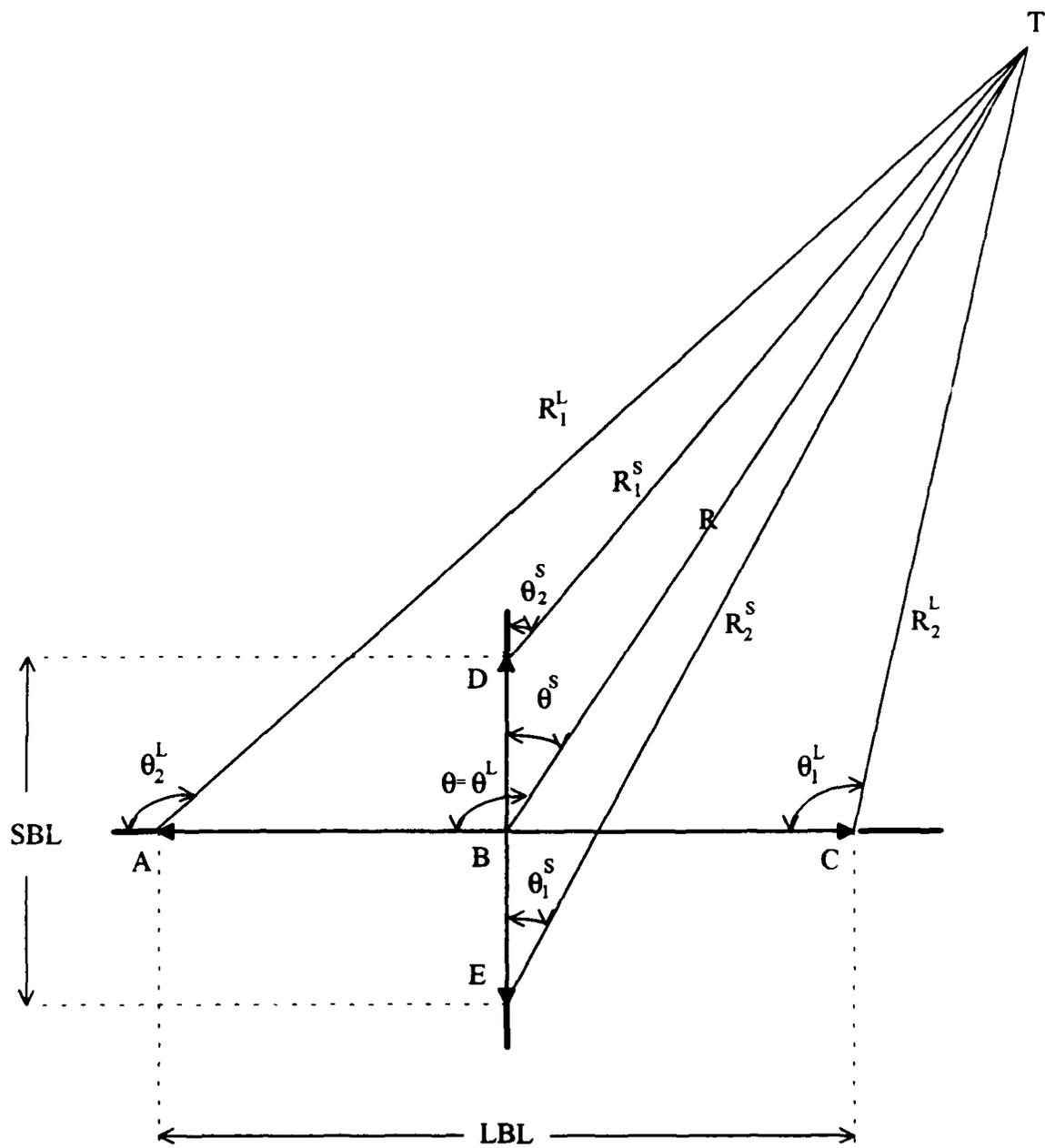
Figure 6 : Dual baseline model scheme

38
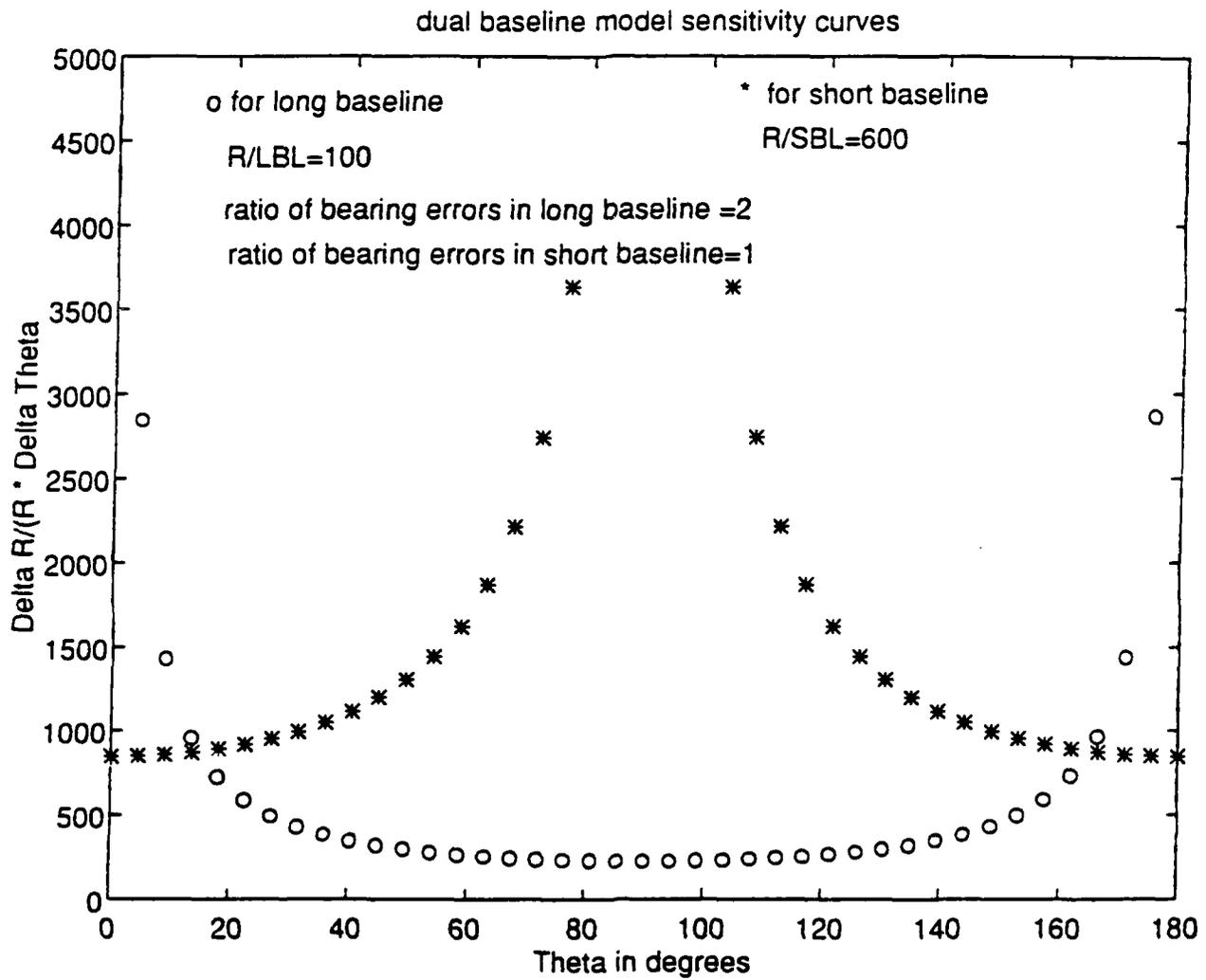
Figure 7: Dual baseline first example (R/LBL=100, R/SBL=600, a^L=2, a^S=1)
(via program in Appendix E. B)
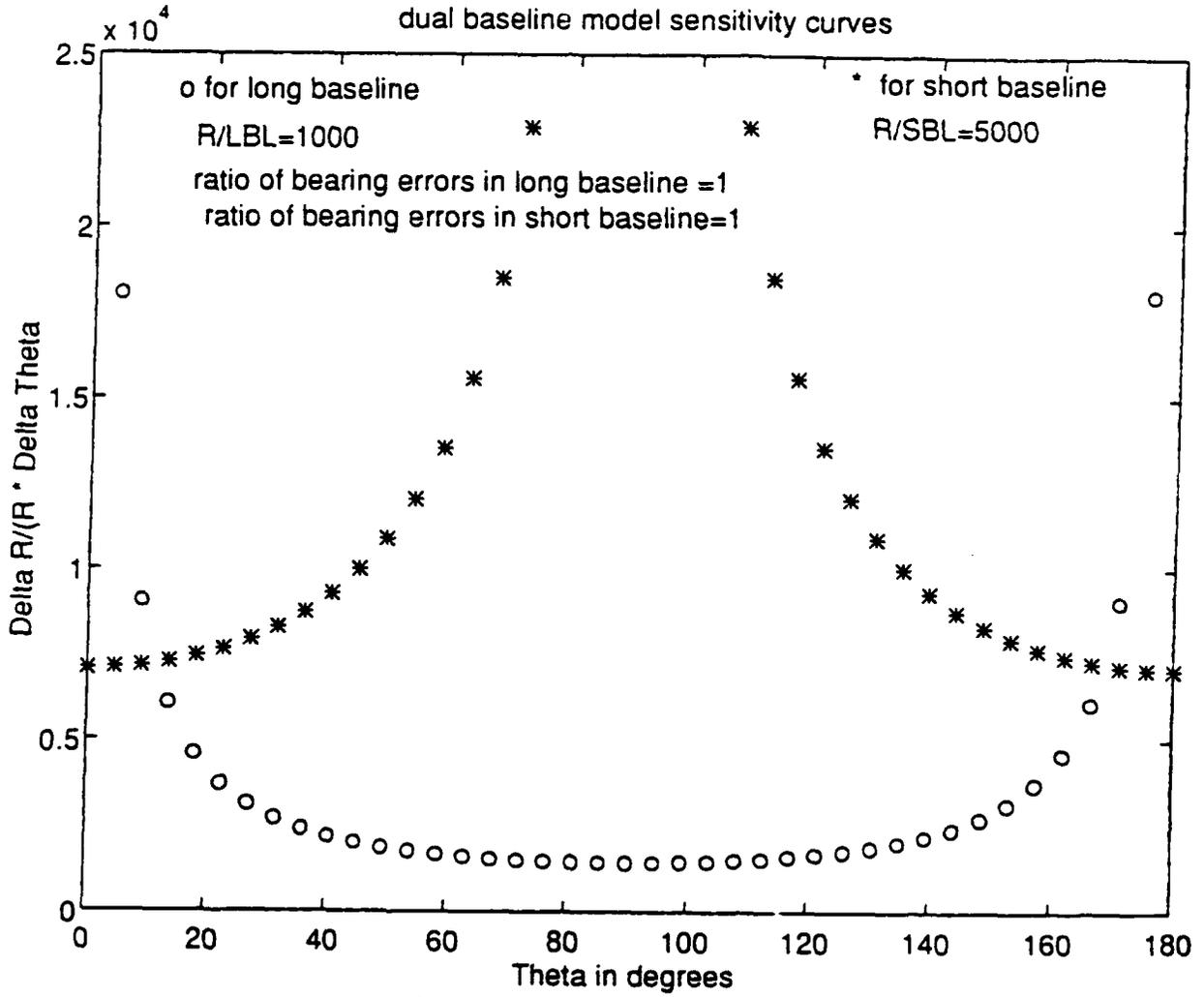
Figure 8: Dual baseline second example(R/LBL=1000, R/SBL=5000, a^L=1, a^S=1)
(via program in Appendix E.B)
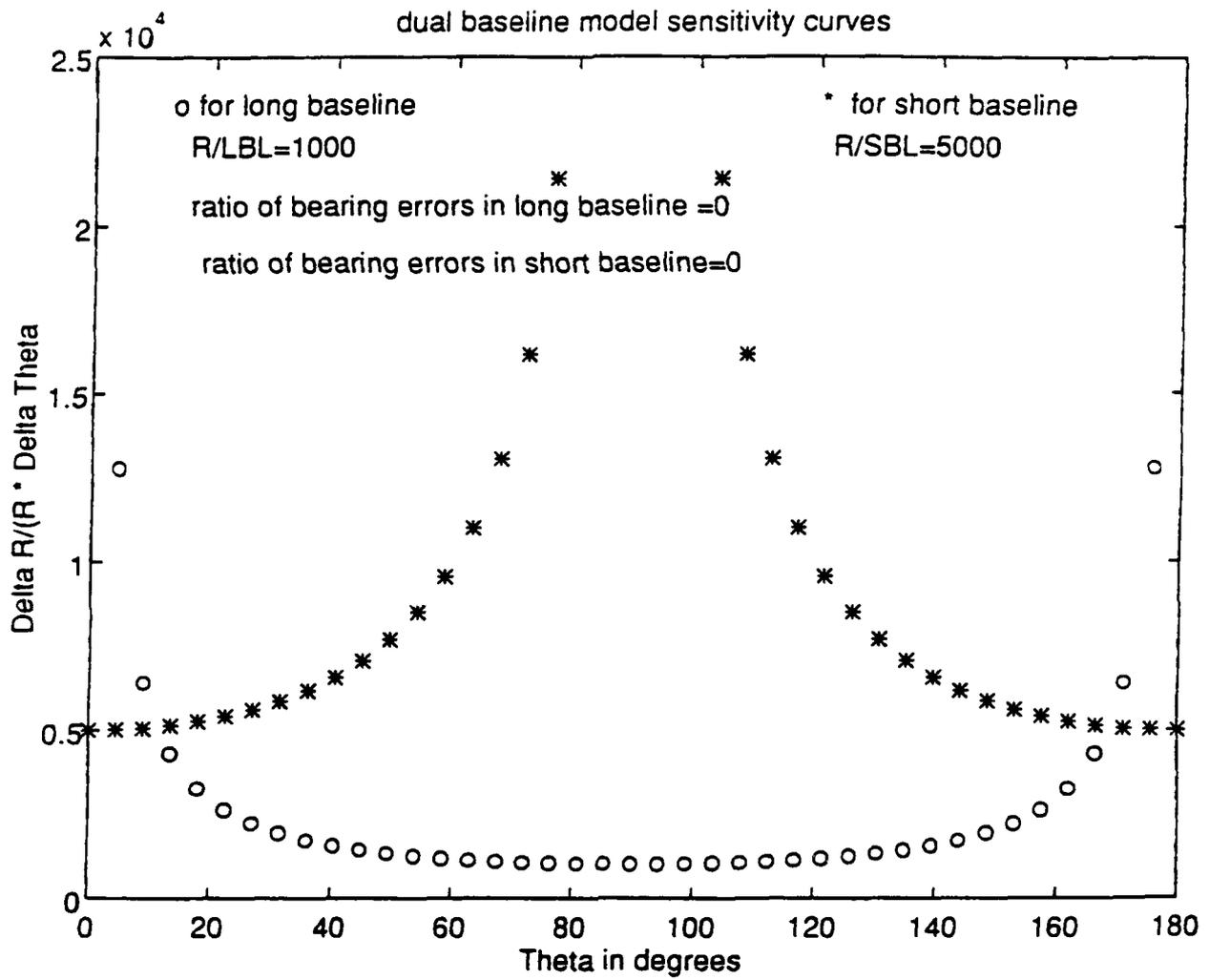
Figure 9: Dual baseline third example(R/LBL=1000, R/SBL=5000, $a^L = a^S = 0$)
(via program in Appendix E. B)
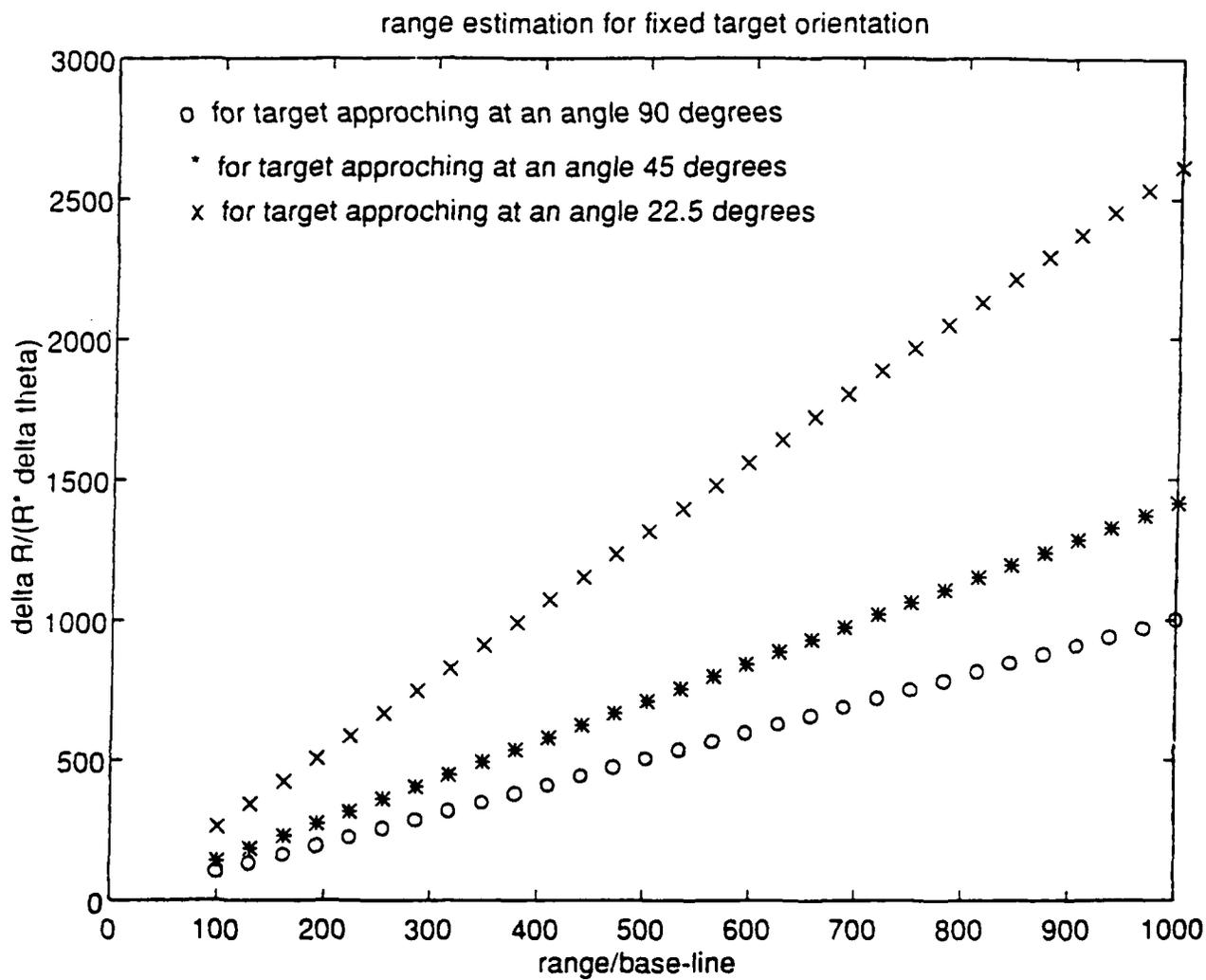
Figure 10: **Range sensitivity** for fixed target orientation (θ= 90°, 45°, and 22.5°)
(via program in Appendix E. C)

range estimation for fixed target orientation

o for target approching at an angle 90 degrees

* for target approching at an angle 80 degrees

x for target approching at an angle 10 degrees
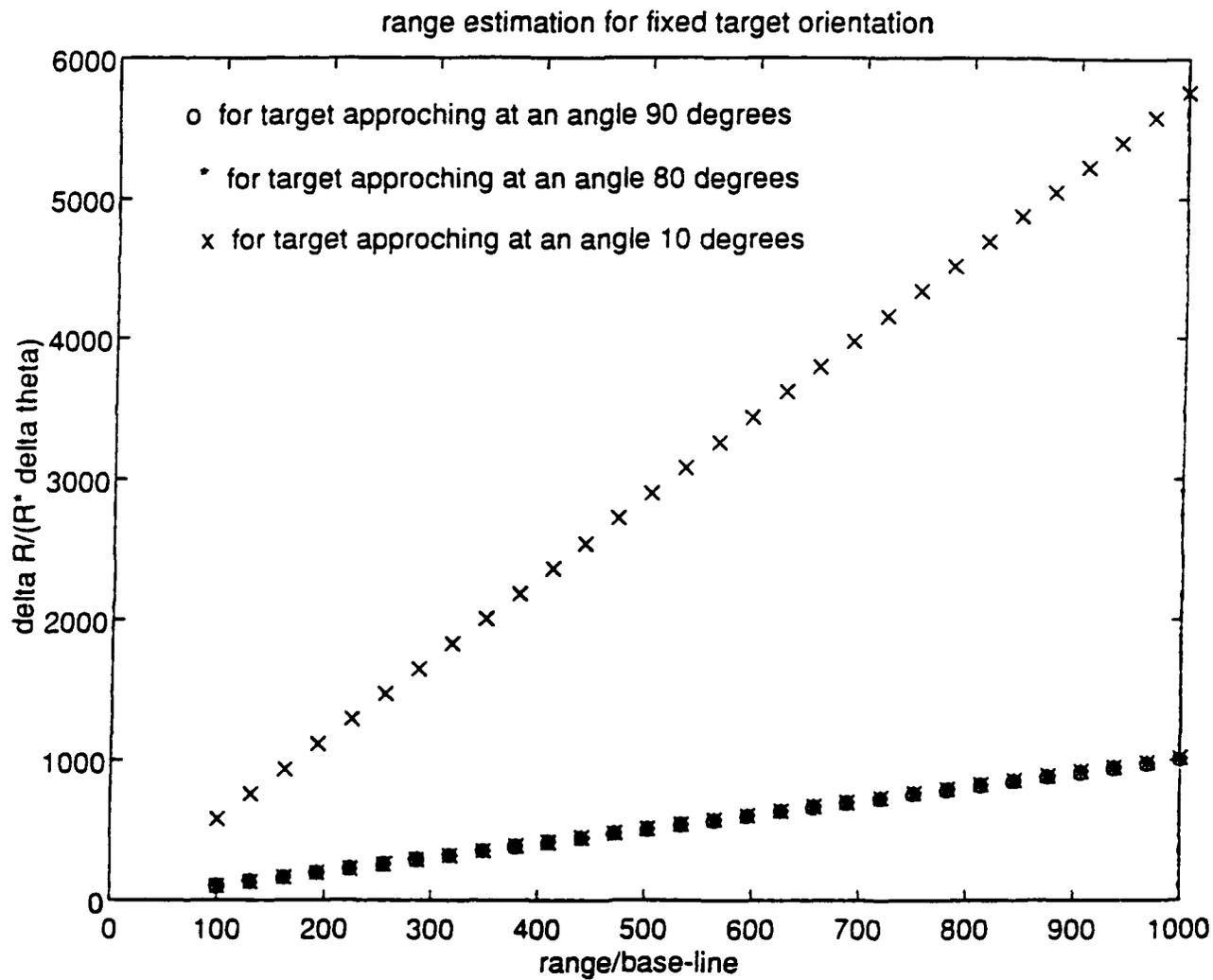
Figure 11: Range sensitivity for fixed target orientation (θ= 90°, 80°, and 10°)
(via program in Appendix E. C)

43

IV. RANGE LIMITATIONS FOR FIXED SENSITIVITY

A. CHAPTER OVERVIEW

In this chapter a more graphical representation for R_{max} versus orientation angle θ will be developed. For target ranges less than R_{max} the triangulation estimation will, by assumption, be within a tolerable precision limit dictated by a maximum sensitivity. Two paradigms for estimation are considered. The first is based on a quadrature addition of terms. In this case an analytic solution can be obtained for the case $a=1$, i.e., equal precision bearing measurements. In the second case the addition occurs as a sum of absolutes. Here after making a reasonable approximation $R/BL >> 1$, a solution for all "a" can be obtained.

B. ANALYSIS BASED ON THE SUM OF ABSOLUTES

Define the normalized range sensitivity for long and short baseline respectively as

$$\left| \left(\frac{\Delta R}{R} \frac{1}{\Delta \theta} \right)^L \right| \equiv c^L \qquad \qquad \left| \left(\frac{\Delta R}{R} \frac{1}{\Delta \theta} \right)^S \right| \equiv c^S \qquad (53\text{a, b})$$

after noting for both LBL and SBL that

$$\frac{1}{2} \frac{\sqrt{1-\sin^2(\theta)}}{\sin(\theta)} < \frac{\sqrt{1-\left(\frac{BL}{R}\sin(\theta)\right)^2}}{\frac{BL}{R}\sin(\theta)} \qquad (53\text{c})$$

44

and after substituting, (35) simplifies to

$$\left(\frac{1}{2}\frac{\sqrt{1-\sin^2(\theta^L)}}{\sin(\theta^L)}\right)(1-a^L)+\left(\frac{\sqrt{1-\left(\frac{LBL}{R}\sin(\theta^L)\right)^2}}{\left(\frac{LBL}{R}\sin(\theta^L)\right)}\right)(1+a^L)=c^L \tag{54a}$$

$$\left(\frac{1}{2}\frac{\sqrt{1-\sin^2(\theta^S)}}{\sin(\theta^S)}\right)(1-a^S)+\left(\frac{\sqrt{1-\left(\frac{SBL}{R}\sin(\theta^S)\right)^2}}{\left(\frac{SBL}{R}\sin(\theta^S)\right)}\right)(1+a^S)=c^S \tag{54b}$$

For typical cases $R >> BL$ (as previously assumed in Chapter II) the first terms, proportional to $(1-a^{L/S})$, are very small compared with the second ones, proportional to $(1+a^{L/S})$, so it is possible to neglect them without significant sacrifice in the accuracy. Then (54) becomes

$$\left(\frac{\sqrt{1-\left(\frac{LBL}{R}\sin(\theta^L)\right)^2}}{\left(\frac{LBL}{R}\sin(\theta^L)\right)}\right)(1+a^L)=c^L \tag{55a}$$

$$\left(\frac{\sqrt{1-\left(\frac{SBL}{R}\sin(\theta^S)\right)^2}}{\left(\frac{SBL}{R}\sin(\theta^S)\right)}\right)(1+a^S)=c^S \tag{55b}$$

Solving (55a) for $\frac{R_{LBL}}{LBL}$, it follows that

$$\left(\frac{R_{LBL}}{LBL}\right)^2 = \sin^2(\theta^L)\frac{(c^L)^2+(1+a^L)^2}{(1+a^L)^2} \qquad \frac{R_{LBL}}{LBL}=\left|\sqrt{\sin^2(\theta)\frac{(c^L)^2+(1+a^L)^2}{(1+a^L)^2}}\right| \tag{55c, d}$$

45

Equation (55d) can be used to create a polar plot of the range measured by the long baseline normalized to the LBL. Solving (55b) for $R_{SBL}/$ SBL, and after (25), it follows that

$$\frac{R_{SBL}}{SBL} = \left| \sqrt{\cos^2(\theta)\frac{(c^S)^2+(1+a^S)^2}{(1+a^S)^2}} \right| \tag{55e}$$

$$\frac{R_{SBL}}{LBL} = \left| \sqrt{\cos^2(\theta)\frac{(c^S)^2+(1+a^S)^2}{(1+a^S)^2}\left(\frac{SBL}{LBL}\right)^2} \right| \tag{55f}$$

Equation (55f) gives the range measured by the short baseline normalized with respect to the LBL for convenient comparison with (54).

C. ANALYSIS BASED ON QUADRATURE ADDITION OF TERMS

After the reasonable assumption that $a = 1$, (33) becomes

$$\left(\frac{\Delta R}{R}\frac{1}{\Delta\theta}\right)^L = \sqrt{\left(\frac{1}{2}\frac{\sqrt{1-\sin^2(\theta^L)}}{\sin(\theta^L)}+\frac{\sqrt{1-\left(\frac{LBL}{R}\sin(\theta^L)\right)^2}}{\left(\frac{LBL}{R}\sin(\theta^L)\right)}\right)^2 + \left(\frac{1}{2}\frac{\sqrt{1-\sin^2(\theta^L)}}{\sin(\theta^L)}-\frac{\sqrt{1-\left(\frac{LBL}{R}\sin(\theta^L)\right)^2}}{\left(\frac{LBL}{R}\sin(\theta^L)\right)}\right)^2} \tag{56a}$$

$$\left(\frac{\Delta R}{R}\frac{1}{\Delta\theta}\right)^S = \sqrt{\left(\frac{1}{2}\frac{\sqrt{1-\sin^2(\theta^S)}}{\sin(\theta^S)}+\frac{\sqrt{1-\left(\frac{SBL}{R}\sin(\theta^S)\right)^2}}{\left(\frac{SBL}{R}\sin(\theta^S)\right)}\right)^2 + \left(\frac{1}{2}\frac{\sqrt{1-\sin^2(\theta^S)}}{\sin(\theta^S)}-\frac{\sqrt{1-\left(\frac{SBL}{R}\sin(\theta^S)\right)^2}}{\left(\frac{SBL}{R}\sin(\theta^S)\right)}\right)^2} \tag{56b}$$

After defining

$$\frac{1}{2}\frac{\sqrt{1-\sin^2(\theta)}}{\sin(\theta)} = \frac{1}{2}\cot(\theta) = k \tag{57}$$

46

and

$$\frac{\sqrt{1-\left(\frac{BL}{R}\sin(\theta)\right)^2}}{\left(\frac{BL}{R}\sin(\theta)\right)} = m \tag{57b}$$

in order to simplify the notation, and after (53), (56) it follows that

$$\sqrt{(k_{LBL}+m_{LBL})^2+(k_{LBL}-m_{LBL})^2} = \sqrt{2(k_{LBL}^2+m_{LBL}^2)} = c^L \tag{58a}$$

and

$$\sqrt{(k_{SBL}+m_{SBL})^2+(k_{SBL}-m_{SBL})^2} = \sqrt{2(k_{SBL}^2+m_{SBL}^2)} = c^S \tag{58b}$$

In (58) only the terms m_{LBL}, and m_{SBL} are R dependent and solving for them it follows that

$$m_{LBL}^2 = \frac{(c^L)^2-2k_{LBL}^2}{2} \qquad \text{and} \qquad m_{SBL}^2 = \frac{(c^S)^2-2k_{SBL}^2}{2} \tag{59a, b}$$

Finally after substituting (57) into (59) this leads to

$$\frac{R}{LBL\sin(\theta^L)} = \sqrt{\frac{(c^L)^2-0.5\cot^2(\theta^L)}{2}+1} \tag{60a}$$

$$\frac{R}{SBL\sin(\theta^S)} = \sqrt{\frac{(c^S)^2-0.5\cot^2(\theta^S)}{2}+1} \tag{60b}$$

47

After referring to Figure 5 and solving (60a) for R_{LBL} it is found that

$$\frac{R_{LBL}}{LBL} = \left| \sqrt{\left(\frac{(c^L)^2 \sin^2(\theta) - 0.5\cos^2(\theta)}{2} + \sin^2(\theta) \right)} \right| \tag{61a}$$

Similarly, solving (60b) for R_{LBL}, and taken into account (24) it follows that

$$\frac{R_{SBL}}{LBL} = \left| \sqrt{\left(\frac{(c^S)^2 \cos^2(\theta) - 0.5\sin^2(\theta)}{2} + \cos^2(\theta) \right) \left(\frac{SBL}{LBL} \right)^2} \right| \tag{61b}$$

Equations (61a, b) can be plotted in polar form in order to show the target's range (normalized to LBL) as it would be measured by a long and short baseline respectively.

D.   RESULTS BASED ON SUM OF THE ABSOLUTES

Following (55d) and (55f), the maximum normalized range LBL and SBL have been plotted in Figures 12, and 13 respectively, versus target orientation θ. This was done for conditions $a^L = a^S = 1$, $c^L = c^S = 500$, and LBL=5 x SBL. For example, using $\theta = 90°$ on Figure 12 indicates that the maximum triangulation range is 250 x LBL. It is seen from Figure 13 that the SBL maximum occurs at $0°$ and it is 50 x LBL as expected. The combined effect is easily visualized in the cartesian representation shown on Figure 14. The solid line is the maximum triangulation range using the short baseline while the small circle plotting symbol is the corresponding long baseline range. As mentioned, the assumption inherent in this scheme is that the baseline producing the most precise estimate for range will automatically be selected with the use of "smart electronics." Therefore the larger of the short and

48

long baseline curves for R_{max} represents the ideal capabilities for the dual baseline scheme. This is shown on Figure 14 with a large circle used as a plotting symbol. The more physical polar representation for this solution is provided in Figure 15. In this figure can be seen the maximum range which is measured via the dual baseline scheme in any direction.

E.   RESULTS BASED ON QUADRATURE ADDITION OF TERMS

Figures 16, 17, 18, and 19 are the counterparts for Figures 12, 13, 14, and 15 with the same data (i.e., $a^L=a^S=1$, $c^L=c^S=500$, and LBL=5 x SBL) but based on (61a), and (61b). It should be noted that these curves have a R_{max} that as expected is approximately $2^{1/2}$ higher (i.e., less conservative) compared with the previous case.

F.   OBSERVATIONS

It is possible to obtain approximate analytic expressions for R_{max} / LBL in terms of the target orientation. In the case of the more conservative sum of absolutes this can be done for arbitrary bearing precision ratios a^L and a^S. Figure 12, obtained using the sum of absolutes paradigm, shows that the maximum value for the long baseline range is approximately 250 x LBL, where 250 is 50% of the long baseline sensitivity. This can be compared with similar long baseline results for the quadrature addition paradigm shown on the Figure 16. Here the maximum value for the long baseline range is approximately 350 x LBL, where 350 is the 70% of the long baseline sensitivity. These observations, which show that the range scales with the sensitivity, can be generalized to convenient rules of thumb for calculating the maximum triangulated range for the long baseline system. The details of this case are presented in Chapter VI. This suggest that for the condition c^L

49

$=c^S=c$ the general appearance of the two curves, independent of scale, will depend on the ratio of the long baseline to the short baseline. This issue is clarified also in greater depth in Chapter VI.

normalized range detected by long baseline (sum of absolutes)
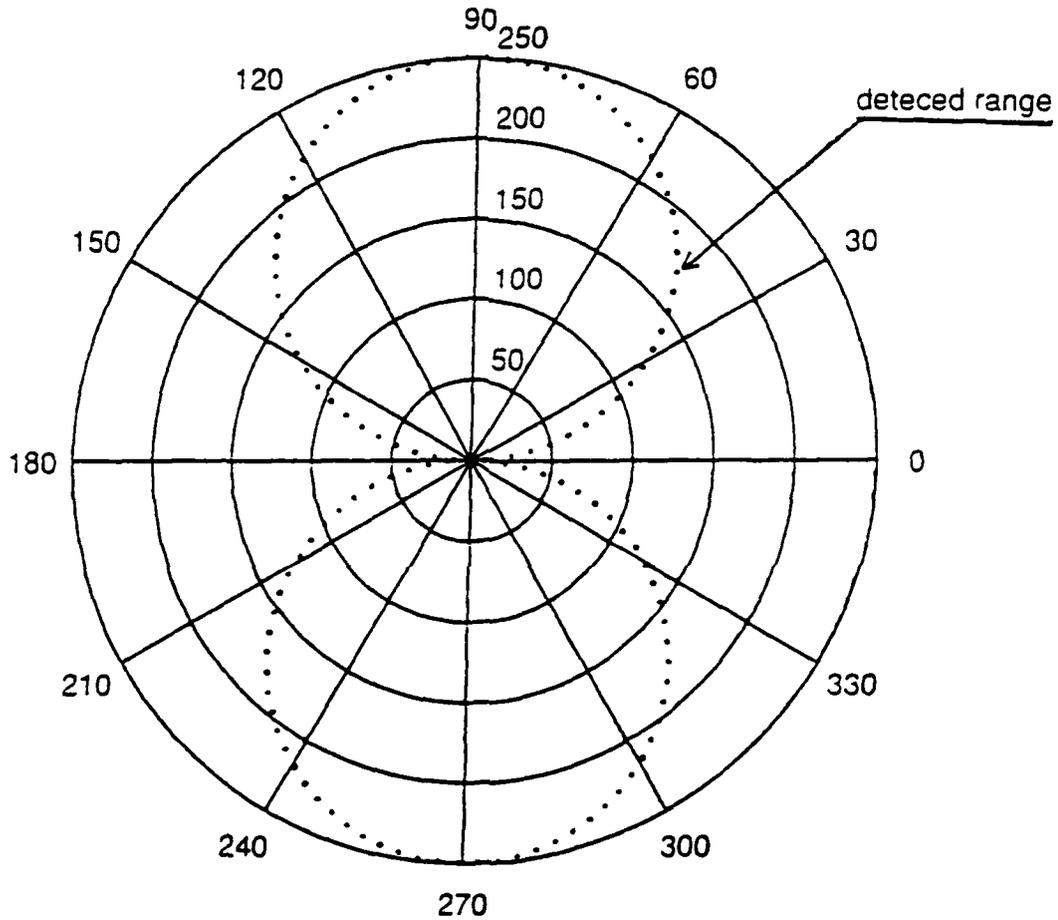
ratio of the bearing errors in long baseline=1   normalized sensitivity of the long baseline =500

Figure 12: Normalized range measured by the long baseline sensors for $a^L=1$, and $c^L=500$ (based on the sum of absolutes and obtained via program in Appendix E. D)

51

normalized range detected by the short baseline(sum of absolutes)
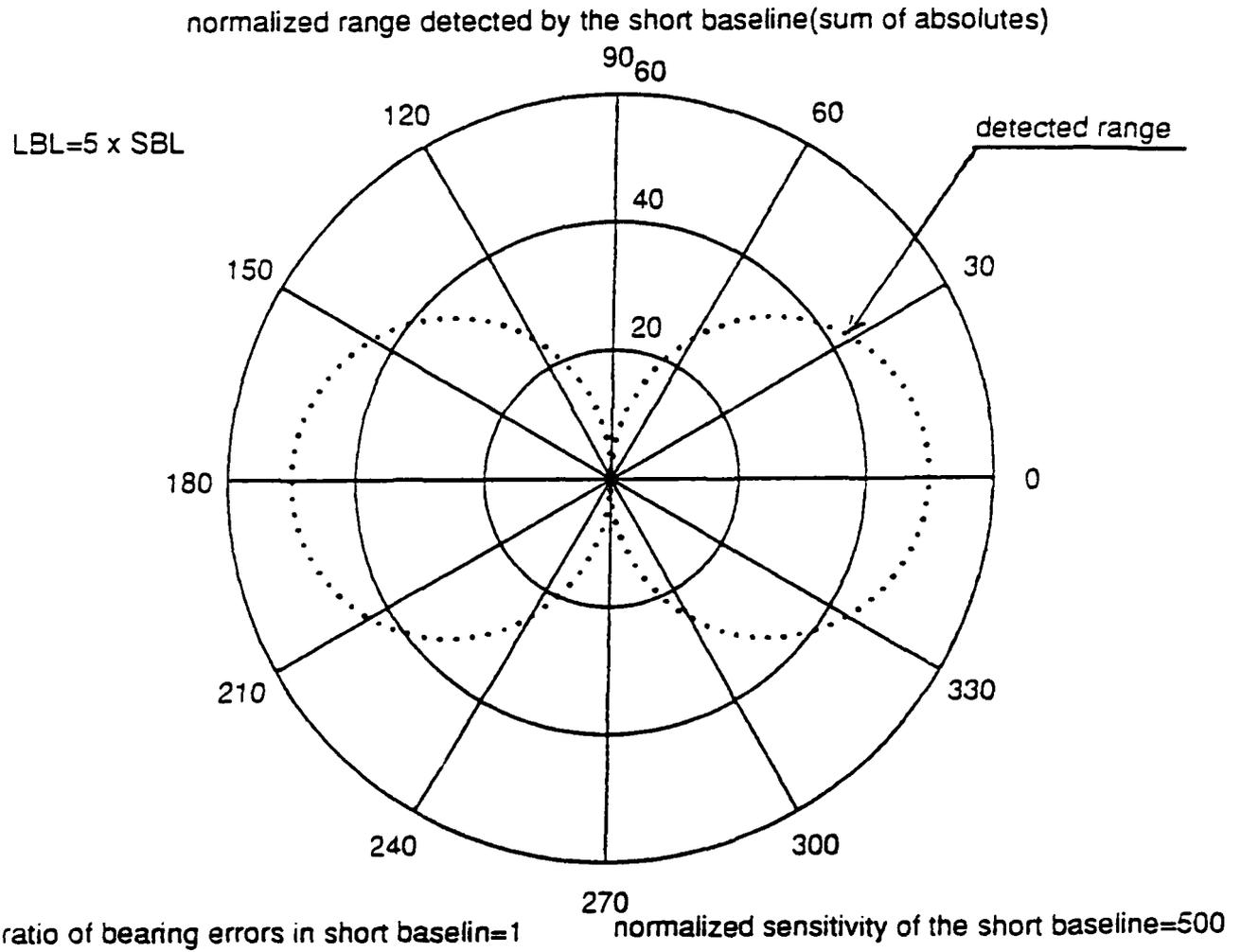
Figure 13: Normalized range measured by the short baseline for $a^s=1$, $c^s=500$, and
SBL/LBL=0.2 (based on the sum of absolutes and obtained via program
in Appendix E. E)

range detected by the dual baseline system in any direction(sum of absolutes)
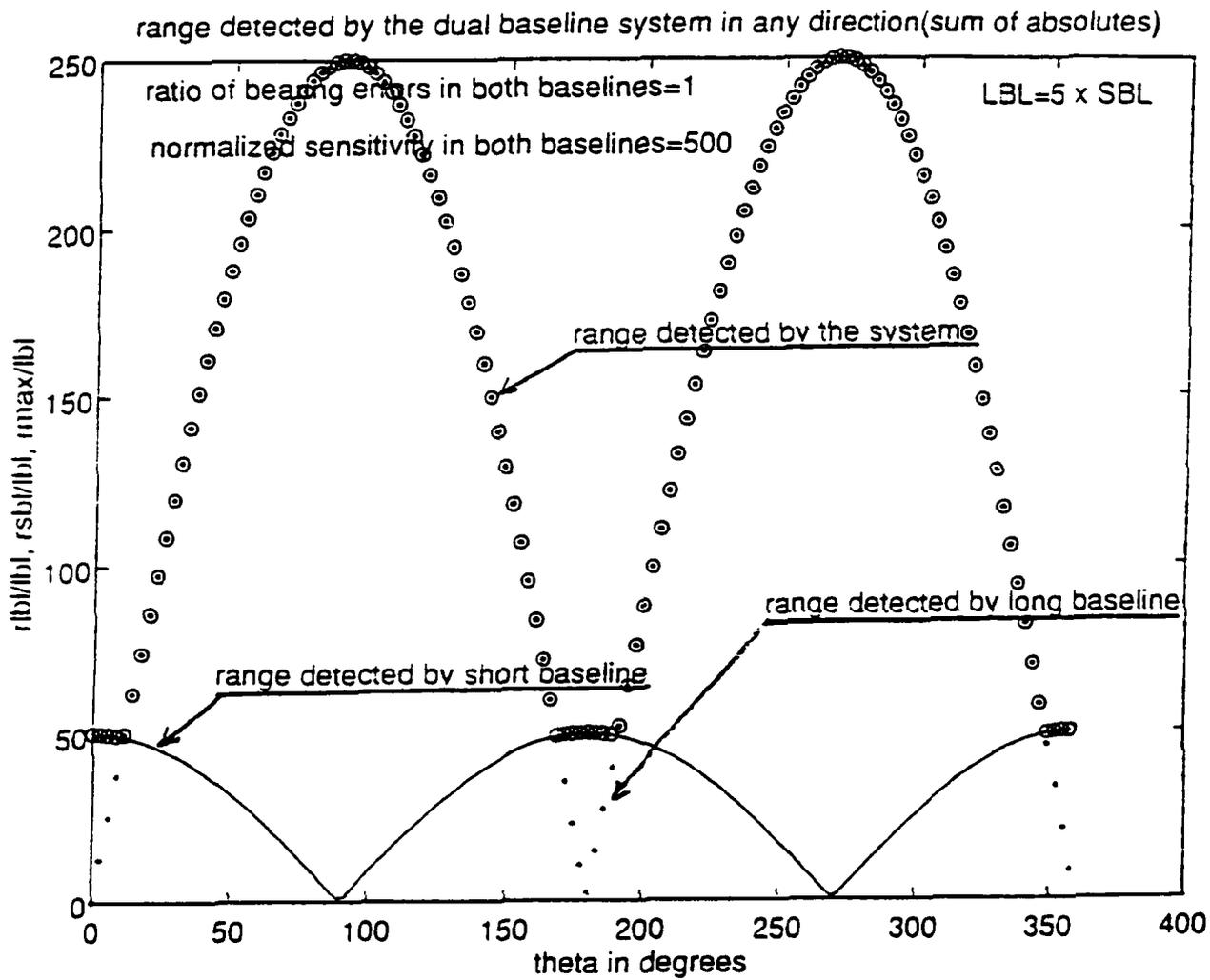
Figure 14: Cartesian plot of the normalized range measured by the short baseline , and the long baseline, showing also the range measured by the entire dual baseline sys-- stem. (based on the sum of absolutes and obtained via program in Appendix E. F)

range detected by the dual baseline system in any direction(sum of absolutes)
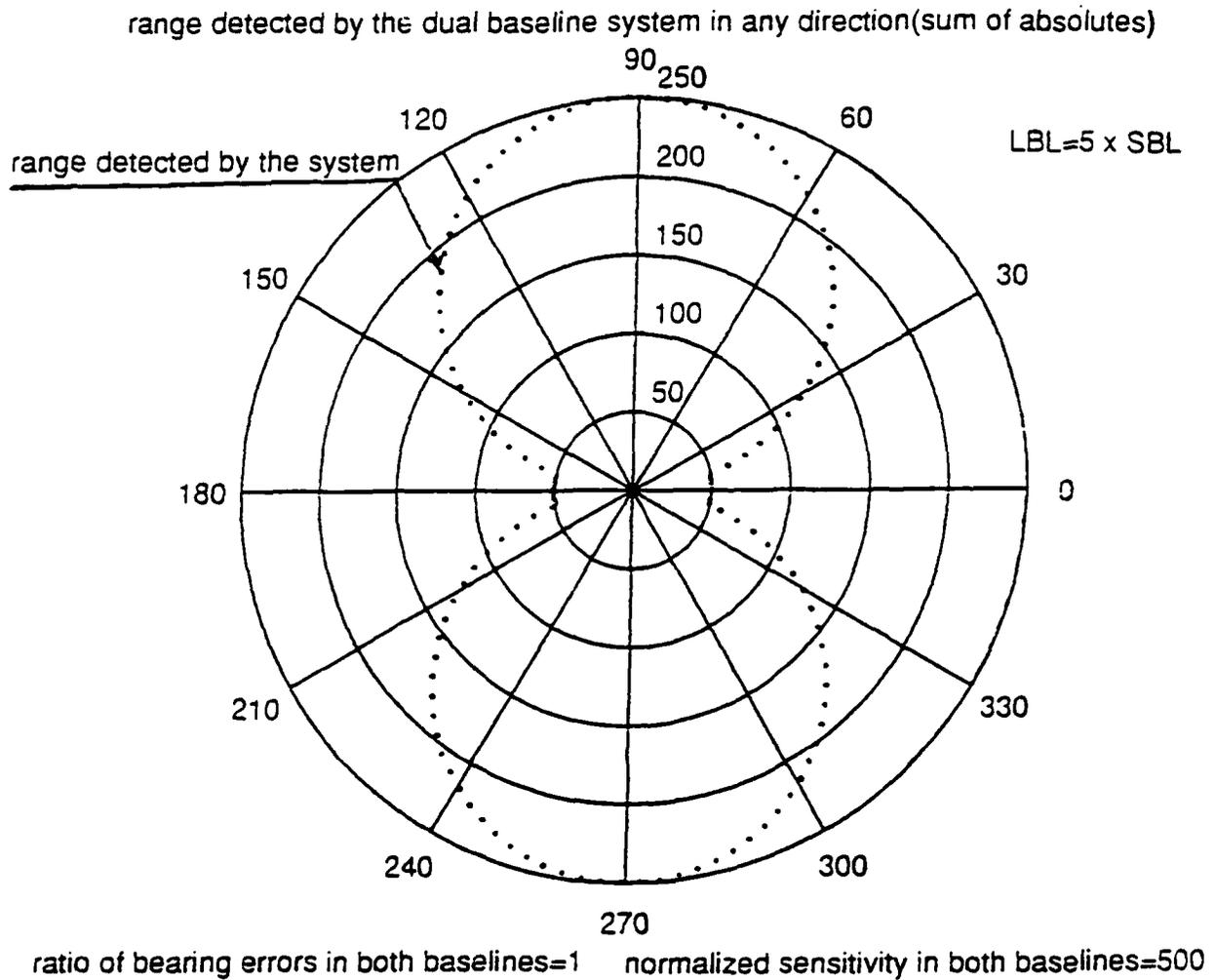
Figure 15: Plot of the normalized range measured by the dual baseline system in any direction. (based on the sum of absolutes and obtained via program in Appendix E. G)

54

normalized range detected by long baseline(quadrature addition of terms)

LBL=5 x SBL

detected range

ratio of the bearing errors in long baseline=1   normalized sensitivity of the long baseline=500
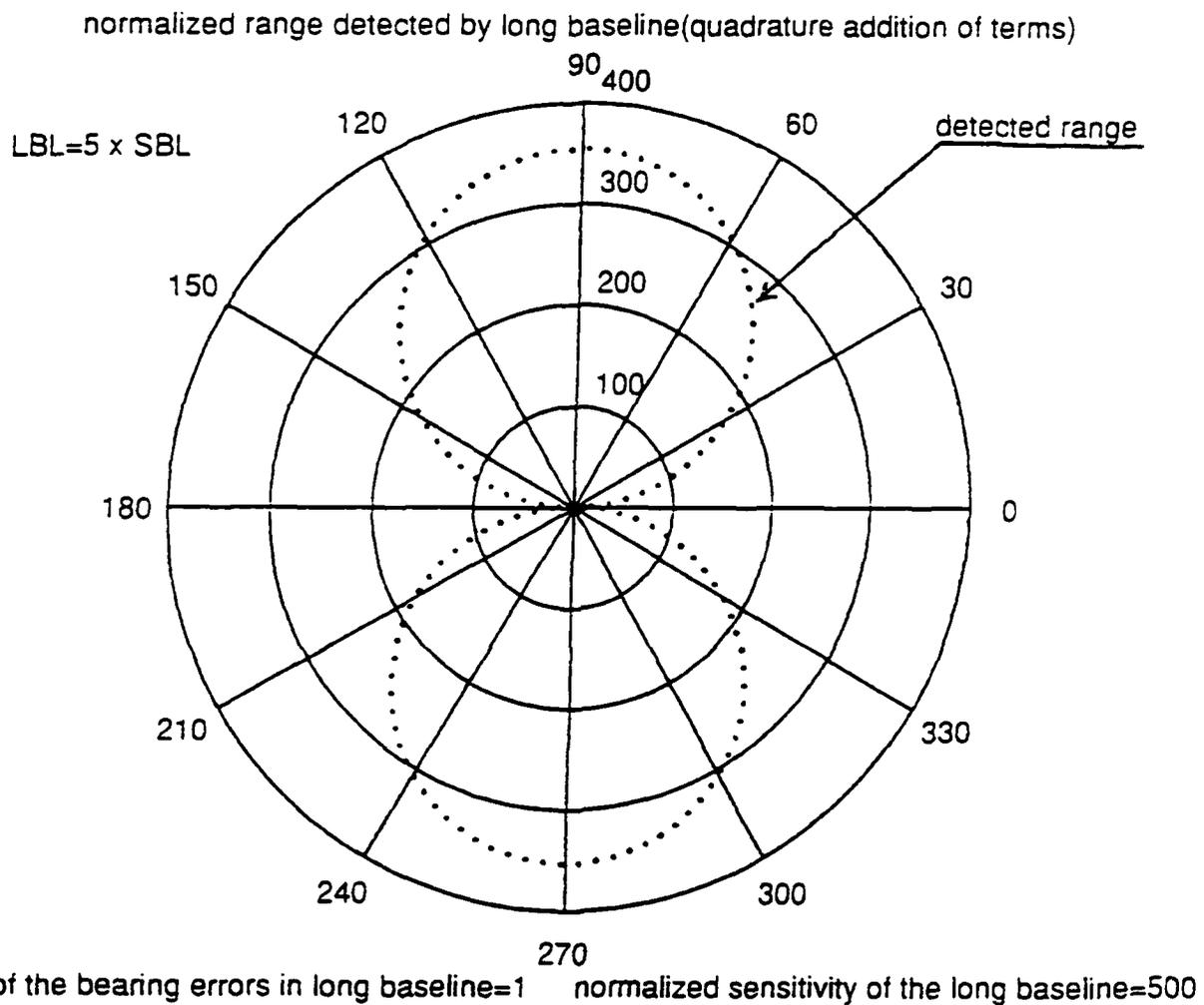
Figure 16 Normalized range measured by the long baseline sensors for a^L=1, and c^L=500
(based on the quadrature addition & obtained via program in Appendix E. H)

normalized range detected by the short baseline(quadrature addition of terms)

LBL=5 x SBL

detected range

ratio of bearing errors in short baseline=1   normalized sensitivity in short baseline=500
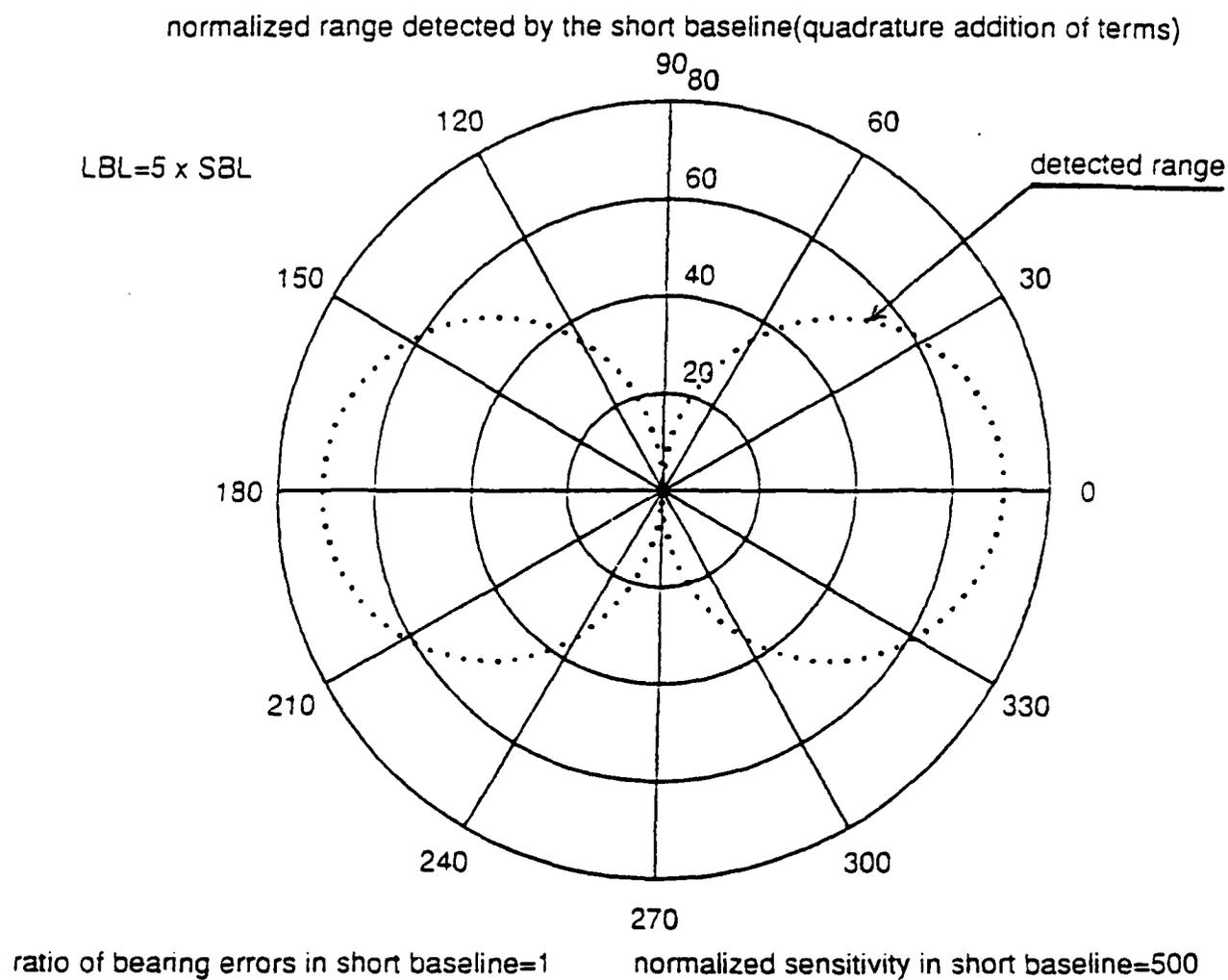
Figure 17: Normalized range measured by the short baseline for $a^s=1$, $c^s=500$, and SBL/LBL=0.2 (based on the quadrature addition and obtained via program in Appendix E. I)

cartesian plot of the range detected by the dual baseline system(quadrature addition)
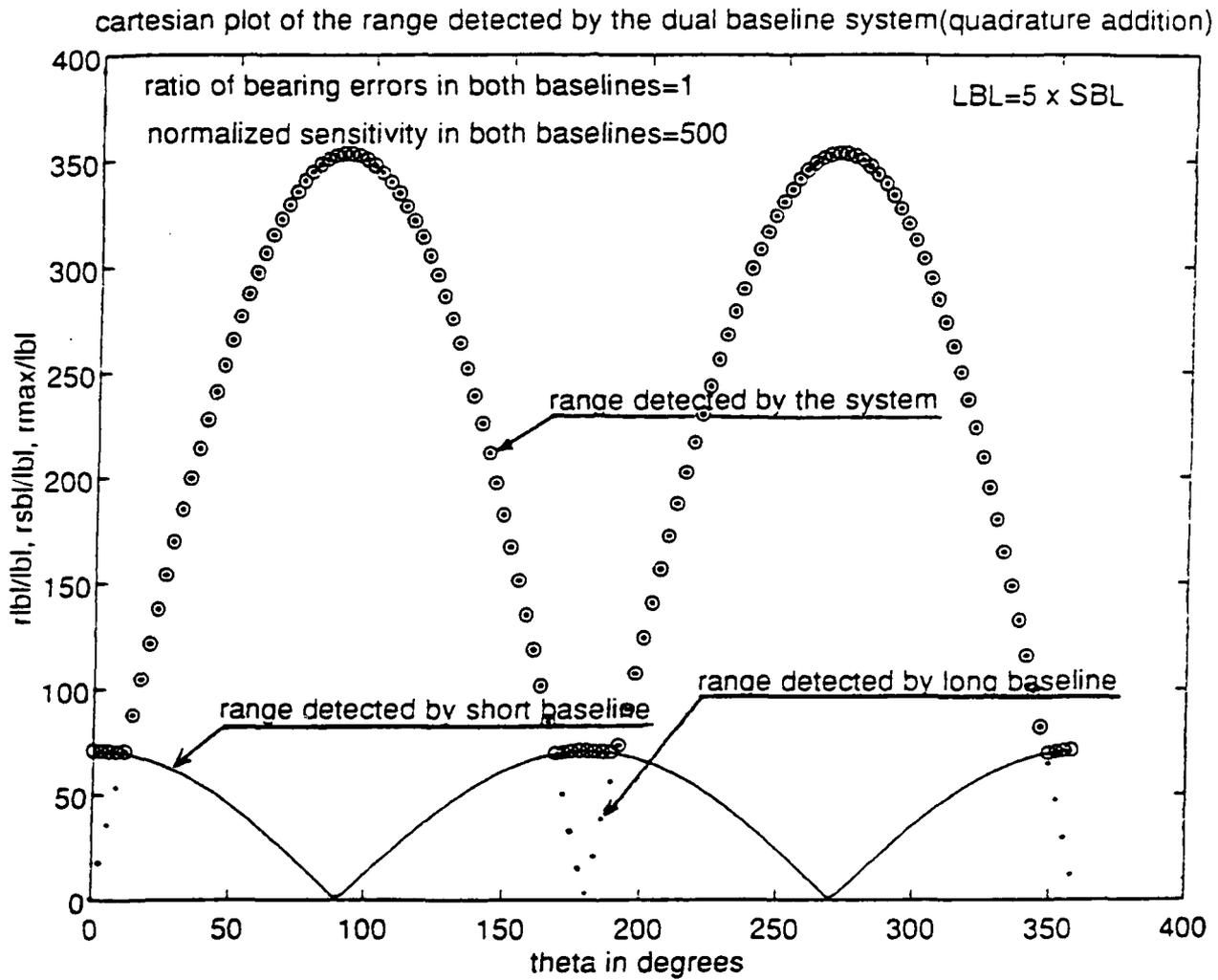
Figure 18: Cartesian plot of the normalized range measured by the short baseline , and the long baseline, showing also the range measured by the entire dual baseline system. (based on the quadrature addition and obtained via program in Appendix E. J)

range detected by the dual baseline system in any direction(quadrature addition)
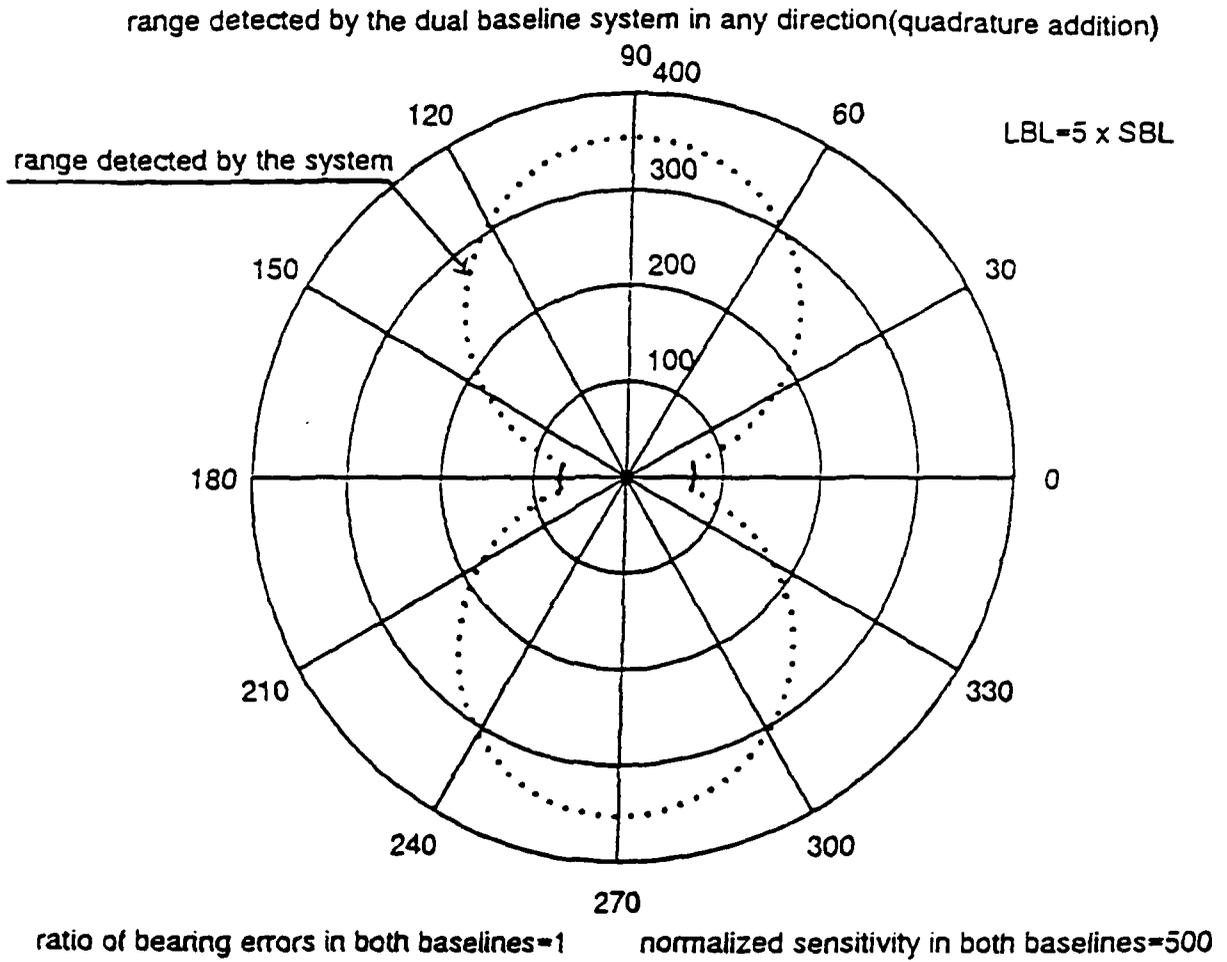
Figure 19: Plot of the normalized range measured by the dual baseline system in any direction. (based on the quadrature addition and obtained via program in Appendix E. K)

V. PHYSICAL LIMITATIONS OF THE TRIANGULATION METHOD

A. INTRODUCTION

The polar plots of the normalized sensitivity that were presented in the previous sections define limitations in the range measurement via the triangulation model. In this chapter the physical limitation due to the optical horizon is considered.

B. GEOMETRIC AND OPTICAL HORIZON [REF. 18]

The line at which the earth's curved surface apparently meets the sky is called the horizon. It can be observed very easily that the distance to the horizon increases as the height of an observer's eye increases above the earth surface. The dependence of sighting distance on the height of the observer's eye is by itself an evidence that the surface of earth is curved. As shown in Figure 20, two types of horizons can be distinguished: the geometric horizon that extends to the point H, and the optical horizon that extends to the point H'. The geometric horizon can be defined as the points where all the straight lines from a given observer tangentially graze the surface of the earth. However, due to refraction an observer can see a longer distance than that of the geometric horizon. This displaced horizon is the only one that can be sensed by an observer and it is called the optical horizon. So, the refraction enables the observer to see over and beyond the earth's surface at H. The distance to which an observer can see depends on the height of the eye and the amount of refraction, and uncertainties in this latter quantity can be troublesome when

59

high accuracy is needed. The uncertainties arise from the fact that the line of sight to the

horizon lies too close to the earth's surface. Because of differences in air and land or water

temperature, abnormal temperature inversions or temperature gradients may occur in the

lowest few meters of the atmosphere. Thus, the amount that the line of sight is bent is a

variable and generally very difficult to predict, leading to a high level unpredictability in

the optical horizon location. Therefore the more conservative estimation for the optical

horizon, based on geometrical consideration alone, will be followed.

C. OPTICAL HORIZON GEOMETRIC ANALYSIS

As may be understood from the Figure 20, no part of the earth's surface whose ele-

vation angle is less than that of the optical horizon can be seen beyond this horizon. How-

ever, an elevated object such as an incoming missile, flying above the surface of the sea,

can be seen beyond this horizon. The geometry for a such an object is shown on Figure

21, and the foregoing analysis refers to an average steady-state condition of the air. From

Figure 21, it is obvious that

$$d = (R_e + t) \cdot \sin \theta_t + (R_e + s) \cdot \sin \theta_s \qquad (65)$$

Again from the same figure

$$\cos \theta_t = \frac{R_e}{R_e + t} \qquad (66a)$$

$$\cos \theta_s = \frac{R_e}{R_e + s} \qquad (66b)$$

60

After (66), (65) becomes

$$d = (R_e + t)\sqrt{1 - \left(\frac{R_e}{R_e+t}\right)^2} + (R_e + s)\sqrt{1 - \left(\frac{R_e}{R_e+s}\right)^2} \qquad (67a)$$

or

$$d = \sqrt{(t^2 + 2R_e t)} + \sqrt{(s^2 + 2R_e s)} \qquad (67b)$$

In (67b) the terms t^2 and s^2 are very small compared to the other terms with factor R_e and can be neglected without error. After this assumption (67b) becomes

$$d \cong \sqrt{2R_e t} + \sqrt{2R_e s} \qquad (68)$$

The geometric analysis ignores the effects of the refraction which can increase the distance to the optical horizon. Therefore (68) represents a conservative estimation for the optical horizon. The relation (68) gives an approximation of the distance at which an object at height t above the surface of the earth can be seen by an observer or sensor at height s above the surface of the earth. Taking $R_e = 6.37 \times 10^6$ meters, (68) can be written as

$$d \cong 3569.6(\sqrt{t} + \sqrt{s}) \qquad \text{meters} \qquad (69)$$

where d, t, and s are expressed in meters.

61

D. EXAMPLES INCORPORATING THE GEOMETRIC HORIZON

The dual baseline triangulation model permits a maximum triangulation range to be estimated within a maximum tolerable error criterion. In the case that the geometric horizon appears at a distance shorter than the dual baseline prediction then the de-facto maximum triangulation range is the geometric horizon. The combined limitations of the dual baseline triangulation system composed of the inherent and physical limitations can be modeled and represented with computer plots. Such plots are presented in Figures (22a, b) and (23a, b) and it can be seen that the limitations in the behavior of the system depends either on the distance from the baseline to the geometric horizon or the parameters of the system itself. The data used to generate these plots are conveniently provided in Table 1. It is noted that the specification $a^L = a^S = 1$ is consistent with the criterion that all bearing sensors have the same precision in bearing measurement. On the other hand the specification $c^L = c^S = c$ is consistent with the condition that the range measurement should be worked with the same precision limit regardless of the baseline used. Note that Figures 22a and 23a are based on the sum of absolutes, while the Figures 22b and 23b are based on the quadrature addition of terms. On all figures, $a^L = a^S = 1$, and $c^L = c^S = 500$.

TABLE 1. DATA FOR THE FIGURES (22, 23)

	t (m)	s (m)	GH (m)	LBL (m)	SBL (m)
Figures 22a, 23a	10	10	22,480	100	20
Figures 22b, 23b	3	3	12,365	20	4
* On all figures $a^L = a^S = 1$, and $c^L = c^S = 500$ ** Figures (22a), and (22b) are based on the sum of absolutes *** Figures (23a), and (23b) are based on the quadrature addition of terms					

62
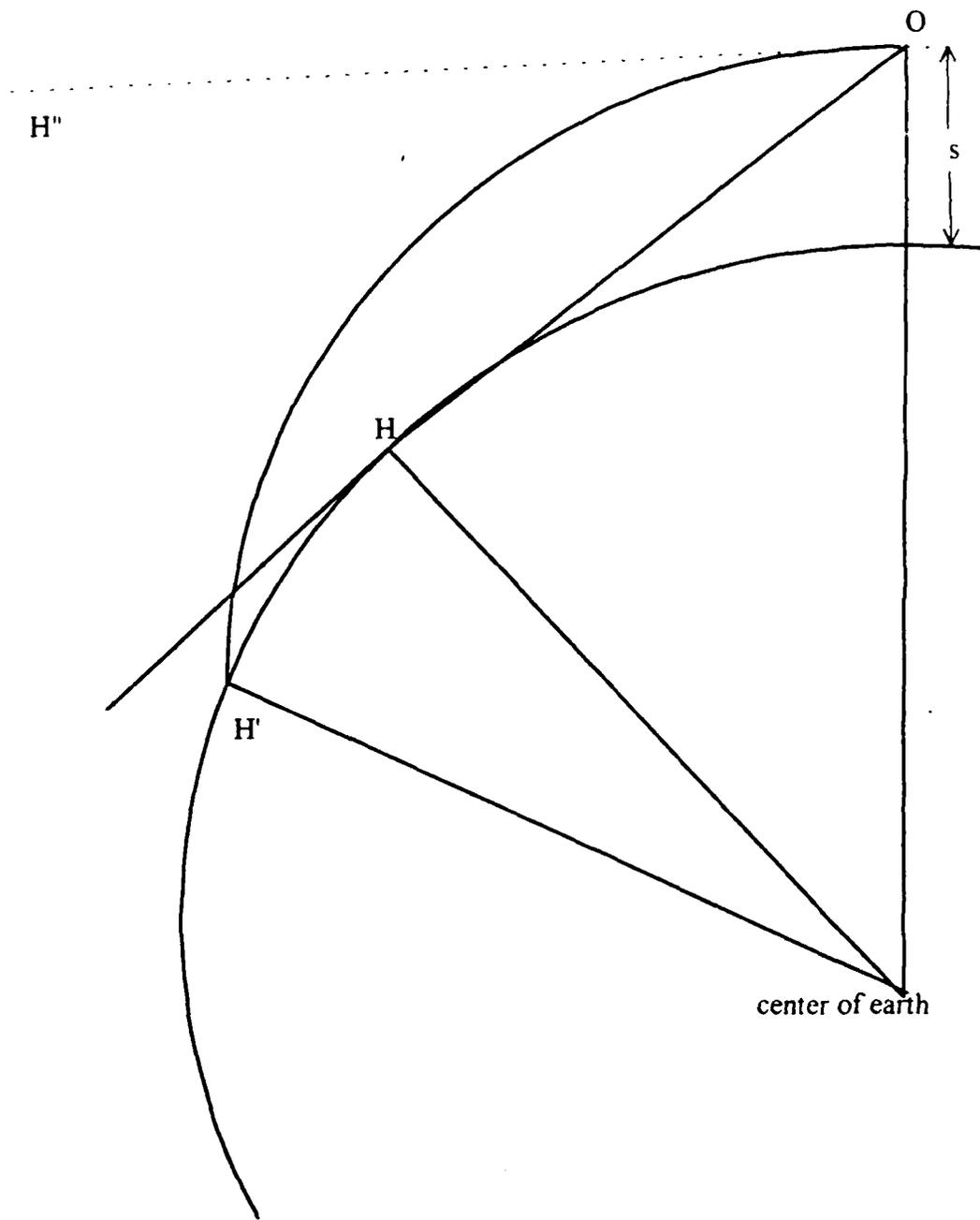
Figure 20: Horizon geometry and effects of refraction (After Ref. 18)
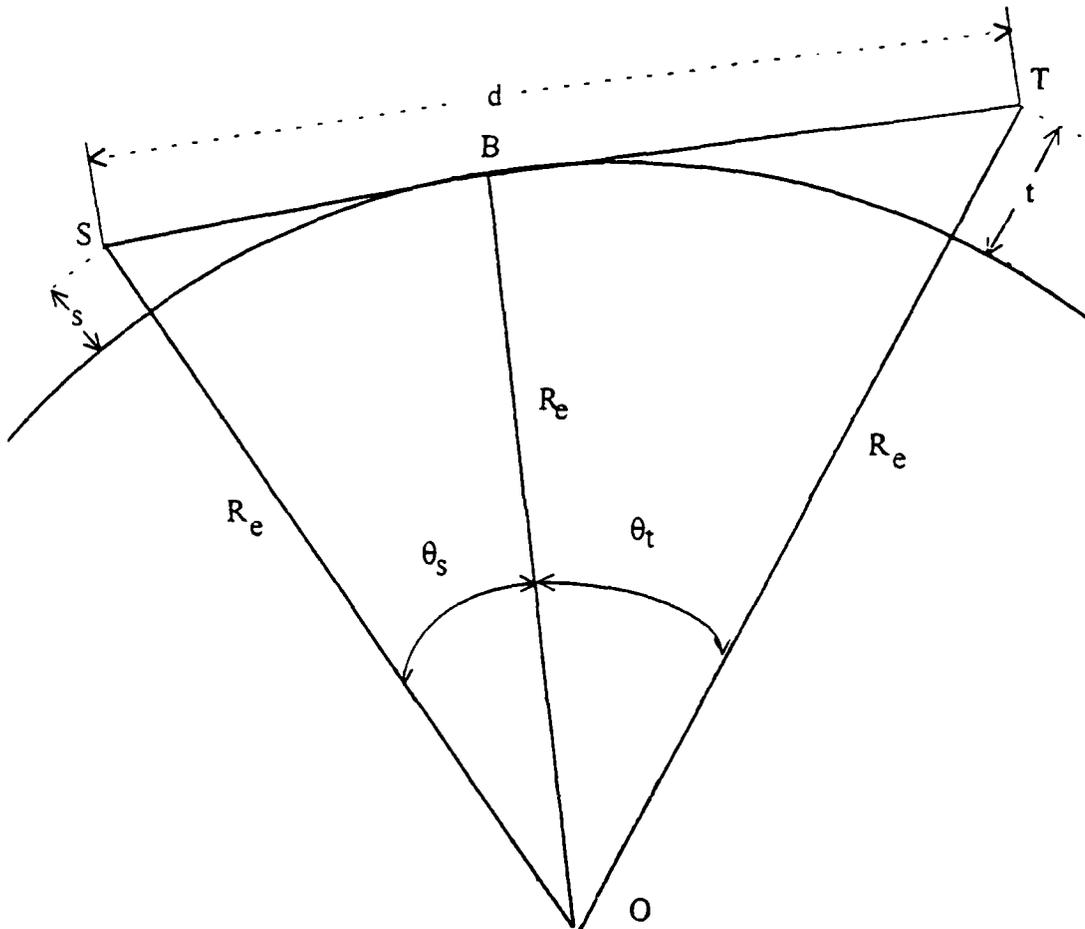
t = height of the target above surface (m)
s = height of the sensor above surface (m)
d = geomerical horizon (m)
R_e = radious of the earth (6.371x 10^6 meters)
O = center of the earth

Figure 21: Geometrical horizon geometry in case that both sensor and target are above the surface of the earth

detected range is limited by the geometric horizon (sum of absolutes)

range detected by the system

detected range

geometric horizon

long baseline length=100m

short baseline length=20m

height of the target above surface=10m

height of the sensor above surface=10m
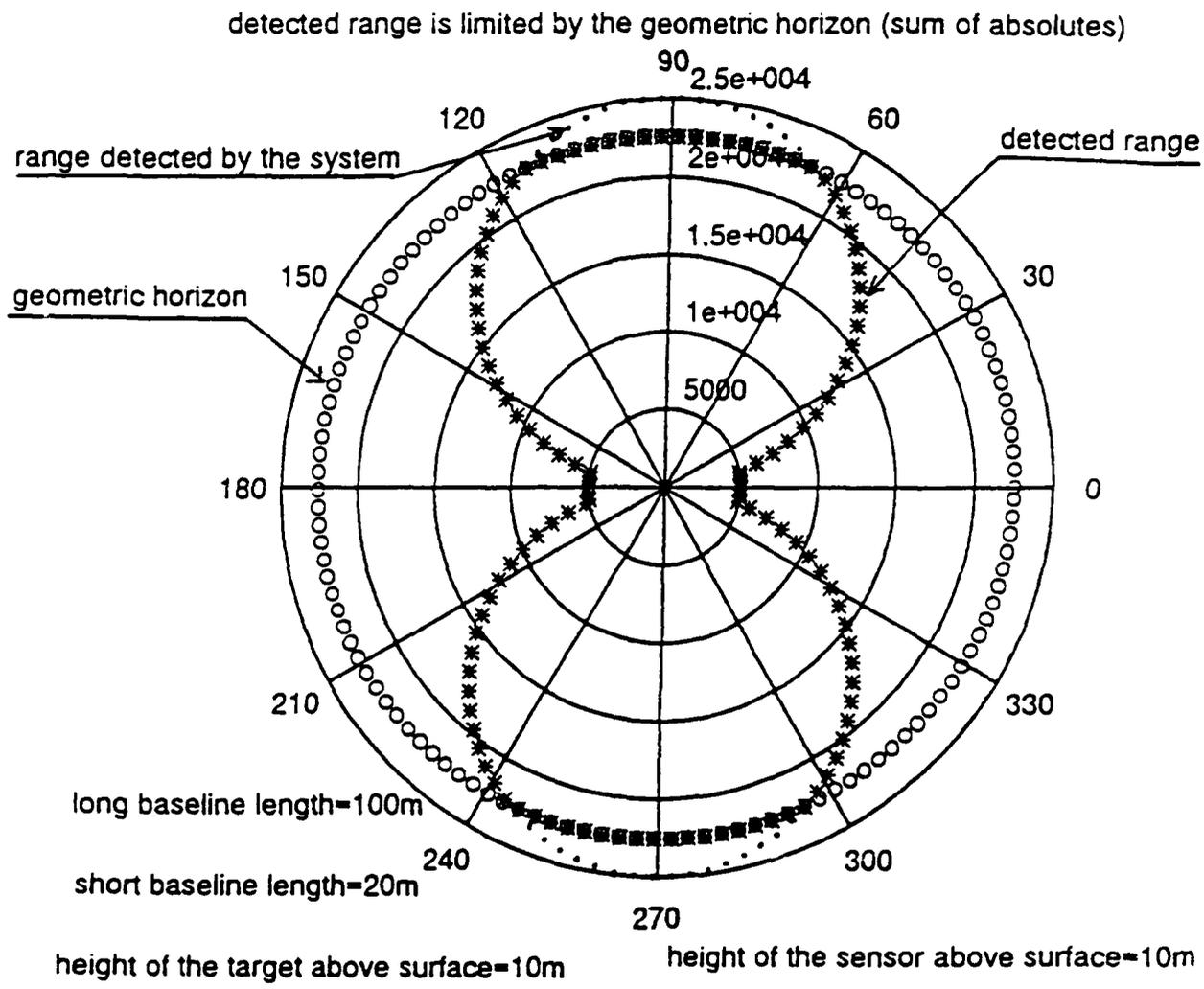
Figure 22a: The maximum measured range is limited due to geometric horizon in 22,480 m instead of 25,000m that can be detected by the system. (based on the sum of absolutes and obtained via program in Appendix E. L)

detected range is limited by the system (sum of absolutes)

range detected by the system

geometric horizon

long baseline length=20m

short baseline length=4m

height of the target above surface=3m

height of the sensor above surface=3m
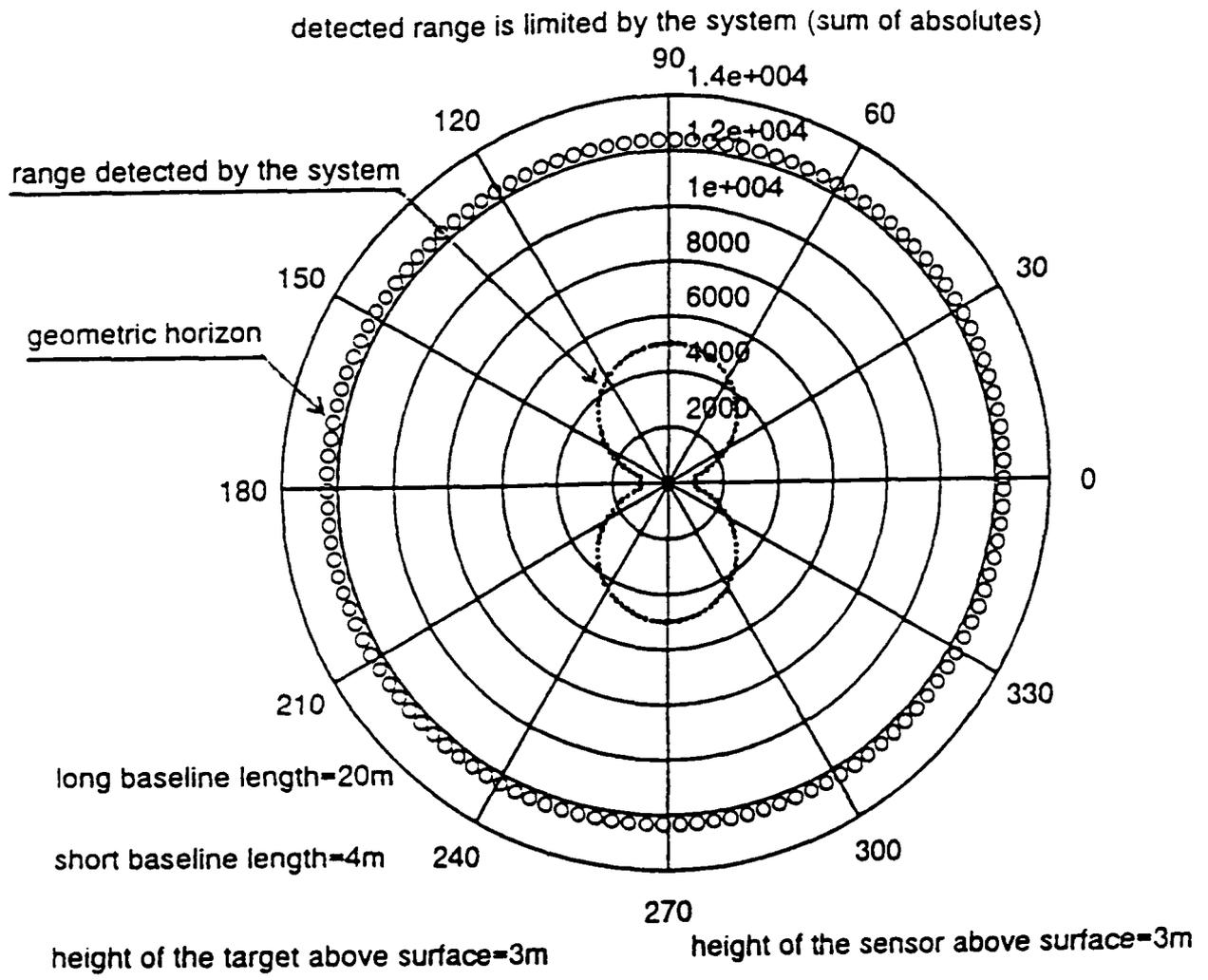
Figure 22b   The maximum detected range is limited to 5,000m due to the method. instead the 12.365m which is the geometric horizon (based on the sum of absolutes and obtained via program in Appendix E.L)

66

detected range is limited by the geometric horizon (quadrature addition)
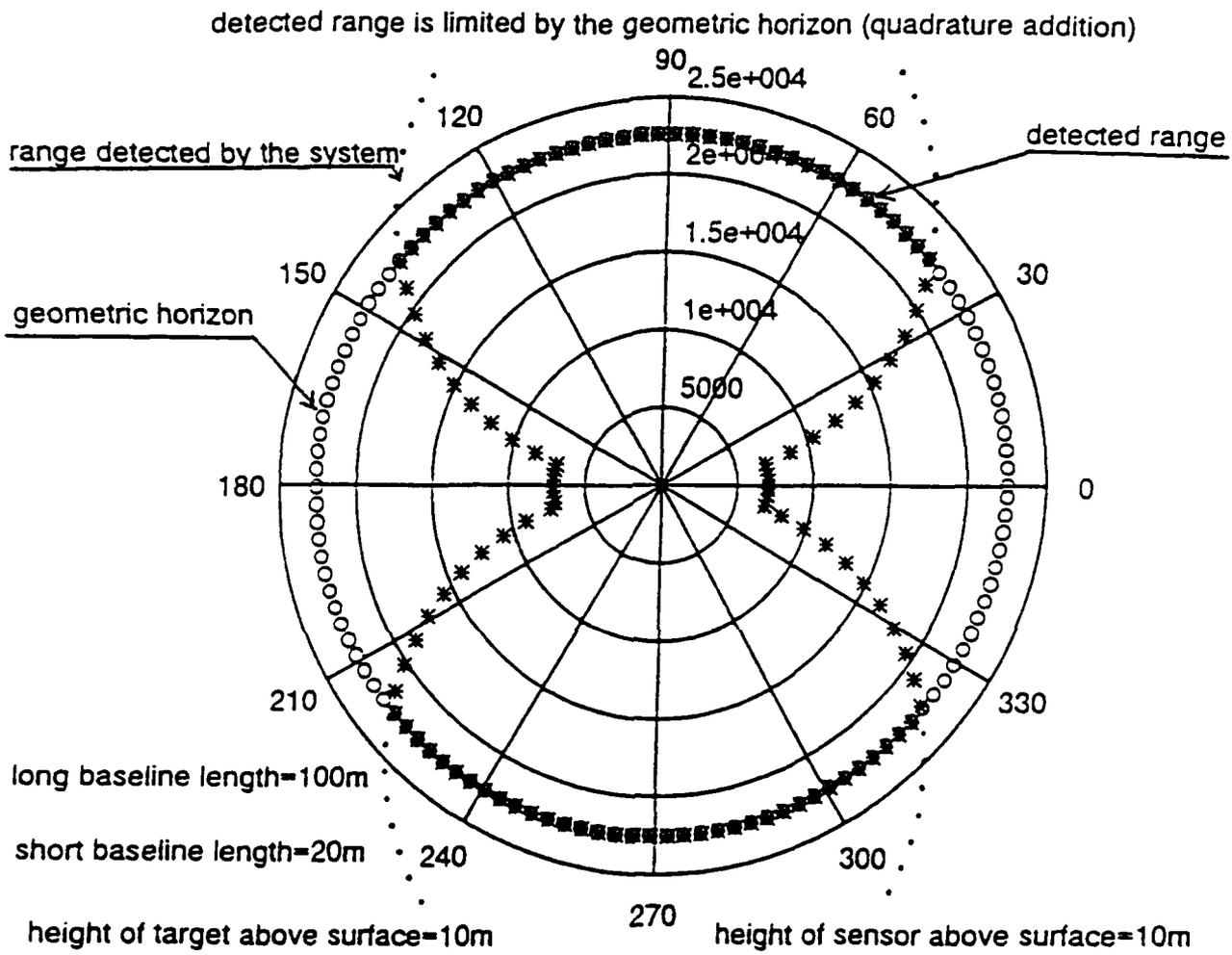
Figure 23a   The maximum measured range is limited due to geometric horizon in 22,480 m instead of 35,000m that can be detected by the system. (based on the quadrature addition of terms and obtained via program in Appendix E. M)

detected range is limited by the system (quadrature addition)

range detected by the system

geometric horizon

long baseline lenght=20m

short baseline length=4m

height of target above surface=3m

height of sensor above surface=3m
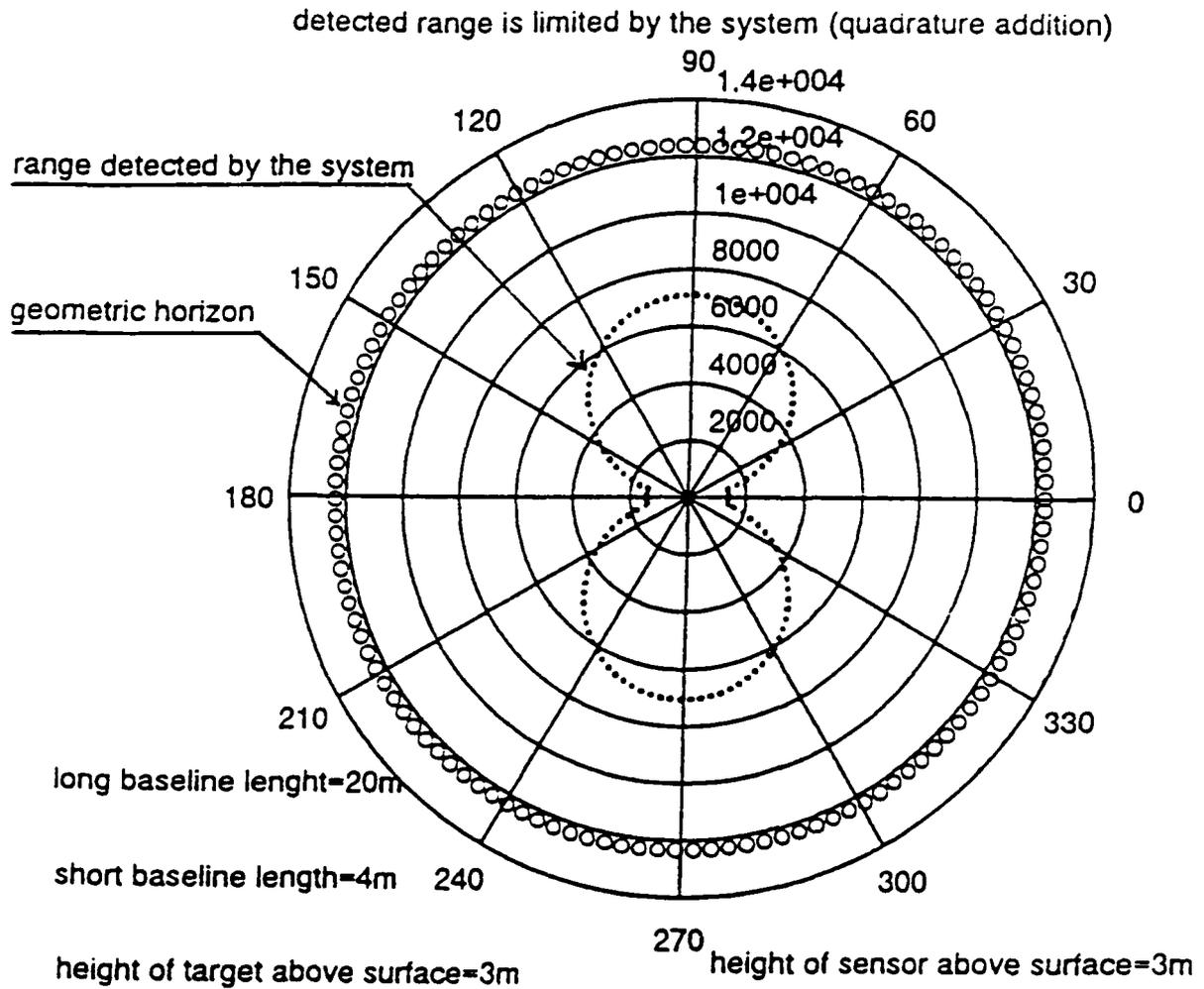
Figure 23b The maximum detected range is limited to 7,000m due to the method, instead the 12.365m which is the geometric horizon (based on the quadrature addition of terms and obtained via program in Appendix E.M)

VI. GENERALIZATION OF THE RESULTS FOR FIXED SENSITIVITY

A.   MOTIVATION

As seen in the previous chapter the condition for fixed sensitivity leads to polar curves for maximum triangulation range using both a LBL and a SBL. The crossing point for these curves, θ_{CROSS}, defines the complimentary application domains for the respective baselines. In this chapter some simple guidelines for predicting θ_{CROSS}, the maximum SBL range, R^S_{max} (at $\theta=0°$), and the maximum LBL range, R^L_{max} (at $\theta=90°$), are derived. This is done for the quadrature addition of terms and the more conservative sum of absolutes.

B.   A SIMPLE FORMULA FOR THE LBL & SBL CROSSOVER

1.   Analysis for the sum of the absolutes

It is observed that in the crossover points of the LBL and SBL polar plots the normalized range in respect to LBL for both baselines has to be equal. That means

$$\frac{R_{LBL}}{LBL} = \frac{R_{SBL}}{LBL} \tag{70a}$$

Taking into account (61), and (62), (70a) becomes

$$\sqrt{\sin^2(\theta)\frac{(c^L)^2+(1+a^L)^2}{(1+a^L)^2}} = \sqrt{\cos^2(\theta)\frac{(c^S)^2+(1+a^S)^2}{(1+a^S)^2}\left(\frac{SBL}{LBL}\right)^2} \tag{70b}$$

69

or

$$\sin^2(\theta)\frac{(c^L)^2+(1+a^L)^2}{(1+a^L)^2} = \cos^2\frac{(c^S)^2+(1+a^S)^2}{(1+a^S)^2}\left(\frac{SBL}{LBL}\right)^2 \qquad (70c)$$

Furthermore (70c) becomes

$$\tan^2(\theta) = \left(\frac{SBL}{LBL}\right)^2 \frac{\frac{(c^S)^2+(1+a^S)^2}{(1+a^S)^2}}{\frac{(c^L)^2+(1+a^L)^2}{(1+a^L)^2}} \qquad (71)$$

Normally in (71), the terms of the form $(c^{L/S})^2$ are much bigger than the terms of the form $(1+a^{L/S})^2$ and dominate, so (71) can be written

$$\tan^2(\theta) \cong \left(\frac{SBL}{LBL}\right)^2 \frac{(c^L)^2}{(c^S)^2} \qquad (72)$$

For the typical case when $c^L=c^S=c$, Equation (72) becomes

$$\tan(\theta) \cong \left(\frac{SBL}{LBL}\right) \qquad (73a, b)$$

and finally

$$\theta_{CROSS} \cong a\tan\left(\frac{SBL}{LBL}\right) \qquad (74)$$

It is worth noting for the correction of (70) that if $a^L=a^S$ and $c^L=c^S$ then (74) is exact

70

2. Analysis based on the quadrature addition of terms

Similarly to the previous case at the crossover points the normalized ranges of both baseline systems are equal. This implies that

$$\left(\frac{R_{LBL}}{LBL}\right)^2 = \left(\frac{R_{SBL}}{LBL}\right)^2 \tag{75}$$

and finally after (63) and (65), (75) gives

$$\frac{(c^L)^2 \sin^2(\theta^L) - 0.5\cos^2(\theta^L)}{2} + \sin^2(\theta^L) = \left(\frac{(c^S)^2 \sin^2(\theta^S) - 0.5\cos^2(\theta^S)}{2} + \sin^2(\theta^S)\right)\left(\frac{SBL}{LBL}\right)^2 \tag{76}$$

and after (24), and (25), (76) become

$$\frac{(c^L)^2 \sin^2(\theta) - 0.5\cos^2(\theta)}{2} + \sin^2(\theta) = \left(\frac{(c^S)^2 \cos^2(\theta) - 0.5\sin^2(\theta)}{2} + \cos^2(\theta)\right)\left(\frac{SBL}{LBL}\right)^2 \tag{77}$$

or

$$\frac{(c^L)^2 \sin^2(\theta) - 0.5\left(1 - \sin^2(\theta)\right)}{2} + \sin^2(\theta) = \left(\frac{(c^S)^2\left(1 - \sin^2(\theta)\right) - 0.5\sin^2(\theta)}{2} + \left(1 - \sin^2(\theta)\right)\right)\left(\frac{SBL}{LBL}\right)^2 \tag{78}$$

After assuming that $c^L = c^S = c$ and substituting $\sin^2(\theta)$ with "y," in (78), it follows that

$$0.5c^2 y - 0.25 + 1.25y = (0.5c^2 - 0.5c^2 y + 1 - 1.25y)\left(\frac{SBL}{LBL}\right)^2 \tag{79a}$$

71

and finally

$$\left(0.5c^2 + 1.25 + 0.5c^2\left(\tfrac{SBL}{LBL}\right)^2 + 1.25\left(\tfrac{SBL}{LBL}\right)^2\right)y = 0.25 + 0.5c^2\left(\tfrac{SBL}{LBL}\right)^2 + \left(\tfrac{SBL}{LBL}\right)^2 \qquad (79b)$$

Solving for "y," that is $\sin^2(\theta)$, and after back substitution into (77), it follows that

$$\sin^2(\theta) = \frac{0.25 + 0.5c^2\left(\tfrac{SBL}{LBL}\right)^2 + \left(\tfrac{SBL}{LBL}\right)^2}{1.25 + 0.5c^2 + 0.5c^2\left(\tfrac{SBL}{LBL}\right)^2 + 1.25\left(\tfrac{SBL}{LBL}\right)^2} \qquad (80)$$

It can be observed at this point, that after dividing both terms of the ratio by c^2 and neglecting the very small terms that follow, (78) becomes

$$\sin^2(\theta) = \frac{0.5\left(\tfrac{SBL}{LBL}\right)^2}{0.5 + 0.5\left(\tfrac{SBL}{LBL}\right)^2} \qquad (81a)$$

or

$$\sin(\theta) \approx \frac{\left(\tfrac{SBL}{LBL}\right)}{\sqrt{1 + \left(\tfrac{SBL}{LBL}\right)^2}} \qquad (81b)$$

and finally

$$\theta_{CROSS} \cong a\sin\left(\frac{1}{\sqrt{\left(\tfrac{LBL}{SBL}\right)^2 + 1}}\right) \cong a\tan\left(\tfrac{SBL}{LBL}\right) \qquad (82)$$

72

3. Observations

After the analysis of both methods have been completed the very obvious result is that the crossover point depends only on the ratio of the two baselines and it is approximately independent of the range sensitivity factor c. To demonstrate the above statement the more exact (80) and the approximate (82) crossover angle is plotted in Figure 24 for a fixed baselines ratio $SBL/LBL=0.2$ versus the variable normalized range sensitivity. The approximate form (82) is nearly equivalent to (80).

C. SIMPLE SCALING FORMULA FOR DUAL BASELINE MODEL RANGES

1. Analysis for the sum of the absolutes

As seen in Chapter IV the sensitivity-fixed triangulated ranges, normalized by the LBL, become maximum at the angle of 90°, measured with respect to each baseline. This maximum normalized range can be evaluated from expressions (61) and (62) for the long and short baselines respectively, as follow

$$\frac{R_{LBL(max)}}{LBL}\bigg|_{\theta^L=90^\circ} = \sqrt{\frac{(c^L)^2+(1+a^L)^2}{(1+a^L)^2}} \tag{83a}$$

and

$$\frac{R_{SBL(max)}}{LBL}\bigg|_{\theta^S=90^\circ} = \sqrt{\frac{(c^S)^2+(1+a^S)^2}{(1+a^S)^2}\left(\frac{SBL}{LBL}\right)^2} \tag{83b}$$

After assuming that $c^L=c^S=c$, and $a^L=a^S=1$, (81) becomes

73

$$\frac{R_{LBL(max)}}{LBL} = \sqrt{\frac{c^2+1}{4}} \quad \text{and} \quad \frac{R_{SBL(max)}}{LBL} = \sqrt{\frac{c^2+1}{4}\left(\frac{SBL}{LBL}\right)^2} \qquad \text{(84a, b)}$$

2. Analysis for the quadrature addition of terms

Following the same procedure described above (63), and (64) give

$$\frac{R_{LBL(max)}}{LBL}\bigg|_{\theta^L=90^\circ} = \sqrt{\frac{(c^L)^2}{2}+1} \qquad \text{(85a)}$$

and

$$\frac{R_{SBL(max)}}{LBL}\bigg|_{\theta^S=90^\circ} = \sqrt{\left(\frac{(c^L)^2}{2}+1\right)\left(\frac{SBL}{LBL}\right)^2} \qquad \text{(85b)}$$

Finally supposing $c^L=c^S=c$, (83) follows that

$$\frac{R_{LBL(max)}}{LBL} = \sqrt{\frac{c^2+1}{2}} \quad \text{and} \quad \frac{R_{SBL(max)}}{LBL} = \sqrt{\left(\frac{c^2+1}{2}\right)\left(\frac{SBL}{LBL}\right)^2} \qquad \text{(86a, b)}$$

As expected, a factor of $2^{1/2}$ increase in the less conservative quadrature addition of the terms is seen by comparing with (84).

3. Observations

The most obvious result of the analysis above is that the scale of the R_{max} curves increases linearly with the normalized range sensitivity. More specifically for the sum of absolutes paradigm the maximum ranges satisfy the following rules of thumb

74

$$R_{LBL}(m) \cong \frac{c}{2} \times LBL(m) \qquad \text{and} \qquad R_{SBL}(m) \cong \frac{c}{2} \times SBL(m) \qquad \text{(87a, b)}$$

Similarly, for the quadrature addition of terms paradigm the maximum ranges satisfy the following relations

$$R_{LBL}(m) \cong \frac{c}{\sqrt{2}} \times LBL(m) \qquad \text{and} \qquad R_{SBL}(m) \cong \frac{c}{\sqrt{2}} \times SBL(m) \qquad \text{(88a, b)}$$

For both paradigms the crossover angle is given by the rule of thumb

$$\theta_{CROSS} \cong a\tan\left(\frac{SBL}{LBL}\right) \qquad \text{(89)}$$

The general characteristics of the dual baseline triangulated ranges and baseline crossing points are shown on Figure 25.

comparison crossover angle approximations
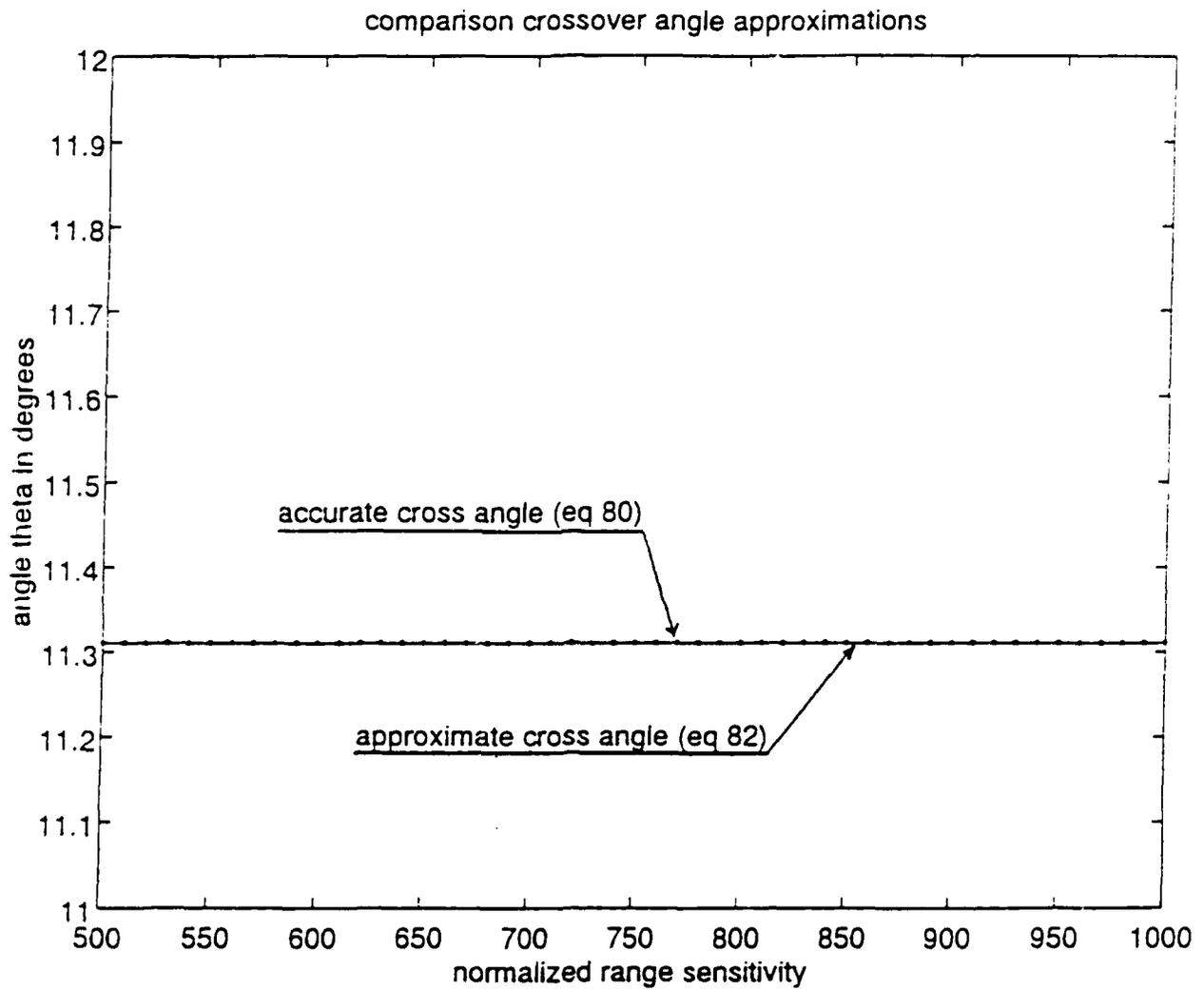
Figure 24a   Crossover angle of long and short baseline based on the accurate expression
(80) and the approximate expression (82). There is not discrepancy betw een
them in this area of the scale of the y axis. (via program in Appendix E. N)

76

comparison between crossover angle approximations
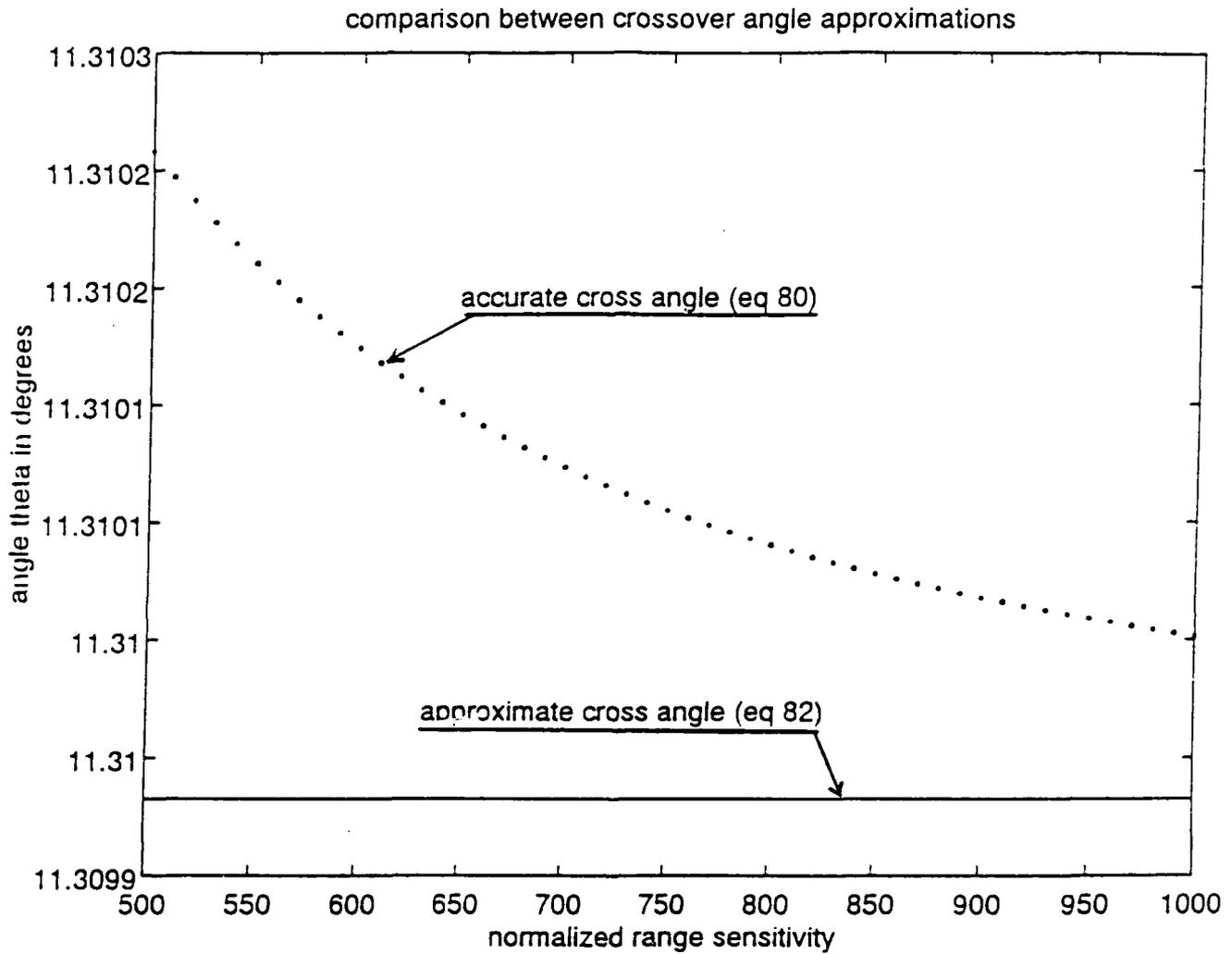
Figure 24b: Crossover angle of long and short baseline based on the accurate expression (80) and the approximate expression (82). The discrepancy between the two expressions becomes obvious as the scale on the y axis goes to the third decimal point. (via program in Appendix E. N)

$$\frac{R_{LBL(max)}}{LBL} \cong \frac{c}{2} \qquad \text{case A}$$

$$\frac{R_{LBL(max)}}{LBL} \cong \frac{c}{\sqrt{2}} \qquad \text{case B}$$

$$\theta_{CROSS} \cong atan\left(\frac{SBL}{LBL}\right)$$

$$\frac{R_{SBL(max)}}{LBL} \cong \frac{c}{2}\cdot\left(\frac{SBL}{LBL}\right) \qquad \text{case A}$$

$$\frac{R_{SBL(max)}}{LBL} \cong \frac{c}{\sqrt{2}}\cdot\left(\frac{SBL}{LBL}\right) \qquad \text{case B}$$
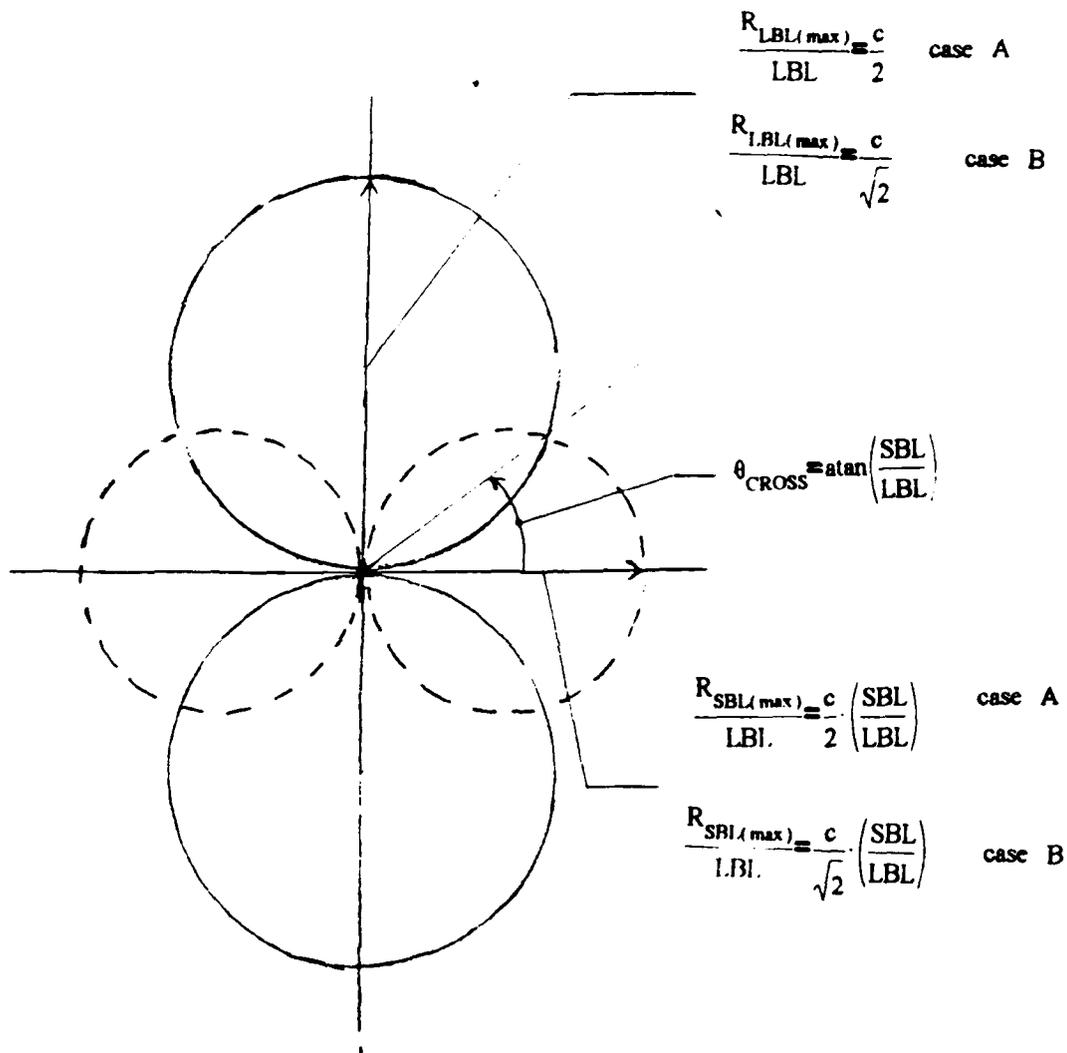
(case A : sum of absolutes , case B : quadrature addition of terms)

Figure 25 : Properties which characterize the performance of the dual baseline triangula-
tion scheme. The maximum normalized range which can be detected by the
system is linearly dependent on the sensitivity. The crossover angle of the
long and short baseline approximately depends only on the ratio of the two
baselines.

78

VII. CONCLUSIONS

A. RESULTS OF THE WORK

A dual baseline scheme based on the triangulation principle proposed for passive

range measurements was presented and its performance was examined in this work. In

Chapter II the approximations on which the proposed model was based were examined,

and the general characteristics of the triangulation principle were reviewed. The conclu-

sion was that the approximations $R>>BL$, and $R=R_1=R_2$ have not noticeably changed the

accuracy of the model, and that for angles close to $0°$ and $180°$ due to "geometric dilution"

no range measurements can be performed. Furthermore it was shown that the precision in

the range measurement was dependent on the precision in the bearing measurement. Lastly

it was shown that the more distant the target to be triangulated is from the baseline the

more inaccurate the measurement. In Chapter III, feasible modeling for a dual baseline tri-

angulation scheme was examined. It was shown that two orthogonal baselines eliminate

the "geometric dilution" problem and that, in general, the larger baseline will have a

higher measurement accuracy. Finally, for further study of the characteristics of the dual

baseline scheme two gauges were proposed. The first one is based on the quadrature addi-

tion of the terms which express the range sensitivity of each sensor for each baseline, and

the second one is approximate and is based on the sum of absolutes of the same terms. It

was shown in Appendix D that the latest one is more conservative with respect to the er-

ror in the range measurement, and it can be used for arbitrary bearing precision of the

sensors. Instead, the less conservative quadrature addition of terms can be used only for the case when the sensors have the same bearing precision. In Chapter IV the performance of the dual baseline model was studied by the above mentioned gauges through the polar plots of the normalized range versus the target orientation angle. The conclusion from this chapter was that with the use of the conservative sum of absolutes the predicted maximum range is $2^{1/2}$ less than the range predicted by the quadrature addition of terms. In Chapter V the physical limitation in the range measurements due to optical horizon was considered. The effect of refraction introduces a complicated situation in the prediction of the optical horizon. Thus, a more conservative estimation for the optical horizon based on the geometrical consideration alone was taken. It was shown in this chapter that the predicted maximum range depends more generally on sensor and target height above the earth's surface, and the ratio of the two baseline lengths. Therefore the range measurement can be limited either due to the optical horizon or the dual baseline system. In Chapter VI the general features of the polar plots that are characteristics of the dual baseline method were considered. It was shown that the maximum range scales with the range sensitivity of the baselines. In the case when the normalized sensitivity in both baselines is the same then the general appearance of the two curves will depend only on the ratio of the long baseline to the short baseline. More specifically, the crossover angle of the two curves, to a high degree of approximation, depends only on the ratio of the two baselines, and it is independent of the range sensitivities.

B.   FUTURE DEVELOPMENTS

The dual baseline model was studied under the assumption that the mean bearing error was zero, but in the real world that is not true. Thus future work is needed to enhance the model to handle systematic errors in the bearing measurements. This future work could employ the "circulation method" instead of triangulation. A second point for future development could be the implementation of the dual baseline model with some "smart electronics" which would switch between baselines at a performance crossover point .

APPENDIX A: LIST OF SYMBOLS

A. SYMBOLS IN ENGLISH

BL: the baseline (platform length) in the triangulation method (m)

c: normalized range sensitivity in triangulation method

$c^{L/S}$: normalized range sensitivity in long/short baseline

d: distance to the geometrical horizon (m)

LBL: the long baseline in the dual baseline triangulation scheme (m)

R: the range from the middle of the baseline to the target (m)

R_e: radious of the earth (6.371×10^6 meters)

R_{LBL}: *the range from the middle of the long baseline to the target* (m)

R_{SBL}: the range from the middle of the short baseline to the target (m)

$R_{1/2}$: the range from the first second sensor to the target (m)

SBL: the short baseline in the dual baseline triangulation scheme (m)

s: height of the sensor above the surface of the earth (m)

t: height of the target above the surface of the earth (m)

B. SYMBOLS IN GREEK

a : ratio of the mean values of the bearing errors in the triangulation method

$a^{L/S}$: ratio of the mean values of the bearing errors in long/short baseline

$\Delta\theta_{1/2}$: bearing error of the first/second sensor (rad)

82

θ : the target orientation angle measured from the middle of the baseline (degrees)

$\theta^{L,S}$: angle to the target measured from the middle of both baseline (degrees)

$\theta_{1,2}$: angle to the target measured from the first/second sensor (degrees)

$x_{1,2}^{L,S}$: independent random variable having zero mean and unity standard deviation in

long/short baseline in respect of first/second sensor

APPENDIX B: MATHEMATICAL PROOFS

A.   SINGLE BASELINE MODEL

1.   Single baseline model analysis

The distance from the middle of the baseline to the target given by Equation (4) is repeated here

$$R = \frac{BL}{2}\left(\frac{\sin\theta_2\sqrt{1-\left(\frac{BL}{2R}\sin\theta_1\right)^2}+\sin\theta_1\sqrt{1-\left(\frac{BL}{2R}\sin\theta_2\right)^2}}{\sin(\theta_2-\theta_1)}\right)$$
(B. 1)

The derivatives of (B.1) with respect θ_1, and θ_2 are respectively

$$\frac{dR}{d\theta_1} \cong \frac{BL}{2}\left[\frac{\cos\theta_1}{\sin(\theta_2-\theta_1)}\left(\sqrt{1-\left(\frac{BL}{2R}\sin\theta_2\right)^2}-\frac{\left(\frac{BL}{2R}\right)^2\sin\theta_1\sin\theta_2}{\sqrt{1-\left(\frac{BL}{2R}\sin\theta_1\right)^2}}\right)-g(\theta_1,\theta_2,R)\right]$$
(B. 2)

$$\frac{dR}{d\theta_2} \cong \frac{BL}{2}\left[\frac{\cos\theta_2}{\sin(\theta_2-\theta_1)}\left(\sqrt{1-\left(\frac{BL}{2R}\sin\theta_1\right)^2}-\frac{\left(\frac{BL}{2R}\right)^2\sin\theta_1\sin\theta_2}{\sqrt{1-\left(\frac{BL}{2R}\sin\theta_2\right)^2}}\right)+g(\theta_1,\theta_2,R)\right]$$
(B. 3)

where

$$g(\theta_1,\theta_2,R) = \frac{\cos(\theta_2-\theta_1)}{\sin^2(\theta_2-\theta_1)}\left(\sin\theta_2\sqrt{1-\left(\frac{BL}{2R}\sin\theta_1\right)^2}+\sin\theta_1\sqrt{1-\left(\frac{BL}{2R}\sin\theta_2\right)^2}\right)$$
(B. 4)

84

and

$$\Delta R = \frac{dR}{d\theta_1}\Delta\theta_1 + \frac{dR}{d\theta_2}\Delta\theta_2 \tag{B.5}$$

The expressions (B.2), (B.3), and (B. 4) above are approximate because the derivatives of the small terms proportional to $(BL/R)^2$ on the RHS of Eq. (B.1) have not been included. The terms

$$\frac{\sqrt{1-\left(\frac{BL}{2R}\sin\theta_2\right)^2}}{\sin(\theta_2-\theta_1)} \quad \text{and} \quad \frac{\sin\theta_2\sqrt{1-\left(\frac{BL}{2R}\sin\theta_1\right)^2}}{\sin(\theta_2-\theta_1)} \tag{B.6}$$

can be factored out of Equations (B.2), and (B.4). Also the terms

$$\frac{\sqrt{1-\left(\frac{BL}{2R}\sin\theta_1\right)^2}}{\sin(\theta_2-\theta_1)} \quad \text{and} \quad \frac{\sin\theta_1\sqrt{1-\left(\frac{BL}{2R}\sin\theta_2\right)^2}}{\sin(\theta_2-\theta_1)} \tag{B.7}$$

can be factored out between Equations (B.3), and (B.4). Then Equation (B.2), after Equation (B.6), becomes

$$\frac{dR}{d\theta_1} = (f_1 + f_2) \tag{B.8a}$$

where

$$f_1 = \frac{\sqrt{1-\left(\frac{BL}{2R}\sin\theta_2\right)^2}}{\sin(\theta_2-\theta_1)}(\cos\theta_1 + \sin\theta_1\cot(\theta_2-\theta_1)) \tag{B.8b}$$

85

and

$$f_2 = \frac{\sin\theta_2 \sqrt{1-\left(\frac{BL}{2R}\sin\theta_1\right)^2}}{\sin(\theta_2-\theta_1)} \left(\cot(\theta_2 - \theta_1) - \frac{\left(\frac{BL}{2R}\right)^2 \sin\theta_1\cos\theta_1}{1-\left(\frac{BL}{2R}\sin\theta_1\right)^2} \right) \tag{B. 8c}$$

Similarly, Equation (B.3), after Equation (B.7), becomes

$$\frac{dR}{d\theta_2} = \left(f_1' + f_2' \right) \tag{B. 9a}$$

where

$$f_1' = \frac{\sqrt{1-\left(\frac{BL}{2R}\sin\theta_1\right)^2}}{\sin(\theta_2-\theta_1)} (\cos\theta_2 - \sin\theta_2\cot(\theta_2 - \theta_1)) \tag{B. 9b}$$

and

$$f_2' = -\frac{\sqrt{1-\left(\frac{BL}{2R}\sin\theta_2\right)^2}}{\sin(\theta_2-\theta_1)} \left(\cot(\theta_2 - \theta_1) + \frac{\left(\frac{BL}{2R}\right)^2 \sin\theta_2\cos\theta_2}{1-\left(\frac{BL}{2R}\sin\theta_2\right)^2} \right) \tag{B. 9c}$$

Equation (B. 5), after (B. 8), (B.9), and after dividing by (B.1), becomes

$$\frac{\Delta R}{R} = \left(\frac{\sqrt{1-\left(\frac{BL}{2R}\sin\theta_2\right)^2}(\cos\theta_1+\sin\theta_1\cot(\theta_2-\theta_1))+\sin\theta_2\sqrt{1-\left(\frac{BL}{2R}\sin\theta_1\right)^2}\left(\cot(\theta_2-\theta_1)-\frac{\left(\frac{BL}{2R}\right)^2\sin\theta_1\cos\theta_1}{1-\left(\frac{BL}{2R}\sin\theta_1\right)^2}\right)}{\sin\theta_2\sqrt{1-\left(\frac{BL}{2R}\sin\theta_1\right)^2}+\sin\theta_1\sqrt{1-\left(\frac{BL}{2R}\sin\theta_2\right)^2}} \right) \cdot (\Delta\theta_1) +$$

86

$$\left(\frac{\sqrt{1-\left(\frac{BL}{2R}\sin\theta_1\right)^2}\ (\cos\theta_2-\sin\theta_2\cot(\theta_2-\theta\ ))-\sin\theta_1\sqrt{1-\left(\frac{BL}{2R}\sin\theta_2\right)^2}\left(\cot(\theta_2-\theta_1)+\frac{\frac{BL}{2R}^2\sin\theta_2\cos\theta_2}{1-\frac{BL}{2R}\sin\theta_2}^2\right)}{\sin\theta_2\sqrt{1-\left(\frac{BL}{2R}\sin\theta_1\right)^2}+\sin\theta_1\sqrt{1-\left(\frac{BL}{2R}\sin\theta_2\right)^2}} \right) \cdot (\Delta\theta_2) \quad \text{(B. 10)}$$

as cited in the main text.

2.   Single baseline model analysis (R>>BL)

A reasonable assumption that R>>BL can be made, and it follows from Equation (4) that

$$R \cong \frac{BL}{2}\left(\frac{\sin\theta_2+\sin\theta_1}{\sin(\theta_2-\theta_1)} \right) \quad \text{(B. 11)}$$

The derivatives of (B.11) with respect θ_1, and θ_2 are

$$\frac{dR}{d\theta_1} = \frac{BL}{2}\left(\frac{\cos\theta_1}{\sin(\theta_2-\theta_1)} - g'(\theta_1,\theta_2) \right) \quad \text{(B. 12)}$$

and

$$\frac{dR}{d\theta_2} = \frac{BL}{2}\left(\frac{\cos\theta_2}{\sin(\theta_2-\theta_1)} - g'(\theta_1,\theta_2) \right) \quad \text{(B. 13)}$$

87

where

$$g'(\theta_1, \theta_2) = \frac{\cos(\theta_2 - \theta_1)(\sin\theta_1 + \sin\theta_2)}{\sin^2(\theta_2 - \theta_1)} \qquad \text{(B.14)}$$

Equations (B.12), and (B.13) after (B.14) can be re-expressed as follow

$$\frac{dR}{d\theta_1} = \frac{BL}{2}\frac{1}{\sin(\theta_2 - \theta_1)}(\cos\theta_1 + \cot(\theta_2 - \theta_1)(\sin\theta_1 + \sin\theta_2)) \qquad \text{(B.15)}$$

and

$$\frac{dR}{d\theta_2} = \frac{BL}{2}\frac{1}{\sin(\theta_2 - \theta_1)}(\cos\theta_2 - \cot(\theta_2 - \theta_1)(\sin\theta_2 - \sin\theta_1)) \qquad \text{(B.16)}$$

Combining Equations (B.15), and (B.16), and after dividing by (B.11) leads to

$$\frac{\Delta R}{R} = \left(\frac{\cos\theta_1}{\sin\theta_2 + \sin\theta_1} + \cot(\theta_2 - \theta_1)\right) \cdot (\Delta\theta_1) + \left(\frac{\cos\theta_2}{\sin\theta_2 + \sin\theta_1} - \cot(\theta_2 - \theta_1)\right) \cdot (\Delta\theta_2) \quad \text{(B.17)}$$

as cited in the main text.

B.   DUAL BASELINE MODEL

Following the substitutions suggested by Equations (23), (24), (26), and (27) the expressions for $\left(\frac{\Delta R}{R}\frac{1}{\Delta\theta}\right)^L$, and $\left(\frac{\Delta R}{R}\frac{1}{\Delta\theta}\right)^S$ are obtained for the various approximation cases of the dual baseline model analysis introduced in Chapter III.

1. Dual baseline model analysis

a. Long baseline (LBL)

$$\left(\frac{\Delta R}{R}\frac{1}{\Delta\theta}\right)^{L} = \left\{\frac{\sqrt{1-\left(\frac{LBL}{2R}\sin\theta_2^L\right)^2}\left(\cos\theta_1^L+\sin\theta_1^L\cot\left(\theta_2^L-\theta_1^L\right)\right)+\sin\theta_2^L\sqrt{1-\left(\frac{LBL}{2R}\sin\theta_1^L\right)^2}\left(\cot\left(\theta_2^L-\theta_1^L\right)-\frac{\left(\frac{LBL}{2R}\right)^2\sin\theta_1^L\cos\theta_1^L}{1-\left(\frac{LBL}{2R}\sin\theta_1^L\right)^2}\right)}{\sin\theta_2^L\sqrt{1-\left(\frac{LBL}{2R}\sin\theta_1^L\right)^2}+\sin\theta_1^L\sqrt{1-\left(\frac{LBL}{2R}\sin\theta_2^L\right)^2}}\right\}\chi_1^L +$$

$$+\left\{\frac{\sqrt{1-\left(\frac{LBL}{2R}\sin\theta_1^L\right)^2}\left(\cos\theta_2^L+\sin\theta_2^L\cot\left(\theta_2^L-\theta_1^L\right)\right)-\sin\theta_1^L\sqrt{1-\left(\frac{LBL}{2R}\sin\theta_2^L\right)^2}\left(\cot\left(\theta_2^L-\theta_1^L\right)-\frac{\left(\frac{LBL}{2R}\right)^2\sin\theta_2^L\cos\theta_2^L}{1-\left(\frac{LBL}{2R}\sin\theta_2^L\right)^2}\right)}{\sin\theta_2^L\sqrt{1-\left(\frac{LBL}{2R}\sin\theta_1^L\right)^2}+\sin\theta_1^L\sqrt{1-\left(\frac{LBL}{2R}\sin\theta_2^L\right)^2}}\right\}\chi_2^L a^L \quad (B.18)$$

b. Short baseline (SBL)

$$\left(\frac{\Delta R}{R}\frac{1}{\Delta\theta}\right)^{S} = \left\{\frac{\sqrt{1-\left(\frac{SBL}{2R}\sin\theta_2^S\right)^2}\left(\cos\theta_1^S+\sin\theta_1^S\cot\left(\theta_2^S-\theta_1^S\right)\right)+\sin\theta_2^S\sqrt{1-\left(\frac{SBL}{2R}\sin\theta_1^S\right)^2}\left(\cot\left(\theta_2^S-\theta_1^S\right)-\frac{\left(\frac{SBL}{2R}\right)^2\sin\theta_1^S\cos\theta_1^S}{1-\left(\frac{SBL}{2R}\sin\theta_1^S\right)^2}\right)}{\sin\theta_2^S\sqrt{1-\left(\frac{SBL}{2R}\sin\theta_1^S\right)^2}+\sin\theta_1^S\sqrt{1-\left(\frac{SBL}{2R}\sin\theta_2^S\right)^2}}\right\}\chi_1^S +$$

$$+\left\{\frac{\sqrt{1-\left(\frac{SBL}{2R}\sin\theta_1^S\right)^2}\left(\cos\theta_2^S+\sin\theta_2^S\cot\left(\theta_2^S-\theta_1^S\right)\right)-\sin\theta_1^S\sqrt{1-\left(\frac{SBL}{2R}\sin\theta_2^S\right)^2}\left(\cot\left(\theta_2^S-\theta_1^S\right)-\frac{\left(\frac{SBL}{2R}\right)^2\sin\theta_2^S\cos\theta_2^S}{1-\left(\frac{SBL}{2R}\sin\theta_2^S\right)^2}\right)}{\sin\theta_2^S\sqrt{1-\left(\frac{SBL}{2R}\sin\theta_1^S\right)^2}+\sin\theta_1^S\sqrt{1-\left(\frac{SBL}{2R}\sin\theta_2^S\right)^2}}\right\}\chi_2^S \alpha^S \quad (B.19)$$

2. Dual baseline model (R>>BL)

a. Long baseline (LBL)

$$\left(\frac{\Delta R}{R}\frac{1}{\Delta\theta}\right)^{L} = \left(\frac{\cos\theta_1^L}{\sin\theta_2^L+\sin\theta_2^L}+\cot\left(\theta_2^L-\theta_1^L\right)\right)\cdot\chi_1^L + \left(\frac{\cos\theta_2^L}{\sin\theta_2^L+\sin\theta_1^L}-\cot\left(\theta_2^L-\theta_1^L\right)\right)\cdot\chi_2^L \cdot a^L \quad (B.20)$$

89

b.   Short baseline (SBL)

$$\left(\frac{\Delta R}{R}\frac{1}{\Delta H}\right)^{S} = \left(\frac{\cos\theta_1^S}{\sin\theta_2^S+\sin\theta_1^S} + \cot\left(\theta_2^S - \theta_1^S\right)\right)\cdot\chi_1^S + \left(\frac{\cos\theta_2^L}{\sin\theta_2^S+\sin\theta_1^S} - \cot\left(\theta_2^S - \theta_1^L\right)\right)\ \chi_2^S\cdot a^L \qquad \text{(B.21)}$$

APPENDIX C: EXACT EXPRESSION FOR THE RANGE

A. GENERALITIES

From Figure 2 the expression (3b), which relates the range of the target to the apex angles on the baseline, had been derived. Solving (3b) for R gives the exact expression that has to be used to solve the problem in the triangulation method.

B. ANALYSIS

In order to simplify the notation the following definitions are introduced

$$sx \equiv \sin(\theta_2 - \theta_1) \qquad \text{(C. 1a)}$$

$$sy \equiv \sin\theta_2 \qquad \text{(C. 1b)}$$

$$sw \equiv \sin\theta_1 \qquad \text{(C. 1c)}$$

Then from (3b)

$$sx = \frac{BL}{2R}\left(sy \cdot \sqrt{1 - \left(\frac{BL}{2R} \cdot sw\right)^2} + sw \cdot \sqrt{1 - \left(\frac{BL}{2R} \cdot sy\right)^2} \right) \qquad \text{(C. 2)}$$

After substituting

$$Z = \left(\frac{BL}{2R}\right) \qquad \text{(C. 3)}$$

symbolic processing using MAPLE [Ref.19], produces

$$4Z^4 sy^2(-1 + Z^2 sw^2)sw^2(-1 + Z^2 sy^2) = (Z^2 sy^2 - 2Z^4 sy^2 sw^2 + Z^2 sw^2 - sw^2)^2 \quad (C.4)$$

and then again symbolic processing produces the two solutions

$$(Z_1)^2 = \frac{1}{2} \frac{-2sx^2 sy^2 - 2sw^2 sx^2 + 4\sqrt{-sx^4 sy^2 sw^2(-1 + sx^2)}}{-4sw^2 sy^2 sx^2 - sy^4 + 2sw^2 sy^2 - sw^4} \quad (C.5a)$$

$$(Z_2)^2 = \frac{1}{2} \frac{-2sx^2 sy^2 - 2sw^2 sx^2 - 4\sqrt{-sx^4 sy^2 sw^2(-1 + sx^2)}}{-4sw^2 sy^2 sx^2 - sy^4 + 2sw^2 sy^2 - sw^4} \quad (C.5b)$$

It can be shown using MAXSYMA [Ref. 20], that the root (C. 5a) is real and (C. 5b) is imaginary. Therefore the exact expression for normalized range in terms of angles θ_1, and θ_2 is

$$\left(\frac{2R}{BL}\right) = \sqrt{2 \cdot \frac{-4sw^2 sy^2 sx^2 - sy^4 + 2sw^2 sy^2 - sw^4}{-2sx^2 sy^2 - 2sw^2 sx^2 + 4\sqrt{-sx^4 sy^2 sw^2(-1 + sx^2)}}} \quad (C.6)$$

92

APPENDIX D: RANGING ERROR IN TRIANGULATION METHOD

A.   GENERALITIES

In single triangulation the target lies at the intersection of the two lines that run from

the sensors. These two lines make angles with the baseline that vary due to mechanical

limitations of the sensors. The variation in the angles, $\Delta\theta_1$ and $\Delta\theta_2$, determine the varia-

tion in the measured range of the target.

B.   APPROXIMATE RANGING ERROR ANALYSIS

Figure 26 shows the geometry of range measurement in the single baseline triangula-

tion scheme. The quadrangle KLMN is established due to variation in the angles. The lines

DE, and FG have values ΔR_1 and ΔR_2 respectively, and approximately represent the un-

certainties in the range of the target from the sensors. The line MK represents the total un-

certainty due to the system and it has value ΔR. In first approximation the error

quadrangle can be treated as a parallelogram and the following relation is derived from

parallelogram on Figure 26

$$\Delta R_Q \cong \Delta R_{PARALLELOGRAM} \equiv \Delta R_P \qquad \qquad (D.\ 1)$$

or

$$\Delta R_P = \sqrt{(\Delta R_1)^2 + (\Delta R_2)^2 + 2|\Delta R_1| \cdot |\Delta R_2|\cos\phi} \qquad \qquad (D.\ 2)$$

93

where "ϕ" is the angle between ΔR_1 with ΔR_2.

For R>>BL, as shown in Figure 27, $\phi \cong 0°$, and therefore

$$\cos \phi \cong 1 \qquad\qquad (D.3)$$

Thus, it follows from Equation (D. 2) that

$$\Delta R_P - \Delta R < |\Delta R_1| + |\Delta R_2| \qquad\qquad (D.4)$$

and therefore via comparison with (D.2) it follows that

$$\sqrt{(\Delta R_1)^2 + (\Delta R_2)^2} \leq |\Delta R_1| + |\Delta R_2| \qquad\qquad (D.5)$$

In fact, under the case that

$$|\Delta R_1| = |\Delta R_2| \qquad\qquad (D.6)$$

e.g. at a point of symmetry, and

$$\cos \phi \cong 1 \qquad\qquad (D.7)$$

the sum of quadratures estimate will be $2^{1/2}$ smaller than the sum of absolutes. So, in general, the sum of absolutes is a more conservative gauge for the lack of precision in the triangulation measurment.

ERROR   QUADRANGLE

$$\Delta R \leq \left| \Delta R_1 \right| + \left| \Delta R_2 \right|$$

Figure 26: Geometry for ranging error in single baseline triangulation

95
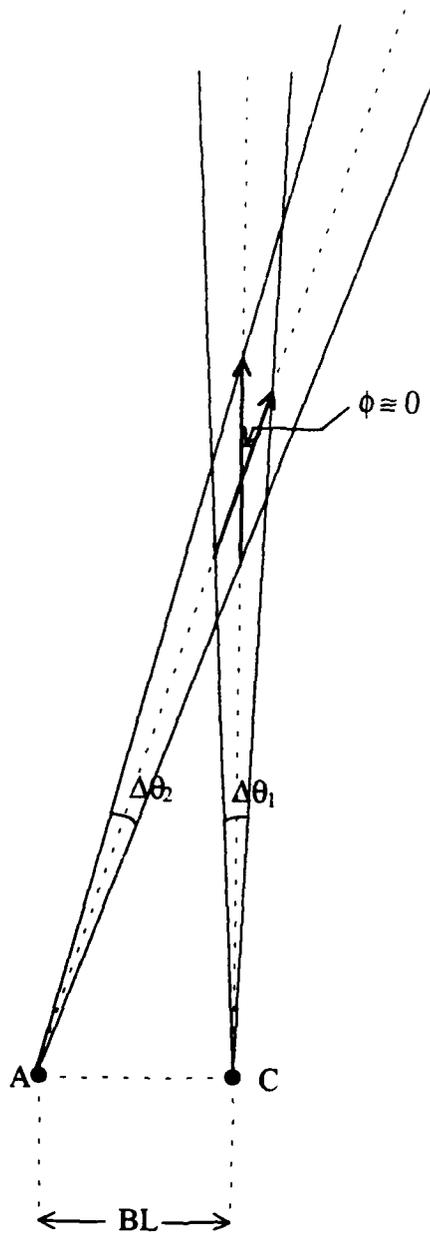
Figure 27 :   Error quadrangle for R>>BL

APPENDIX E: MATLAB CODES

A.   SINGLE BASELINE MODEL

```
clear;
b=input ('put the ratio R/BL=');
y=1./b;
a=input('put the ratio DTH2./DTH1=');
step=pi./40;
theta=0:step:pi;
u=sin(theta);
v=cos(theta);
q=tan(theta);
j=1./q;
c=(b.^2+.5.^2+b.*v).^.5;        % c=R2/BL  eq. 9a ;
d=(b.^2+.5.^2-b.*v).^.5;        % d=R1/BL  eq. 9b ;
theta1=asin(u.*b./c);           %             eq. 10b ;
e=sin(theta1);
f=cos(theta1);
theta2=asin(u.*b./d);           %             eq. 10a ;
g=sin(theta2);
h=cos(theta2);
theta21=asin(1./d.*e);          %             eq. 11 ;
z=tan(theta21);
k=1./z;
l=(.5.*y);                      % l=BL/2R;
m=l.*g;                         % m=(BL/2R)*sin(theta2);
n=(1-m.^2).^.5;
p=l.*e;                         % p=(BL/2R)*sin(theta1);
q=(1-p.^2).^.5;
r=g.*q+e.*n;                    % r=denom. of eq. 7 ;
w=k-(l.^2.*e.*f./q.^2);
x=k+(l.^2.*g.*h./m.^2);
B=n.*(f+e.*k)+g.*q.*w;
C=q.*(h-g.*k)-e.*n.*x;
D=(f./(g+e)+k);
E=(h./(g+e)-k);
F=(sqrt(1-(y.*u).^2)./(y.*u));
% s represents the general solution for single baseline  model  eq. 7 ;
s=((B./r).^2+((C./r).*a).^2).^.5;
```

97

```
% t represents the approximate solution (R>>BL) eq. 15 ;
t=(D.^2+(E.*a).^2).^.5;
% z represents the approximate solution (R>>BL,R1=R2=R) eq. 21 ;
z=((.5.*j+F).^2+((.5.*j-F).*a).^2).^.5;
theta=theta.*180./pi;
plot(theta,s,'*',theta,t,'o',theta,z,'+');
axis([0 180 0 .....]);
xlabel('Theta in degrees');
ylabel('|delta R / (R * delta theta)|');
title('comparison of single baseline model sensitivity curves');
gtext('* for more accurate case (equation 7)');
gtext('o for R>>BL approximation case (equation 15)');
gtext(' + for R>>BL & R=R1=R2 approximation case (equation 21) ');
gtext('R/BL=');
gtext('a=');
```

B. DUAL BASELINE MODEL

```
clear;
rovlbl=input('put the ratio R/LBL=');      %  rovlbl=R/LBL;
y=1./rovlbl;                               %  y=LBL/R;
rovsbl=input('put the ratio R/SBL=');      %  rovsbl=R/SBL;
x=1./rovsbl;                               %  x=SBL/R;
a=input('put the ratio DTHL2/DTHL1=');
aa=input('put the ratio DTHS2./DTHS1=);
step=pi./40;
theta=0:step:pi;
u=sin(theta);
v=cos(theta);
m=(1-sin(theta).^2).^.5;
k=v./u;                  % k=cot(theta);
c=y.*u;                  % c=(LBL/R)*sin(theta);
b=(1-c.^2).^.5;          % b=(1-((LBL/R)*sin(theta)^2)^.5;
d=(1-(-v.^2)).^ 5;       % d=(1-(-cos(theta)^2)^.5;
g=x.*(-v);               % g=(SBL/R)*(-cos(theta));
f=(1-g.^2).^.5;          % f=(1-((SBL/R)*(-cos(theta)))^2)^.5;
% the following relation is for LBL model eq. 33a ;
l=((1/2.*k+b./c).^2+((1/2.*k-b./c).*a).^2).^.5;
% the following relation is for SBL model eq. 33b ;
s=((1/2.*d/(-v)+f./g).^2+((1/2.*d./(-v)-f./g).*aa).^2).^.5;
theta=theta.*180./pi;
plot(theta,l,'o',theta,s,'*');
axis([0, 180, 0, 2.5*10^4]);
title(' dual baseline model sensitivity curves');
```

```
xlabel('Theta in degrees');
ylabel('Delta R/(R * Delta Theta');
gtext('o for long baseline');
gtext('* for short baseline');
gtext('R/LBL=');
gtext('R/SBL=');
gtext('a=');
gtext('ratio of bearing errors in long baseline=');
gtext('ratio of bearing errors in short baseline=');
```

C. RANGE LIMITATIONS FOR FIXED TARGET ORIENTATION

```
clear;
maxrovbl=input(' input the  maximum ratio of r/bl   ');
minrovbl=input(' input the  minimum ratio of r/bl   ');
thetv=1:3;
thetv(1)= input (' angle1 in degrees  other than 0,pi');
thetv(1)=pi/180*thetv(1);
thetv(2)= input (' angle2 in degrees  other than 0,pi');
thetv(2)=pi/180*thetv(2);
thetv(3)= input (' angle3 in degrees  other than 0,pi');
thetv(3)=pi/180*thetv(3);
nmax=input(' input the # points ');
long=1:nmax;
long1=1:nmax;
long2=1:nmax;
long3=1:nmax;
longv=long'*thetv;
difr= (maxrovbl-minrovbl)/(nmax-1);
for k=1:3;
thet=thetv(k);
for i=1:nmax;
rovbl(i)= minrovbl+difr*(i-1);
  rovbll=rovbl(i);
  v=sin(thet) ;
  z=tan(thet);
  x=1./z;
long(i)= 1/2.*x + (sqrt(1-((1./rovbll).*v).^2))./((1./rovbll).*v)) ;    %eq. 47 ;
longv(i,k)=long(i);
end ;
end;
for i=1:nmax ;
long1(i)=longv(i,1);
```

99

```
long2(i)=longv(i,2);
long3(i)=longv(i,3);
ee ;
plot(rovbl,long1,'o',rovbl,long2,'*',rovbl,long3,'x') ;
title ( ' symmetrical analysis ' )
xlabel (' range/base-line ') ;
ylabel (' delta R/(R* delta theta)  ') ;
gtext('o for target approching at an angle -- degrees');
gtext('* for target approching at an angle -- degrees');
gtext('x for target approching at an angle -- degrees');
```

D.   LONG BASELINE POLAR PLOT (SUM OF ABSOLUTES)

```
clear;
%al=input('put the ratio of the bearing errors DTH2L/DTH1L=');
al=1;
%cl=input('put the critical value of the normalized sensitivity=');
cl=500;
theta=0:0.05:2*pi;
% rlovlbl represents the eq.55d ;
rlovlbl=abs((sin(theta).^2.*((cl.^2+(1+al).^2.)/(1+al).^2)).^.5);
polar(theta,rlovlbl);
title('normalized range detected by long baseline (sum of absolutes)');
gtext('ratio of the bearing errors in long baseline=');
gtext('normalized sensitivityof the long baseline=');
gtext('detected range');
```

E.   SHORT BASELINE POLAR PLOT (SUM OF ABSOLUTES)

```
clear;
%as=input('put the ratio of ratio of the bearing errors DTH2S/DTH1S=');
as=1;
%f=input('ratio of the two baselines  SBL(m)/LBL(m)=');
f=0.2;
% cs=input('put the critical value of the normalized sensitivity=');
cs=500;
theta=0:0.05:2*pi;
% rsovlbl represents the eq.55f ;
rsovlbl=abs((cos(theta).^2.*((cs.^2+(1+as).^2)./(1+as).^2) *f.^2).^.5);
polar(theta,rsovlbl);
title('normalized range detected by the short baseline (sum of absolutes)');
gtext('LBL=5 x SBL');
gtext('ratio of the bearing errors in short baseline=');
```

gtext('normalized sensitivity of the short baseline=');
gtext('detected range');

F. LBL & SBL CARTESIAN PLOT (SUM OF ABSOLUTES)

```
clear;
%cl=input('critical value of the normalized sensitivity in long baseline=');
cl=500;
%al=input('ratio of the bearing errors in LBL (DTH2/DTH1)=');
al=1;
%f=input('ratio (SBL(m) /LBL(m)=');
f=0.2;
%cs=input('critical value of the normalized sensitivity in short baseline =');
cs=500;
%as=input('ratio of the bearing errors in SBL (DTH2/DTH1)=');
as=1;
theta=0:0.05:2*pi;
rlovlbl=abs((sin(theta).^2.*((cl.^2+(1+al).^2)./(1+al).^2)).^.5);    % eq. 55d ;
rsovlbl=abs((cos(theta).^2.*((cs.^2+(1+as).^2)./(1+as).^2).*...
f.^2).^.5);                                                          % eq. 55f ;
rmax=max(rlovlbl,rsovlbl);
%polar(theta,rmax);
theta=theta.*180./pi;
plot(theta,rlovlbl,'.',theta,rsovlbl,'-.',theta,rmax,'o');
%gtext('al=2');
%gtext('cl=500');
%gtext('SBL/LBL=0.2');
xlabel('theta in degrees');
%ylabel('rlbl/lbl, rsbl/lbl, rmax/lbl');
title('cartesian plot of the range detected by the dual baseline system (sum of absolutes)');
gtext('ratio of the bearing errors in both baselines=1');
gtext('normalized sensitivity in both baselines=500');
gtext('LBL=5 x SBL');
gtext('range detected by short baseline');
gtext('range detected by long baseline');
gtext('range detected by the system');
```


G. LBL & SBL POLAR PLOT (SUM OF ABSOLUTES)

```
clear;
%cl=input('critical value of normalized sensitivity in long baseline=');
cl=500;
```

```
%al=input('ratio of the bearing errors in long baseline (DTH2L/DTH1L)=');
al=1;
%f=input('ratio (SBL(m) /LBL(m)=');
f=0.2;
%cs=input('critical value of normalized sensitivity in short baseline =');
cs=500;
%as=input('ratio of the bearing errors in short baseline (DTH2S/DTH1S)=');
as=1;
theta=0:0.05:2*pi;
rlovlbl=abs((sin(theta).^2.*((cl.^2+(1+al).^2)./(1+al).^2)).^.5);    % eq. 55d ;
rsovlbl=abs((cos(theta).^2.*((cs.^2+(1+as).^2)./(1+as).^2).*...
f.^2).^.5);                                                          % eq. 55f ;
rmax=max(rlovlbl,rsovlbl);
polar(theta,rlovlbl,'.',theta,rsovlbl,'-.',theta,rmax,'o');
title('range detected by the dual baseline system in any direction(sum of absolutes)');
gtext('ratio of bearing errors in both baselines=1');
gtext('normalized sensitivity in both baselines=500');
gtext('LBL=5 x SBL');
```

H.   LONG BASELINE POLAR PLOT (QUADRATURE ADDITION OF TERMS)

```
 clear;
theta=0:0.05:2*pi;
%cll=input('critical value of the normalized sensitivity in long baseline=');
cll=500;
% rlovlbl  represents eq. 61a ;
rlovlbl=abs(((1/2.*(cll.^2.*sin(theta).^2-0.5.*cos(theta).^2)+sin(theta).^2)).^0.5);
polar(theta,rlovlbl);
title('normalized range detected by long baseline (quadrature addition of terms)');
gtext('ratio of the bearing errors in long baseline=1');
gtext('normalized sensitivity of the long baseline=500');
title('detected range');
```

I.   SBL POLAR PLOT (QUADRATURE ADDITION OF TERMS)

```
 clear;
theta=0:0.05:2*pi;
%css=input('critical value of the normalized sensitivity in short baseline=');
css=500;
%f=input('ratio SBL(m) /LBL(m)=');
f=0.2;
% rsovlbl represents eq. 61b;
rsovlbl=abs(((1/2.*(css.^2.*cos(theta).^2-0.5.*sin(theta).^2)+...
```

```
cos(theta).^2).*f.^2).^0.5);
polar(theta,rsovlbl);
gtext('ratio of the bearing errors in short baseline=1');
gtext('normalized sensitivity of the short baseline=500');
title('normalized range detected by the short baseline (quadrature addition of terms');
gtext('LBL=5 x SBL');
gtext('detected range');
```

J. LBL & SBL CARTESIAN PLOT (QUADRATURE ADDITION OF TERMS)

```
clear;
%cll=input('critical value of the normalized sensitivity in long baseline=');
cll=500;
%ff=input('ratio SBL(m) / LBL(m)=');
ff=0..
%css=input('critical value ot the normalized sensitivity in short baseline=');
css=500;
theta=0:0.05:2*pi;
% rlovlbl represents eq. 61a ;
rlovlbl=abs(((1/2.*(cll.^2.*sin(theta).^2-...
0.5.*cos(theta).^2)+sin(theta).^2)).^0.5);
%rsovlbl represents eq. 61b;
rsovlbl=abs(((1/2.*(css.^2.*cos(theta).^2-0.5.*sin(theta).^2)+...
cos(theta).^2).*ff.^2).^0.5);
rmax=max(rlovlbl,rsovlbl);
plot(theta,rlovlbl,'.',theta,rsovlbl,'-.',theta,rmax,'o');
xlabel('theta in degrees');
ylabel('rlbl/lbl, rsbl/lbl, rmax/lbl');
titie('cartesian plot of the range detected by the dual baseline system(quadrature
addition)');
gtext('ratio of bearing errors in both baselines =1');
gtext('normalized sensitivity in both baselines=500');
gtext('LBL=5 x SBL');
gtext(' range detected by short baseline');
gtext('range detected by long baseline');
```

K. LBL & SBL POLAR PLOT (QUADRATURE ADDITION OF TERMS)

```
clear;
%cll=input('critical value of the normalized sensitivity in long baseline=');
cll=500;
%ff=input('ratio SBL(m) / LBL(m)=');
ff=0.2;
```

```
%css=input('critical value of the normalized sensitivity in short baseline=');
css=500;
theta=0:0.05:2*pi;
% rlovlbl represents eq. 61a ;
rlovlbl=abs(((1/2.*(cll.^2.*sin(theta).^2-0.5.*cos(theta).^2)+sin(theta).^2)).^0.5);
% rsovlbl represents eq. 61b ;
rsovlbl=abs(((1/2.*(css.^2.*cos(theta).^2-0.5.*sin(theta).^2)+...
cos(theta).^2).*ff.^2).^0.5);
rmax=max(rlovlbl,rsovlbl);
polar(theta,rmax);
theta=theta.*180./pi;
title('range detected by the dual baseline system in any direction (quadrature addition)');
gtext('ratio of bearing errors in both baselines=1');
gtext('normalized sensitivity in both baselines=500');
gtext('LBL=5 x SBL');
gtext('ass=1');
gtext('range detected by the system');
```

L. LIMITATIONS IN THE MEASURMENT OF THE RANGE (S. A)

```
clear;
% S.A is for the sum of absoluets;
%al=input('ratio of the bearing errors in the long baseline( DTH2L/DTH1L)=');
al=1;
%cl=input('critical value of the normalized sensitivity in long baseline=');
cl=500;
%lbl=input('length of the long baseline(m)=');
lbl=100/20;
theta=0:0.05:2*pi;
% rl represents the eq. 55d;
rl=abs((sin(theta).^2.*lbl.^2.*((cl.^2+(1+al).^2)./...
(1+al).^2)).^0.5);
%as=input('ratio of the bearing errors in short baseline (DTH2S/DTH1S)=');
as=1;
%cs=input('critical value of the normalized sensitivity in short baseline=');
cs=500;
%sbl=input('length of SBL(m)=');
sbl=20/4;
% rs represents the eq. 55f;
rs=abs((cos(theta).^2.*sbl.^2.*((cs.^2+(1+as).^2)./...
(1+as).^2)).^.5);
rmax=max(rl,rs);
```

```matlab
% re represents the radius of the earth (6.371 x 10^6 meters);
re=6.371*10.^6;
%s=input('height of the sensor above surface (m)=');
s=10/3;
%t=input('height of the target above surface (m)=');
t=10/3;
% d represents the eq. 68;
d=(2.*re.*t).^.5+(2.*re.*s).^.5;
% r represents the geometrical horizon;
r=(d.^2.*cos(theta).^2+d.^2.*sin(theta).^2).^.5;
if d>rmax
    polar(theta,r);
    hold on
    polar(theta,rmax);
else
    polar(theta,rmax);
    hold on
    polar(theta,r);
end;
title('detected range is limited by the geometric horizon / by the system (sum of absolutes)');
gtext('long baseline length=100/20m');
gtext('short baseline length =20/4 m');
gtext('height of the target above surface=10/3m');
gtext('height of the sensor above surface =10/3m');
gtext('geometric horizon');
gtext('range detected by the system');
gtext('detected range');
```

M.   LIMITATIONS IN THE MEASURMENT OF THE RANGE (Q. A)

```matlab
clear;
% Q.A is for the quadrature addition of terms;
%cll=input('critical value of the normalized sensitivity in long baseline=');
cll=500;
%lbl=input('length of the long baseline(m)=');
lbl=100/20;
%sbl=input('length of the short baseline(m)=');
sbl=20/4;
%css=input('critical value of the normalized sensitivity in short baseline=');
css=500;
theta=0:0.05:2*pi;
% rl represents eq. 61a;
```

```
rl=abs(((1/2.*(cll.^2.*sin(theta).^2-0.5.*cos(theta).^2)+...
sin(theta).^2).*lbl.^2).^0.5);
% rs represents eq. 61b;
rs=abs(((1/2.*(css.^2.*cos(theta).^2-0.5.*sin(theta).^2)+...
cos(theta).^2).*sbl.^2).^0.5);
rmax=max(rl,rs);
% re represents the radious of the earth (6.371x 10^6 meters);
re=6.371*10.^6;
%s=input('height of sensor above surface (m)=');
s=10/3;
%t=input('height of terget above surface (m)=');
t=10/3;
% d represents eq. 68;
d=(2.*re.*t).^.5+(2.*re.*s).^.5;
% r  represents the geometrical horizon;
r=(d.^2.*cos(theta).^2+d.^2.*sin(theta).^2).^.5;
if d>rmax
   polar(theta,r);
   hold on
   polar(theta,rmax);
else
   polar(theta,rmax);
   hold on
   polar(theta,r);
end;
title('detected range is limited by the geometric horizon/by the system (quadrature
addition)');
gtext('long baseline length=100/20m');
gtext('short baseline length=20/4m');
gtext('height of the target above the surface = 10/3m');
gtext('heigt of the sensor above the surface= 10/3m');
gtext('geometric horizon');
gtext('range detected by the system');
gtext('detected range');
```

N.   CROSSOVER ANGLE

```
clear;
% f=input('ratio of the two baselines SBL(m)/LBL(m)=');
f=0.2;
% c is the normalized sensitivity of both baselines which assumed to be the same;
% clower= input ('lower limit of the normalized sensitivity=');
clower=500;
```

```
% cupper+input ('upper limit of the normalized sensitivity =');
cupper=1000;
%cstep=input ('step of normalized sensitivity');
cstep=10;
c=clower:cstep:cupper;
theta1=atan(f.*(c./c));                    % eq. 82 ;
theta2=asin(sqrt((0.25+0.5.*c.^2.*f.^2+...
f.^2)./(1.25+0.5.*c.^2+0.5.*c.^2.*f.^2+f.^2))); % eq. 80 ;
theta1=theta1.*180/pi;
theta2=theta2.*180/pi;
plot(c,theta1);
hold on;
plot(c,theta2,'.');
axis([500 1000  11.3  11.4 ]);
xlabel('normalized range sensitivity');
ylabel('angle theta in degrees');
title('comparison crossover angle approximations');
gtext('accurate cross angle (eq. 80)');
gtext('approximate cross angle (eq. 82)');
```

LIST OF REFERENCES

1. A. N. Steinberg, "Sensor and Data Fusion," *The Infrared Electro-Optical Handbook*, vol. 8, ed. Stanley Robinson, Bellingham, WA, SPIE Optical Engineering Press, pp. 309-313, 1993.

2. R. G. Wiley, *Electronic Intelligence, The Interception of Radar Signals*, Dedham, MA, Artech House, pp. 255-267, 1985.

3. J. Sparagna and others, "Passive ECM: Emitter Techniques," *The Microwave Journal*, pp.45-74, 1971.

4. J. P. Ovrebo and others, "*Passive Infrared Ranging Device Using Absorption Bands of Water Vapor or Carbon Dioxide*," U. S. Patent 3,103,586, September 10, 1963.

5. J. R. Jennes Jr., and others, "*Apparatus for Passive Infrared Range Finding*," U. S. Patent 3,117,228, January 7, 1964.

6. D. V. Lowry, *Target range estimation based on passive detection of infrared emissions*, Master's Thesis, Naval Postgraduate School, Monterey, CA, September 1987.

7. S. Hirakawa, *Passive determination of temperature over range using spectral band measurement of photon emitted*, Master's Thesis, Naval Postgraduate School, Monterey, CA, September 1991.

8. J. H. Dick, *Analysis of two color passive infrared ranging utilizing the AE-4128 infrared camera system*, Master's Thesis, Naval Postgraduate School, Monterey, CA, December 1993.

9. W. J. Smith, *Modern Optical Engineering: the Design of Optical Systems*, 2d ed., New York, NY, Mcgraw Hill, pp. 254-256, 1990.

10. J. Strong, "*Infrared Range Finder*," U. S. Patent 3,005,913, October 1961.

11. J. R. Ester, Jr., "*Closure Time Computer*," U. S. Patent 2,993,121, July 18, 1961.

12. J. S. Acceta, "Infrared and track systems," *The Infrared and Electro-Optical Handbook*, vol. 5, ed. Steven Campana, Bellingham, WA, SPIE Optical Engineering Press, pp. 342-343, 1993.

13. D. L. Fried, "Resolution, signal to noise ratio and measurements precision," *Optical Society of America Journal*, vol. 69, pp. 399-406, March 1979.

14. W. H. Foy, "Position-location solutions by Tailor-series estimation," *IEEE Transactions on Aerospace and Electronic Systems*, vol. AES-12, No 2, pp. 187-193, March 1976.

15. J. S. Acceta, "Infrared and track systems,"*The Infrared and Electro-Optical Handbook*, vol. 5, ed. Steven Campana, Bellingham WA, SPIE Optical Engineering Press, pp. 336-337, 1993.

16. J. L. Poirot and Ghassan, "Position Location: Triangulation versus circulation," *IEEE Transactions on Aerospace and Electronic Systems*, vol. AES-14, No 1, pp. 48-53, January 1978.

17. R. J. Pieper and A. W. Cooper, "*A Triangulation Method for Passive Ranging,*" Technote NACIT-94-1, delivered JHU/APL, November 1993.

18. E. J. McCartney, "*Optics of the Atmosphere,*" pp. 94-100, New York, NY, John Wiley&Sons Inc., 1976.

19. MAPLE, Waterloo Maple Software, Ontario, Canada N2L 5J2.

20. MAXSYMA, Symbolics Inc., Burligton, MA, 0183, January 1988.

INITIAL DISTRIBUTION LIST

No. Copies

1. Defense Technical Information Center   2
   Cameron Station
   Alexandria, Virginia 22304-6145

2. Library, Code 52   2
   Naval Postgraduate School
   Monterey, California 93943-5101

3. Chairman, Code EC   1
   Department of Electrical and Computer Engineering
   Naval Postgraduate School
   Monterey, California 93943-5121

4. Chairman, Code PH   1
   Department of Physics
   Naval Postgraduate School
   Monterey, California 93943-5117

5. Prof. Ron J. Pieper, Code EC/Pr   1
   Department of Electrical and Computer Engineering
   Naval Postgraduate School
   Monterey, California 93943-5121

6. Prof. A. W. Cooper, Code PH/Cr   1
   Department of Physics
   Naval Postgraduate School
   Monterey, California 93943-5117

7. Dennis V. Webster   1
   Surface Combat Systems (FPI)
   The Johns Hopkins University, Applied Physics Lab.
   Laurel Maryland. 20723-6099

8. Commander, NAVAL SEASYSTEMS COMMAND   1
   ATTN: LCDR. J. W. Wilson, PMS-400B30
   Washington, DC 20363

9. Program Executive Office- Theater Air Defense (TAD)   1
   ATTN: Mr. J. E. Misanin, Code PEO (TAD) D234
   Naval Sea Systems Command
   Washington, DC 20363-5100

10. LTCOL Pelegris Gerasimos
    Dimarxiou 110 Aegaleo (Agios Spyridonas)
    ATHENS GREECE

1